NAVAL POSTGRADUATE SCHOOL
MONTEREY, CALIFORNIA

THESIS

ASSESSMENT OF SHALLOW WATER NEAR SURFACE RESPONSE OF SUBMERSIBLE VEHICLES

by

Ufuk Toprak

June, 1996

Thesis Advisor: Fotis A. Papoulias

Approved for public release; distribution is unlimited.

DISCLAIMER NOTICE

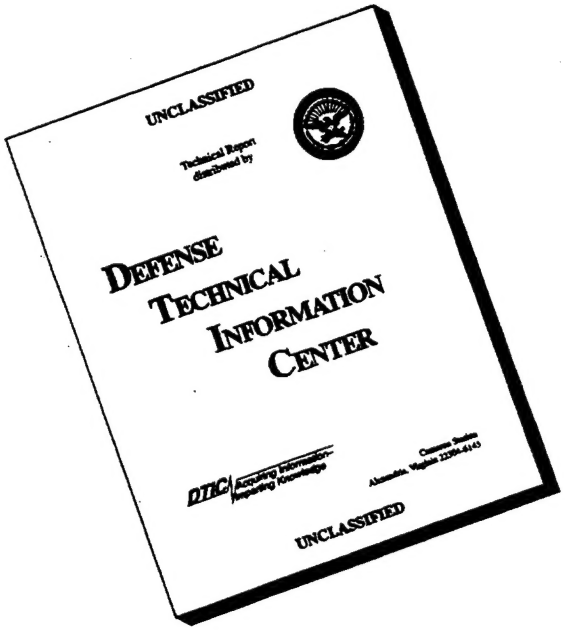

THIS DOCUMENT IS BEST QUALITY AVAILABLE. THE COPY FURNISHED TO DTIC CONTAINED A SIGNIFICANT NUMBER OF PAGES WHICH DO NOT REPRODUCE LEGIBLY.

REPORT DOCUMENTATION PAGE

Form Approved OMB No. 0704-0188

1. AGENCY USE ONLY *(Leave blank)*	2. REPORT DATE June 1996	3. REPORT TYPE AND DATES COVERED Master's Thesis

4. TITLE AND SUBTITLE ASSESSMENT OF SHALLOW WATER NEAR SURFACE RESPONSE OF SUBMERSIBLE VEHICLES

5. FUNDING NUMBERS

6. AUTHOR(S) Ufuk Toprak

7. PERFORMING ORGANIZATION NAME(S) AND ADDRESS(ES)
Naval Postgraduate School
Monterey CA 93943-5000

8. PERFORMING ORGANIZATION REPORT NUMBER

9. SPONSORING/MONITORING AGENCY NAME(S) AND ADDRESS(ES)

10. SPONSORING/MONITORING AGENCY REPORT NUMBER

11. SUPPLEMENTARY NOTES The views expressed in this thesis are those of the author and do not reflect the official policy or position of the Department of Defense or the U.S. Government.

12a. DISTRIBUTION/AVAILABILITY STATEMENT
Approved for public release; distribution is unlimited.

12b. DISTRIBUTION CODE

13. ABSTRACT *(maximum 200 words)* Vertical plane response of submersible vehicles in the proximity of a free surface in both deep and shallow waters is evaluated using a potential flow, strip theory solver. Three criteria, namely periscope submergence, sail broaching, and collision are used to quantify the response. These criteria combined with the vehicle's response amplitude operators in regular sinusoidal waves along with a statistical description of the seaway lead to an assessment of an overall operability index for the vehicle. The operability index is calculated within a given range for sea states and sea directions and for various vehicle speeds and operating depths. The results indicate that a certain combination of depth and speed can lead to a significant improvement in vehicle operations.

14. SUBJECT TERMS SUBMERSIBLE VEHICLES, PERISCOPE DEPTH OPERATIONS, OPERABILITY INDEX, STRIP THEORY			15. NUMBER OF PAGES 127 16. PRICE CODE
17. SECURITY CLASSIFICATION OF REPORT Unclassified	18. SECURITY CLASSIFICATION OF THIS PAGE Unclassified	19. SECURITY CLASSIFICATION OF ABSTRACT Unclassified	20. LIMITATION OF ABSTRACT UL

NSN 7540-01-280-5500
Standard Form 298 (Rev. 2-89)
Prescribed by ANSI Std. 239-18 298-102

Approved for public release; distribution is unlimited.

ASSESSMENT OF SHALLOW WATER NEAR SURFACE RESPONSE OF SUBMERSIBLE VEHICLES

Ufuk Toprak
Ltjg, Turkish Navy
B.S., Turkish Naval Academy - 1990

Submitted in partial fulfillment
of the requirements for the degree of

MASTER OF SCIENCE IN MECHANICAL ENGINEERING

from the

NAVAL POSTGRADUATE SCHOOL
June 1996

Author: _____
Ufuk Toprak

Approved by: _____
Fotis A. Papoulias , Thesis Advisor

_____
Terry R. McNelley, Chairman
Department of Mechanical Engineering

ABSTRACT

Vertical plane response of submersible vehicles in the proximity of a free surface in both deep and shallow waters is evaluated using a potential flow, strip theory solver. Three criteria, namely periscope submergence, sail broaching, and collision are used to quantify the response. These criteria combined with the vehicle's response amplitude operators in regular sinusoidal waves along with a statistical description of the seaway lead to an assessment of an overall operability index for the vehicle. The operability index is calculated within a given range for sea states and sea directions and for various vehicle speeds and operating depths. The results indicate that a certain combination of depth and speed can lead to a significant improvement in vehicle operations.

TABLE OF CONTENTS

ACKNOWLEDGEMENT

I would like to thank my thesis advisor, Professor Fotis A. Papoulias, for his guidance in this thesis research.

I. INTRODUCTION

When a submarine is at periscope depth beneath a seaway, several exciting forces and moments are encountered. These include first-order oscillatory motions at the prevailing wave frequencies and second-order drifting motions at very low frequencies well outside the wave spectrum of the seaway. These are referred to as the free surface suction forces and moments. In practice these low frequency motions are difficult to control and may give rise to unsatisfactory depth keeping. Standard ways of computing free surface effects rely on combinations of potential flow and semi-empirical coefficient based models. Rankine type sources are distributed along the hull of the ship, which satisfy the free surface boundary condition. Source strength can be computed by satisfying the exact body boundary condition, that no fluid can pass through the hull surface. Discretization of the hull form into a finite set of Hess-Smith type quadrilateral panels allows formulation of algebraic system of equations to be solved for the unknown singularity strengths. [Ref. 1] Combination of forces and moments generated in this way with deep water force predictions can then be utilized to simulate the motion of the boat under waves.

Although such suction forces and moments are difficult to predict, they are slowly varying in time and as a result they can be controlled by either the operators or automatic control systems. Techniques of disturbance estimation and compensation can be employed in order to allow satisfactory real-time estimation of unknown disturbances from depth, pitch angle, and pitch rate measurements [Ref. 2]. In contrast to these second-

order forces, first-order forces cannot be actively controlled in practice since they occur at very high frequencies (in the order of magnitude of a few seconds) which are normally outside the range of hardware response times. Therefore, it is essential that we have a clear understanding of the effects of first-order excitation on boat missions in order to maximize its window of operations. This approach will identify parameter regions where operations may be carried out with higher degrees of confidence of success and with better opportunities for active control. In order to achieve this first we need to have a computational tool which will allow us to determine vehicle motions in the vicinity of a free surface in deep and shallow water. In this work we utilize a strip theory seakeeping prediction program based on the work by Beck and Troesch [Ref. 3].

Accurate submarine maneuvering predictions are essential for operation, to provide optimal and safe submerged operating envelopes. Relative vertical motion is one of the most important response elements that appear to be the most crucial to the submarine operators for successful completion of a mission near a free surface. To decide whether the submarine could complete her mission successfully or not we need to adopt a number of criteria each pertaining to different operational hazards. These criteria can be broadly divided into two major categories, subtle and catastrophic failures. In this study we consider two criteria. One of them is periscope submergence, which is a subtle failure and the other is sail broaching, which is a catastrophic failure.

Subtle failures refer to events which will occur in all types of periscope depth operations, i.e., propeller emergence, mast emergence, periscope submergence. Single occurrence of these events does not constitute failure of operations. However, their

frequency imposes operability limits for a certain sea state. Periscope submergence impairs visual information. The dominant criterion is the number of occurrences per unit time.

Catastrophic failures will probably result in either cancel of operations, failure to complete mission or submarine detection, i.e., broaching, loss of depth control deep. Broaching the sail is defined here as any portion of the sail breaking the surface. It is assumed that submarine detection will occur with probability of one each time a broaching occurs.

In shallow water operations, we employ an additional criterion in addition to the two above. This corresponds to the event of vehicle collision with the sea-bed and is determined statistically based on the absolute vertical motion of either the bow or the stern of the vehicle and its clearance from the sea-bed. Combination of all of the above criteria provides a quantifiable measure of vehicle operability within a certain range of sea-states and directions.

Chapter II of this thesis describes the mathematical foundation for the problem. Chapter III presents results for the operability index of a vehicle for periscope submergence and sail broaching criteria for different sea-states and wave heading angles and deep water operations. In Chapter IV the operability index of the vehicle is presented for periscope submergence, sail broaching, and collision criteria for shallow water operations. Finally, conclusions from this work and recommendations for further research are outlined in Chapter V.

II. EVALUATION OF RESPONSE

A. GEOMETRY OF A SUBMARINE

Froude (1877) [Ref. 4] introduced the concept of a ship with a forward end called the "entrance", a parallel middle body, and an after end called the "run". Chapman (1768) [Ref. 4] introduced the concept of a ship hull with the entrance a portion of an ellipsoid of revolution, and with the run a portion of a parabola of revolution. This concept is tailor-made for use in calculating volumes of modern submarine hulls, as described by Jackson (1983) [Ref. 4]. It was developed by assuming a body of revolution with a length/diameter (L/D) ratio of six and a maximum diameter at $0.4L$. The entrance has a length , L_f , of 2.4 diameters. The run or after end has a length, L_a , of 3.6 diameters. The entrance can be calculated as an ellipsoid of revolution, and the run as a paraboloid of revolution which is rotated about a line parallel to the center-line. The equations of the offsets for each are given below. The hull radius at each station can be found by multiplying the offsets by half the maximum diameter, $D/2$.

If one were to use equations for true ellipsoids and parabolas, the entrance and the run would be too fine for a modern submarine. The displacement can be increased by using larger exponents (n_f and n_a), as in Equations (1) and (2). If even more displacement is required, a parallel middle body of cylindrical shape can be inserted at the maximum diameter. The prismatic coefficient, C_p, is used to calculate volumes and for a cylinder the prismatic coefficient is 1. For a submarine-like body the prismatic coefficient can be evaluated in terms of its geometry. Using the above concept, the length of the parallel middle body (PMB) is the length overall (LOA) less $6D$, that is, LOA-$6D$.

$$y_f = \frac{D}{2}\left[1-\left(\frac{x_f}{L_f}\right)^{n_f}\right]^{1/n_f} \quad \textbf{(1)}$$

$$y_a = \frac{D}{2}\left[1-\left(\frac{x_a}{L_a}\right)^{n_a}\right] \quad \textbf{(2)}$$

Here x_f and x_a are the distances from the maximum diameter. With these concepts, a very simple method of calculating the volume of the entire hull can be developed. This is true for the ends separately and for the PMB. Let V_f, V_a, and V_{PMB} denote, respectively, volume of the entrance, the run, and the parallel middle body, and let C_f and C_a be the prismatic coefficients. The resulting equations are

$$V_f = \frac{\pi D^2}{4}\left(C_{pf}\,2.4D\right) \quad \textbf{(3)}$$

$$V_a = \frac{\pi D^2}{4}\left(C_{pa}\,3.6D\right) \quad \textbf{(4)}$$

$$V_{PMB} = \frac{\pi D^2}{4}\left(L-6D\right) \quad \textbf{(5)}$$

The above can be combined into the following

$$V = \frac{\pi D^3}{4}\left[3.6C_{pa}+\frac{L}{D}-6+2.4C_{pf}\right] \quad \textbf{(6)}$$

Figure 1 illustrates this concept [Ref. 4]. In this study our model submarine's LOA is 109.75 m. (360 ft.), D is 9.15 m. (30 ft.), and the exponents n_a and n_f are 3.0.

B. REGULAR WAVE RESPONSE

In this study our main concern is the effects of surface waves on a near-surface submarine vertical motions. The assumptions here are that the fluid is ideal and the wave

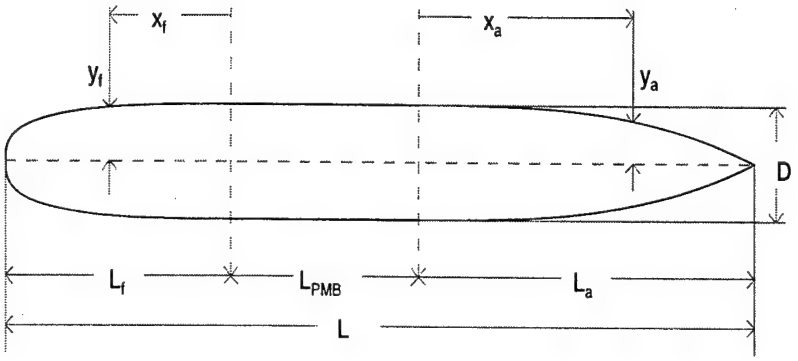

Figure 1. Submarine Geometry [Ref. 4]

and body motions are sufficiently small to linearize. Sea waves and ship motions are based on potential flow theory. In the simplest case it may be assumed that the waves incident upon the body are plane progressive waves of small amplitude, with sinusoidal time dependence. The solution to the water velocity distribution associated with the wave can be simplified to deep and shallow water approximations. When the wave length is greater than 20 times the depth, then shallow water approximations apply and depth becomes the controlling factor. The horizontal component of the velocity is not a function of depth, but is constant from top to bottom. The vertical component of water motion decays linearly from its maximum at the surface to zero at the bottom. The pressure under a shallow-water wave also is not a function of depth, but is just the hydrostatic pressure due to the amount of water above. When the water depth is greater than one quarter the wavelength then the deep water approximations apply and the water depth becomes unimportant. The horizontal and vertical components of velocity are equal and the orbits

become circles which decrease exponentially as a function of depth. Their motions become negligible at a depth equal to one half the wavelength [Ref. 5]. Since we are interested in the vertical motion we consider the motions of a body that is allowed to heave and pitch only. Such motions are usually decoupled, for typical ships, from the horizontal plane motions in sway or yaw. The final coupled form of the heave and pitch equations of a ship in regular wave is then

$$(m + A_{33})\ddot{\eta}_3 + B_{35}\dot{\eta}_3 + C_{33}\eta_3 + A_{35}\ddot{\eta}_5 + B_{35}\dot{\eta}_5 + C_{35}\eta_5 = F_3 e^{i\omega t} \quad (7)$$

$$(I_{55} + A_{55})\ddot{\eta}_5 + B_{55}\dot{\eta}_5 + C_{55}\eta_5 + A_{53}\ddot{\eta}_3 + B_{53}\dot{\eta}_3 + C_{53}\eta_3 = F_5 e^{i\omega t} \quad (8)$$

where m is the ship's mass and I_{55} the mass moment of inertia with respect to the y axis. The A_{jk} terms correspond to added mass. The B_{jk} terms correspond to hydrodynamic damping. Terms involving the coefficients ; i.e., C_{33} , C_{55} , and C_{55} are related to tons per cm immersion, change in displacement per cm, and moment to trim one cm, respectively. The right hand side represents the heave, F_3 , Froude-Krylov and diffraction excitation forces. F_3 and F_5 are taken to be the complex exciting force and moment amplitudes, containing both amplitude and phase information. The previous equations of motion are valid for a ship with zero forward speed. If the ship possesses a forward speed U , this can be assumed, within linearity, constant. The only change in such a case is in the frequency ω due to a Doppler shift effect. In linear theory, the harmonic responses of the vessel, $\eta_j(t)$, will be proportional to the amplitude of the exciting forces and at the same frequency, which is now ω_e (wave frequency of encounter) instead of ω. Consequently ship motions will have the form

$$\eta_j(t) = \overline{\eta}_j e^{i\omega_e t},$$

$$\dot{\eta}_j(t) = i\omega_e \overline{\eta}_j e^{i\omega_e t}, j = 3,5 \qquad \textbf{(9)}$$

$$\ddot{\eta}_j(t) = -\omega_e^2 \overline{\eta}_j e^{i\omega_e t},$$

where $\overline{\eta}_j$ is the complex response amplitude, and j=3 for heave and j=5 for pitch. Substituting equations (9) in (7) and (8), the $e^{i\omega_e t}$ terms cancel out and the resulting equations are

$$\left[-\omega_e^2(m + A_{33}) + i\omega_e B_{33} + C_{33}\right]\overline{\eta}_3 + \left(-\omega_e^2 A_{35} + i\omega_e B_{35} + C_{35}\right)\overline{\eta}_5 = F_3, \qquad \textbf{(10)}$$

$$\left[-\omega_e^2(I_{55} + A_{55}) + i\omega_e B_{55} + C_{55}\right]\overline{\eta}_5 + \left(-\omega_e^2 A_{53} + i\omega_e B_{53} + C_{53}\right)\overline{\eta}_3 = F_5, \qquad \textbf{(11)}$$

In equations (10) and (11) the origin is at the center of gravity, which is assumed to lie on the waterline. In the more general case, the term $m\ddot{\eta}_3$ is substituted by $m\ddot{\eta}_3 - mx_G\ddot{\eta}_5$, and the term $I_{55}\ddot{\eta}_5$ by $I_{55}\ddot{\eta}_5 + m(z_G\ddot{\eta}_1 - x_G\ddot{\eta}_3)$, where η_1 is the surge motion amplitude. In other words, a coordinate coupling is introduced.

The determination of the coefficients and exciting forces and moments amplitudes represents the major problem in ship motions calculations. The problem can be simplified by applying a strip theory approach, where the ship is divided into transverse strips, or segments. The added mass and damping for each strip are relatively easily calculated, using two dimensional potential theory or by suitable two dimensional experiments. The sectional values are appropriately combined to yield values for A_{jk}, B_{jk}, C_{jk}, and F_j.

To solve equations (10) and (11) for the complex amplitudes, the equations are written in the form

$$P\overline{\eta}_3 + Q\overline{\eta}_5 = F_3, \tag{12}$$

$$R\overline{\eta}_3 + S\overline{\eta}_5 = F_5, \tag{13}$$

where

$$P = -\omega_e^2(m + A_{33}) + i\omega_e B_{33} + C_{33},$$

$$Q = -\omega_e^2 A_{35} + i\omega_e B_{35} + C_{35},$$

$$R = -\omega_e^2 A_{53} + i\omega_e B_{53} + C_{53},$$

$$S = -\omega_e^2(I_{55} + A_{55}) + i\omega_e B_{55} + C_{55},$$

The solutions to the coupled equations (12) and (13) is then given by

$$\overline{\eta}_3 = \frac{F_3 S - F_5 Q}{PS - QR}, \tag{14}$$

$$\overline{\eta}_5 = \frac{F_5 P - F_3 R}{PS - QR}. \tag{15}$$

The ratio (η_j/A) is a quantity of fundamental significance, where A is wave amplitude, and is defined by $Z_j(\omega,U,\theta)$. Physically, this is the complex amplitude of body motion in the j-th mode, in response to an incident wave of unit amplitude, frequency ω, and direction θ. The body itself moves with forward speed U. This ratio is generally known as the *transfer function,* or the *response amplitude operator,* RAO. The RAO can be calculated once the added mass, damping, exciting, and hydrostatic forces are known.

The absolute vertical displacement at a point x along the length of the hull, due to heave and pitch is given by

$$\xi_{VA} = \eta_3 - x\eta_5, \tag{16}$$

and since η_3 and η_5 are the complex amplitudes in heave and pitch motion, respectively, ξ_{VA} contains both magnitude and phase information. Particularly of interest in this study is the relative vertical motion between a point in the ship and the surface of the encountered wave. The relative motion in regular waves is found by subtracting the free surface motion from the vertical ship motion at the desired point, taking account of their phase relationship. The free surface motion is composed of the incident wave, the diffracted wave, the radiated wave, and the Kelvin wave due to the ship's steady forward speed. The traditional assumption is that the principal component is the incident wave; i.e., the incident wave is not distorted by the presence of the ship. Then the amplitude of the relative vertical motion in general is given by

$$\xi_{VR} = \xi_{VA} - Ae^{ikx} \ , \tag{17}$$

where A is the wave amplitude and k is the wave number. Then the RAO which requires only the scalar or absolute magnitude is

$$\left|\frac{\xi_{VR}}{A}\right| = \left|\frac{\eta_3 - x\eta_5}{A} - e^{ikx}\right| . \tag{18}$$

The significance of the relative motion response is that the moments of their spectrum provide probability measures related to anticipated deck wetness, bow slamming or particularly for our study sail broaching and periscope submergence.

Figures 2 and 3 show RAO amplitudes and phases versus wave to ship length ratio of our model submarine's heave, pitch, and relative vertical motion at 3 submarine diameter depth and 5 knots forward speed when A equals 5 feet.

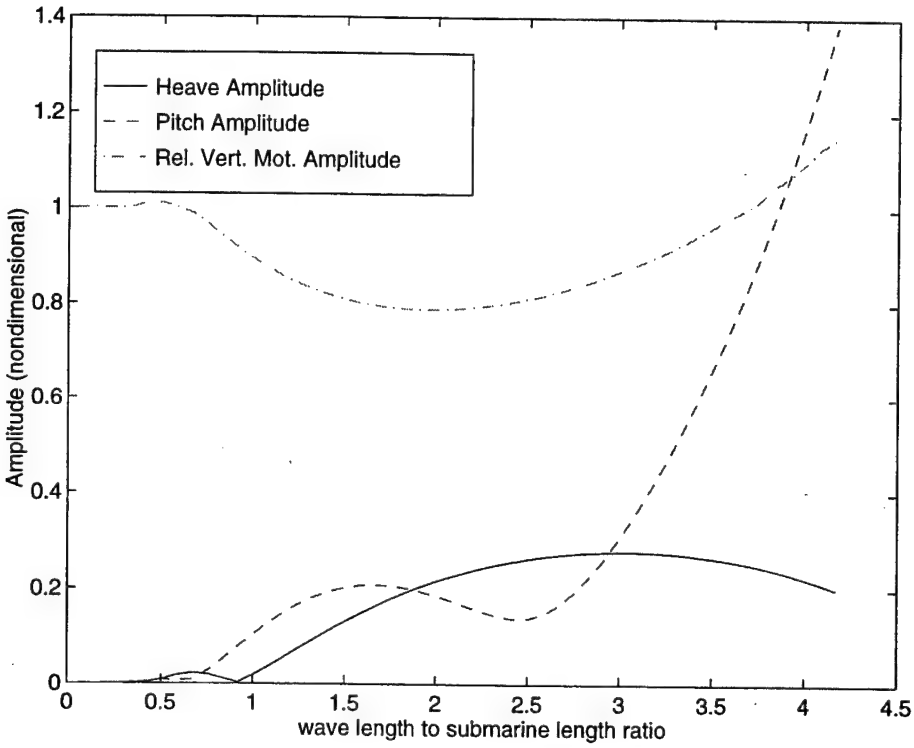

Figure 2. Amplitude of RAO for heave/pitch and relative motion

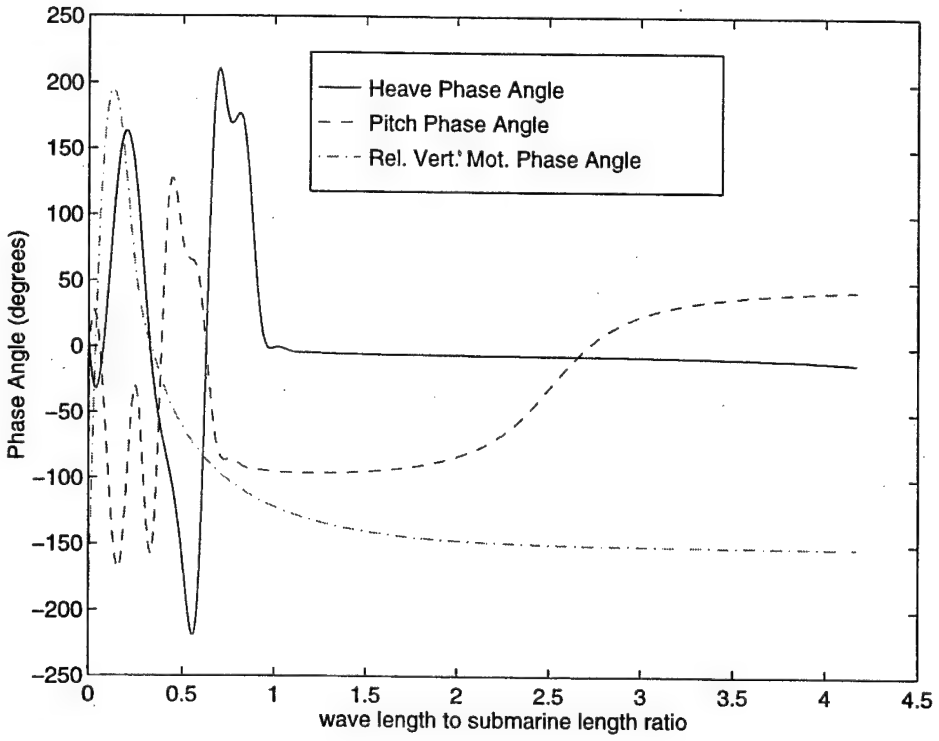

Figure 3. Phase Angle of RAO for heave/pitch and relative motion

C. IRREGULAR WAVE RESPONSE

Wave patterns in an open sea are ever changing with time and space, in a manner that appears to defy analysis be it linear or second order Stokes. Ambient waves on the surface of the sea are dispersive as well as random. Random refers to the character of the wave height distribution. The continuous distribution of sinusoidal waves have continuously distributed amplitude and phase so that in summation the variation of wave height with time is not systematic in any respect, but random. The practically useful data extractable from a random wave record $h(t)$ is its spectral density, $S(\omega)$. The random $h(t)$ record is processed in such a way to produce a curve of $S(\omega)$ versus wave frequency, ω. The spectral density is obtained from a wave height record taken over a time period for which the sea conditions are assumed to be unchanging, in an average sense (stationary). This corresponds to a certain sea state. The function $S(\omega,\theta)$ is called the spectral energy density or simply the energy spectrum. More specifically, this is a directional energy spectrum; it can be integrated over all wave directions to give the frequency spectrum

$$S(\omega) = \int_0^{2\pi} S(\omega,\theta) d\theta \ . \qquad \textbf{(19)}$$

Usually in the fields of ocean engineering and naval architecture it is customary to assume that the waves are long crested which means the fluid motion is two dimensional and the wave crests are parallel. With such a simplification it is possible to use existing information for the frequency spectrum (19), which is based on a combination of theory and full scale observations.

For most purposes we are interested primarily in the larger waves. The most common parameter that takes this into account is the significant wave height, $H_{1/3}$, defined as the average of the highest one third of all waves. This can be computed from

$$H_{1/3} = 4.0(m_0)^{1/2}. \tag{20}$$

In this equation, m_0 is the area under the spectrum $S(\omega)$ integrated over the entire range of frequencies ω. An average frequency of the spectrum can be defined as the expected number of zero upcrossings per unit time, that is, the number of times the wave amplitude passes through zero with positive slope. The final result here is

$$\omega_z = \left(\frac{m_2}{m_0}\right)^{1/2}. \tag{21}$$

The average period between zero upcrossings is

$$T_z = \frac{2\pi}{\omega_z} = 2\pi\sqrt{\frac{m_0}{m_2}} \tag{22}$$

More meaningful frequency parameters can be obtained from the set of moments, which depend on spectrum shape

$$m_n = \int_0^\infty \omega^n S(\omega) d\omega \ , \qquad n=0,1,2,... \tag{23}$$

In particular, the area, m_0, is the variance or the total energy of the spectrum. Also m_2 is variance of velocity and m_4 is variance of acceleration.

A good model for fully developed seas is the classical Pierson-Moskowitz spectrum. This spectral form depends upon a single parameter which is the significant wave height. It is intended to represent point spectrum of a fully-developed sea. Fetch and duration are assumed to sufficiently large so that the sea has reached steady state, in a

statistical sense. This spectral family should be recognized as an asymptotic form, reached after an extended period of steady wind, with no contamination from an underlying swell. Using the spectral family, along with the similarity theory of S. A. Kitaigorodskii, Pierson and Moskowitz (1964) [Ref. 6] arrived at the following analytical formulation for ideal sea spectra,

$$S_1^+(\omega) = \frac{0.0081 g^2}{\omega^5} \exp\left[-0.032 \left(\frac{g}{H_{1/3} \omega^2} \right)^2 \right], \qquad \textbf{(24)}$$

where

$S_1^+(\omega)$ = one-sided incident wave spectrum

g = acceleration of gravity

$H_{1/3}$ = significant wave height

ω = wave frequency

In Figure 4 we can observe typical Pierson-Moskowitz wave spectra for 5 m. significant wave height.

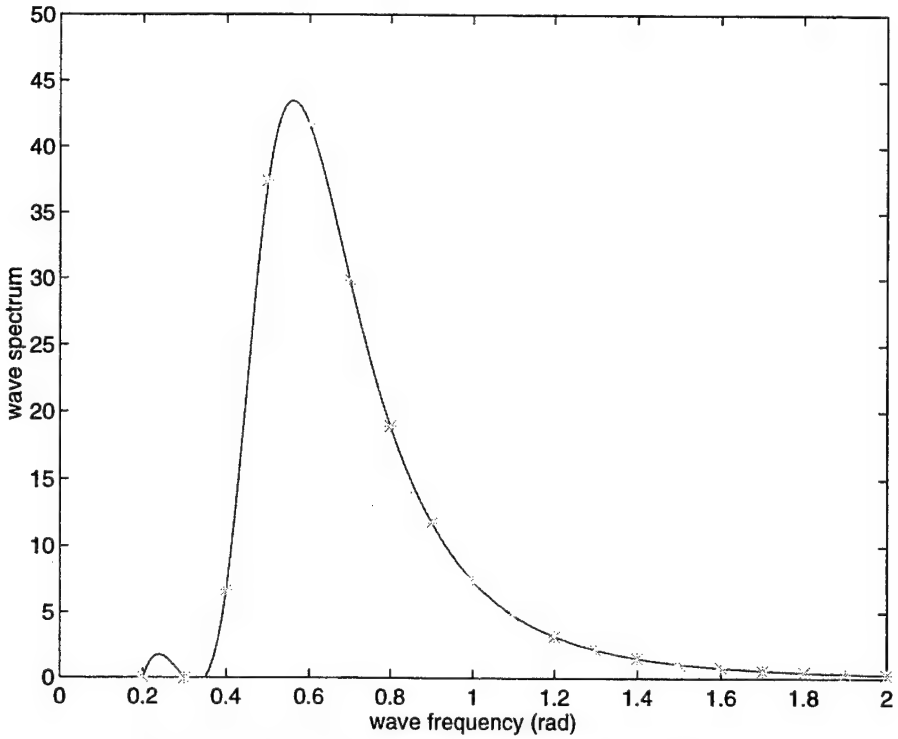

Figure 4. Typical Pierson-Moskowitz wave spectra

Any conclusions drawn on the seakeeping behavior of a ship based on the critical examination of motion response in regular waves can, at best, assume only academic significance. The establishment of the seakeeping behavior of a ship has to be done in a realistic seaway. With the spectral description of sea waves given before, we can return to the subject of body motions and generalize the results of regular harmonic waves. If the sea waves are described by the random distribution , and if the response of the body to each component wave is defined by a response amplitude operator $Z(\omega,\theta)$, the body response will be

$$\eta_j(t) = \Re\iint Z_j(\omega,\theta)e^{i\omega t}dA(\omega,\theta)\ . \qquad \textbf{(25)}$$

The principal assumption here is that linear superposition applies, as it must in any event for the underlying development of the RAO and the spectrum.

Like the waves themselves, the response (25) is a random variable. The statistic of the body response are identical to the wave statistics, except that the wave energy spectrum S is multiplied by the square of the RAO (this is a property of linear systems). Thus, if the subscript R represents any body response, we have

$$S_R(\omega) = |Z_R(\omega)|^2 S(\omega) \ , \qquad \textbf{(26)}$$

where $Z_R(\omega)$ is the RAO of the response R, and $S(\omega)$ the spectrum of the seaway. Equation (26) can then be utilized to obtain the spectrum of the response R. Figure 5 displays the spectrum of response of the relative vertical motion at the top of our model submarine's sail while submarine's forward speed is 5 Knots and it is at 3 submarine diameter depth. Also seaway is modeled by Pierson-Moskowitz spectrum with 5 m. significant wave height and head seas.

To a large extent, equation (26) provides the justification for studying regular wave responses. The transfer function $Z_R(\omega)$ is valid not only in regular waves, where it has been derived, but also in a superposition of regular waves, and ultimately in a spectrum of random waves. Generally speaking, a vessel with favorable response characteristics in regular waves will be good in irregular waves, and vice versa.

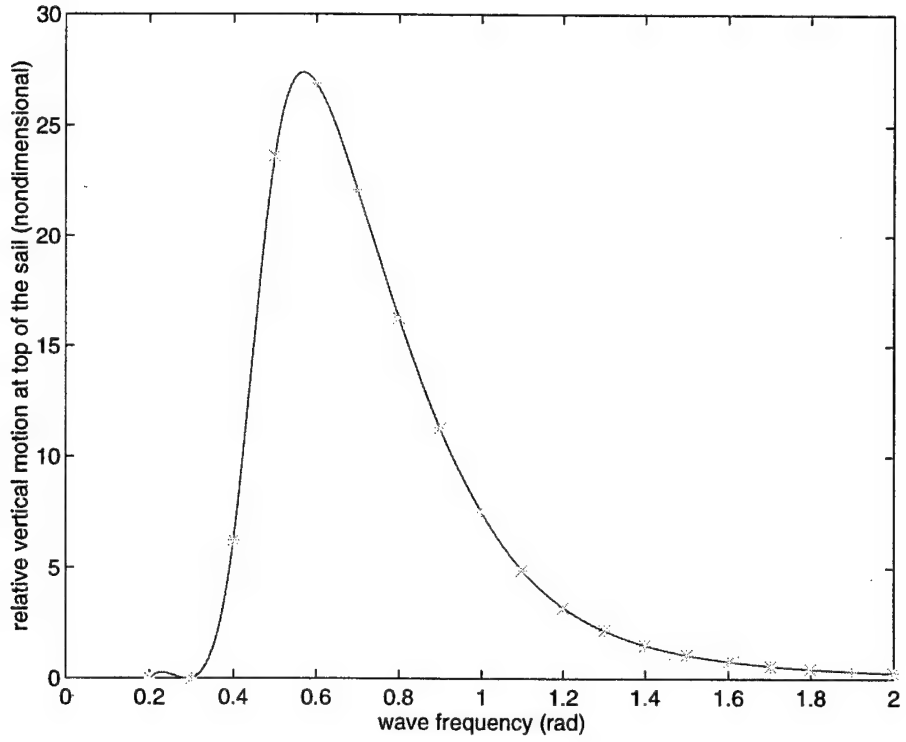

Figure 5. Spectrum of response for relative vertical motion

The average period between zero upcrossings was determined by equation (22), and the number between zero upcrossings per unit time is

$$N_z^R = \frac{1}{2\pi}\sqrt{\frac{m_2^R}{m_0^R}}\ , \tag{27}$$

where m_0^R, m_2^R are the moments of the particular response R, whose spectral density is given by equation (26). Equation (27) can be generalized for the case of the average number of upcrossings above a specified level α as in

$$N_{z,\alpha}^R = \frac{1}{2\pi}\sqrt{\frac{m_2^R}{m_0^R}}\exp\left(-\frac{\alpha^2}{2m_0^R}\right). \tag{28}$$

Equation (28) can be utilized to determine such events deck wetness and bow slamming for a surface ship or periscope submergence and sail broaching for a near surface

submarine. If f represents height of the periscope over calm sea surface level, the number of periscope submergence events per hour is

$$N_p = 3600\frac{1}{2\pi}\sqrt{\frac{m_2}{m_0}}\exp\left(-\frac{f^2}{2m_0}\right), \qquad \textbf{(29)}$$

where m_0 , m_2 are the moments of the vertical relative motion spectrum at periscope. The same equation can be used to estimate the frequency of sail broaching, with f substituted by the distance between top of the sail and encountered wave surface. Of course, m_0 , m_2 are now the moments of the relative motion spectrum at top of the sail. When we calculate the frequency of vehicle collision with the sea-bed for shallow water operations this time m_0 , m_2 are the moments of the absolute motion spectrum at either the bow or the stern of the submarine and f is its clearance from the sea-bed.

III. DEEP WATER RESULTS

A. OPERABILITY INDEX

As we mentioned in the first chapter in this study we considered two criteria when the submarine conducts near surface operations in deep water. One is the number of periscope submergence events per hour, which we can calculate with Equation (29) This number (N_{p1}) was selected as 300, which corresponds to five periscope submergence events per minute. This is an arbitrary number and different numbers could be picked for different operational considerations. Since the same number was used for all cases, the results presented here are representative for all possible choices. The other criterion is the number of sail broachings per hour, which is also calculated from Equation (29). This number (N_{p2}) was selected as one. This places far greater emphasis on sail broaching than periscope submergence since sail broaching is closely related to visual detection.

Now we have the tools to compute the two performance indices defined above in a given seaway. Suppose that the submarine conducts periscope depth operation in a seaway characterized by a significant wave height (Pierson-Moskowitz Wave Spectrum), so that the sea spectrum is defined. For all round the clock boat headings relative to the predominant wave direction for which the operations are to be conducted, a polar plot diagram similar to the one in Figure 6 is prepared. Significant wave heights are represented along the radial direction of the polar plot. The shaded area in the plot shows wave height and wave direction combinations where the selected tactical assessment criterion is exceeded. Letting the polar area of the disk in Figure 6 be A_0 and the subset of

A_o within which the boat can conduct the operation be A, a performance index characterizing the ability of the boat perform this operation in the specified submarine velocity and depth can be defined as $100(A/A_o)$. Generally a submarine's forward speed ranges from three to twelve knots in periscope depth operations. We used three, five, eight and eleven knots submarine forward speeds, U, in our calculations. Depths, h, beneath the surface were selected from 2.5 to 5 boat diameters measured from the keel up. In computing the above index we could easily take into account the probability of occurrence of a particular sea state and wave heading angle in the area of interest by introducing appropriate weight factors. In this study we assumed that all possible sea-states and wave heading angles are equally probable. In the following sections we discuss the results for both criteria/operability indices and also for the combined criterion/operability index, where both criteria are taken into consideration at the same time.

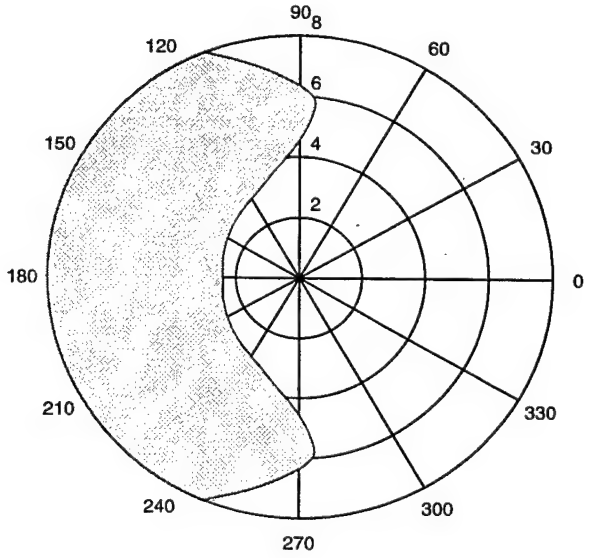

Figure 6. Typical performance assessment of a submarine

B. RESULTS OF PERISCOPE SUBMERGENCE CRITERION

We begin by presenting results with regards to periscope submergence criterion alone. Typical polar plots are shown in Figures 7 through 30. The operability index is presented for different speeds and operating depths in Figures 31 through 40. Based on these results we can draw the following general conclusions:

1. Head seas appear to result in a larger number of expected criterion violations than following seas. This is true regardless of the actual number used in establishing the criterion.
2. For a given sea direction it is possible to reduce criterion violations for higher sea states. This simply means that the motion point moves more in phase with the incoming waves. It should be emphasized, however, that at such high sea states the average wave height may exceed the exposed periscope length. Since the periscope moves in phase with the waves, the operator's visual horizon may be very small. This situation has been reported in practice and although the criterion is not exceeded, operations are very difficult to conduct. Such a situation can only be analyzed with proper visual simulation studies.
3. An optimum operating depth can be found which minimizes the expected number of periscope submergence events. This depth depends on the forward speed, but it appears to be a weak function of speed.

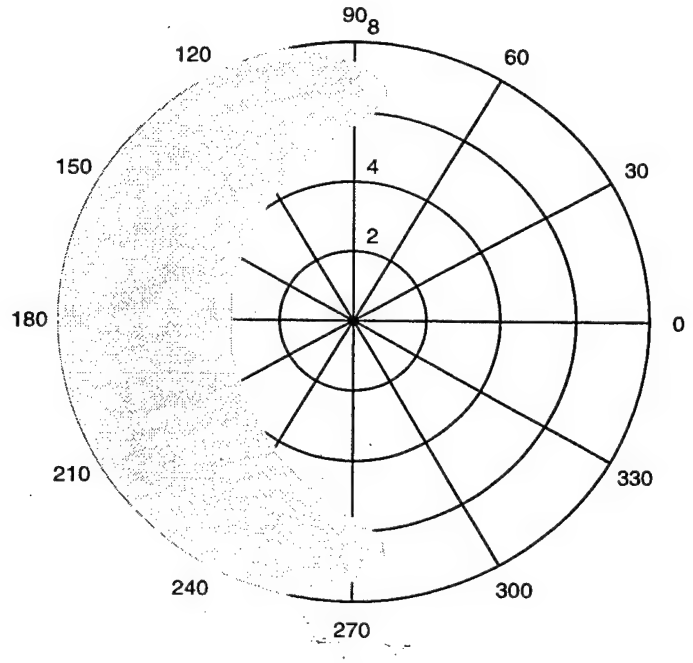

Figure 7. Sea state-polar plot, showing SOE for a submarine U=3 Knots, h=2.5D

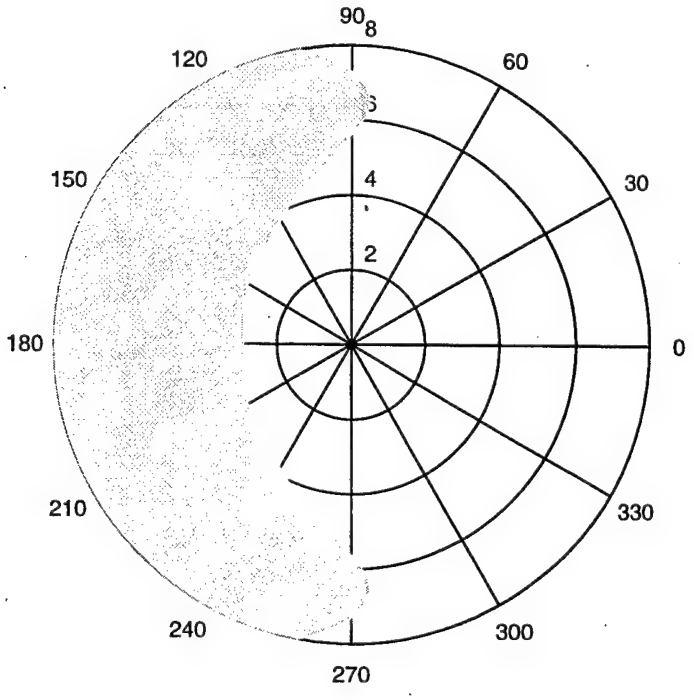

Figure 8. Sea state-polar plot, showing SOE for a submarine U=5 Knots, h=2.5D

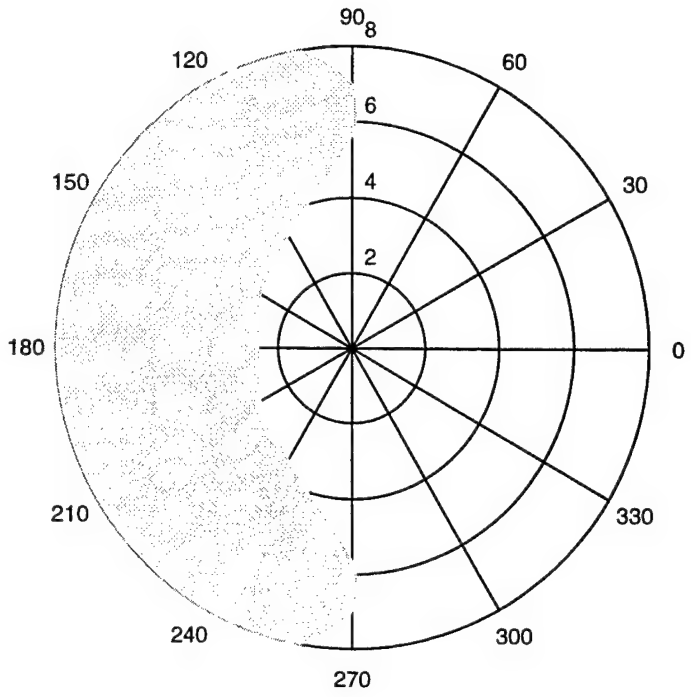

Figure 9. Sea state-polar plot, showing SOE for a submarine U=8 Knots, h=2.5D

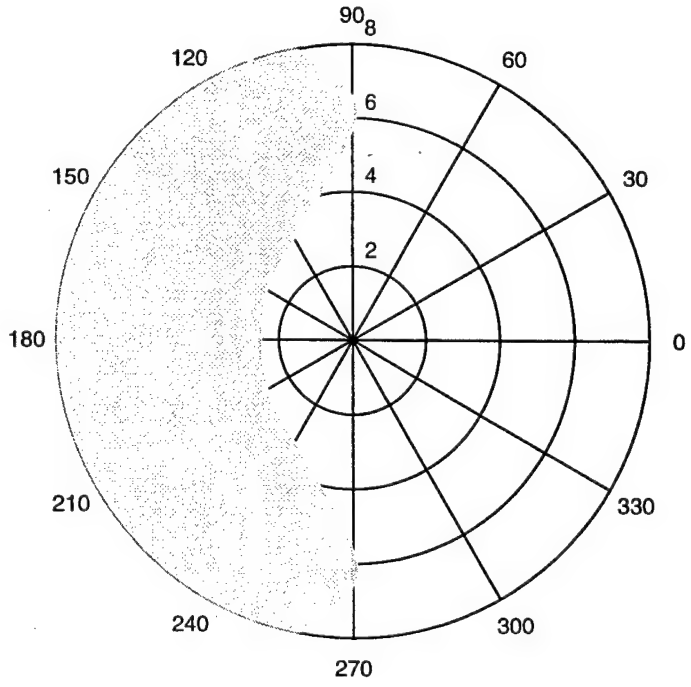

Figure 10. Sea state-polar plot, showing SOE for a submarine U=11 Knots, h=2.5D

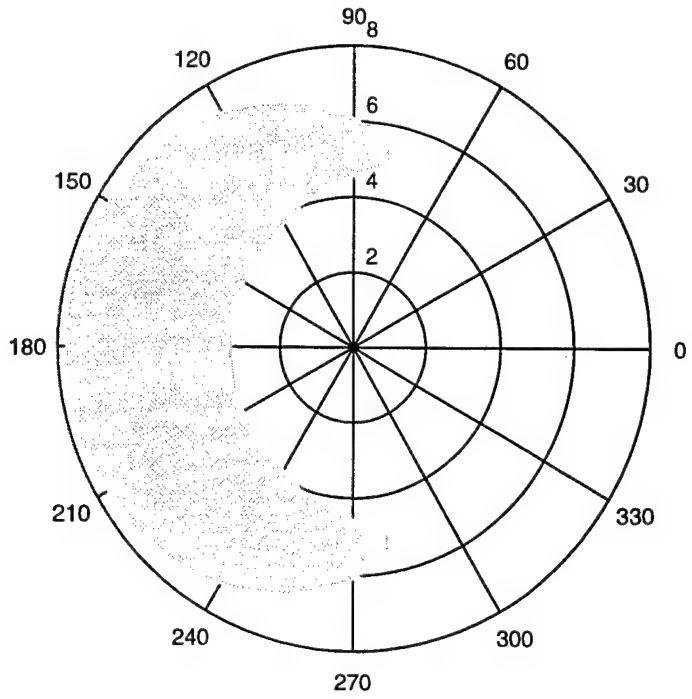

Figure 11. Sea state-polar plot, showing SOE for a submarine U=3 Knots, h=3D

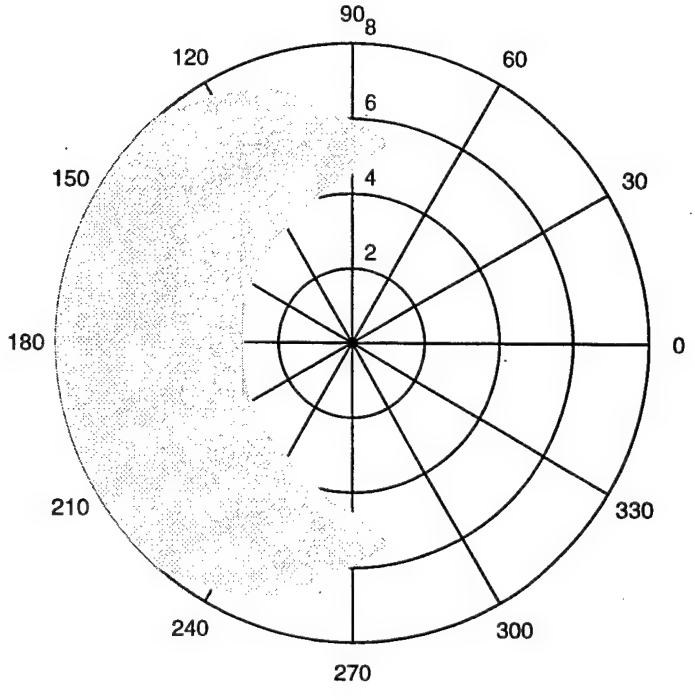

Figure 12. Sea state-polar plot, showing SOE for a submarine U=5 Knots, h=3D

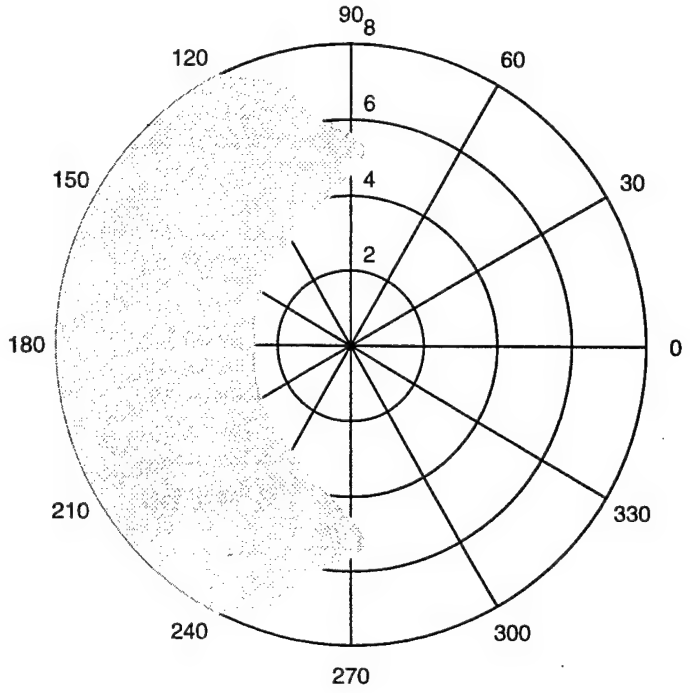

Figure 13. Sea state-polar plot, showing SOE for a submarine U=8 Knots, h=3D

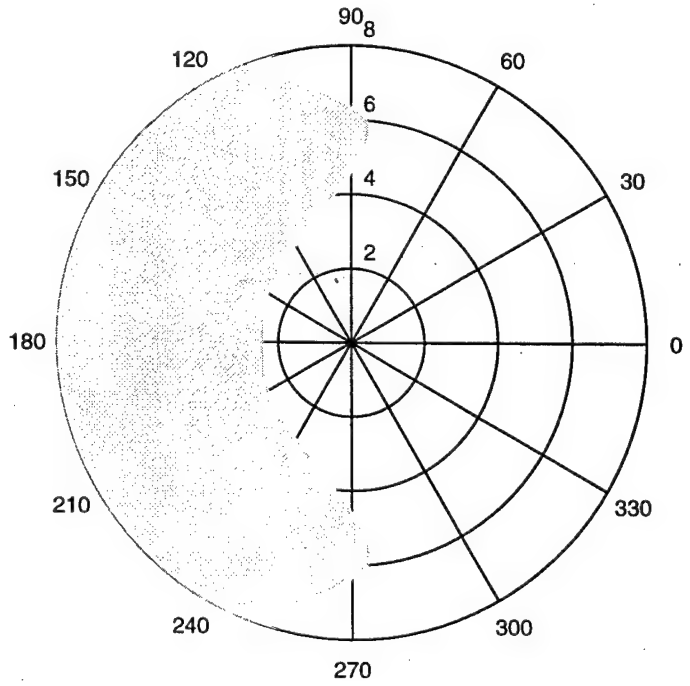

Figure 14. Sea state-polar plot, showing SOE for a submarine U=11 Knots, h=3D

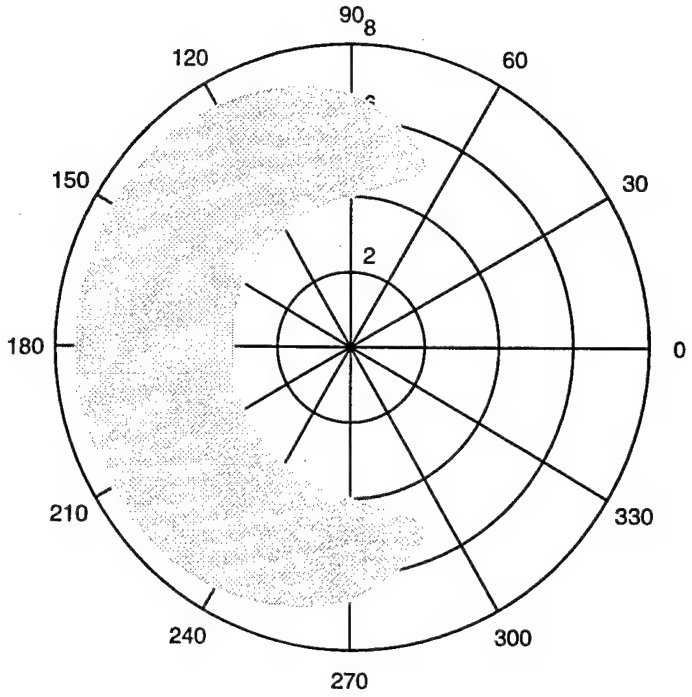

Figure 15. Sea state-polar plot, showing SOE for a submarine U=3 Knots, h=3.5D

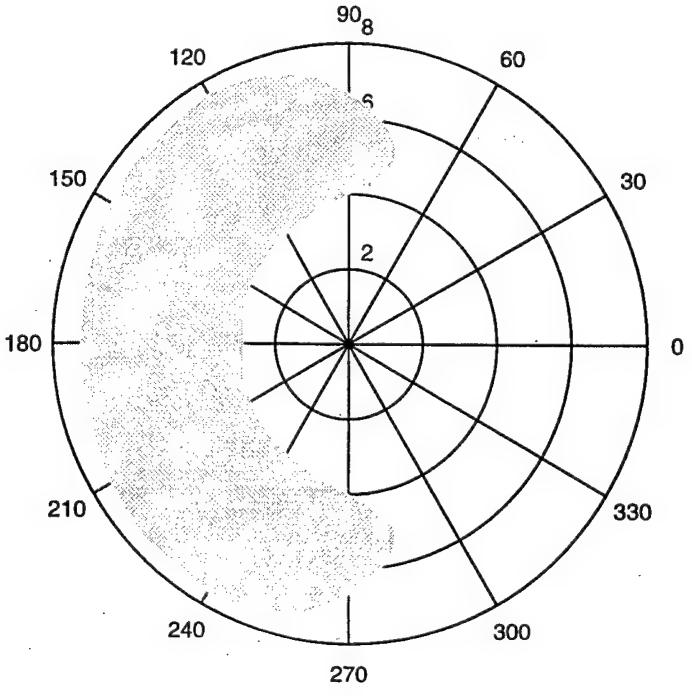

Figure 16. Sea state-polar plot, showing SOE for a submarine U=5 Knots, h=3.5D

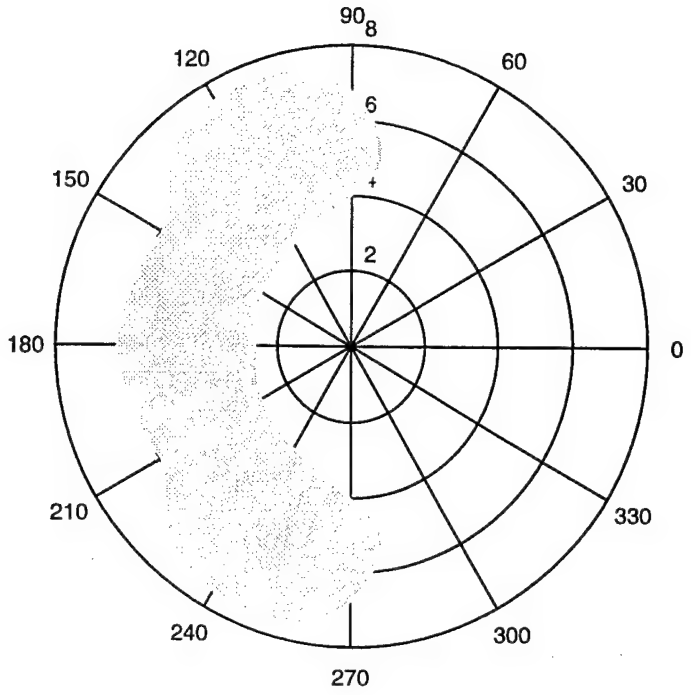

Figure 17. Sea state-polar plot, showing SOE for a submarine U=8 Knots, h=3.5D

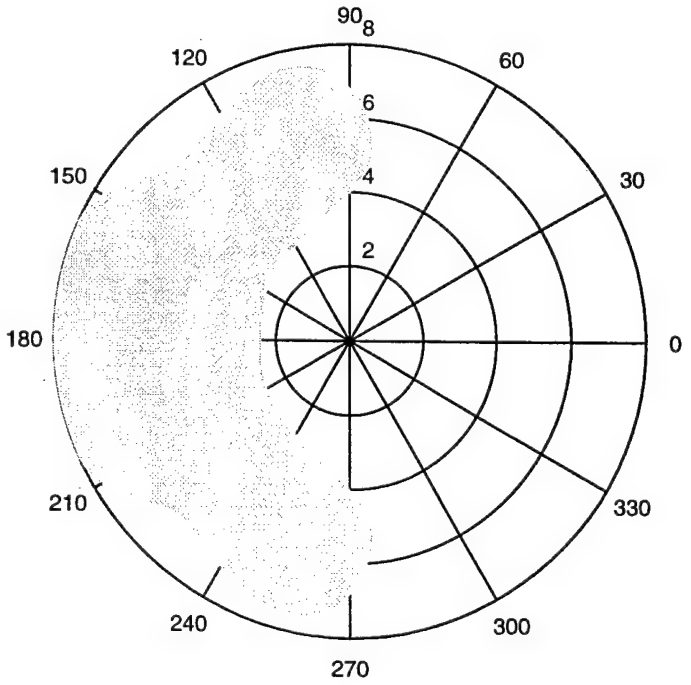

Figure 18. Sea state-polar plot, showing SOE for a submarine U=11 Knots, h=3.5D

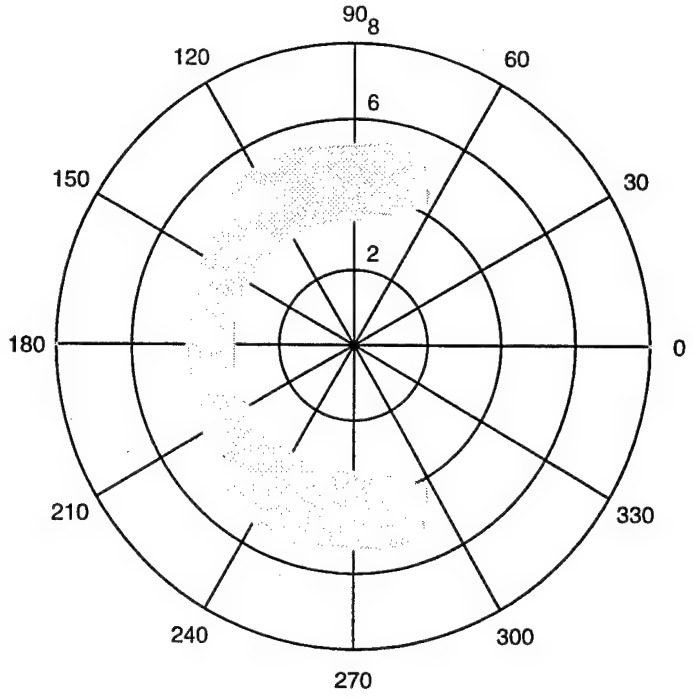

Figure 19. Sea state-polar plot, showing SOE for a submarine U=3 Knots, h=4D

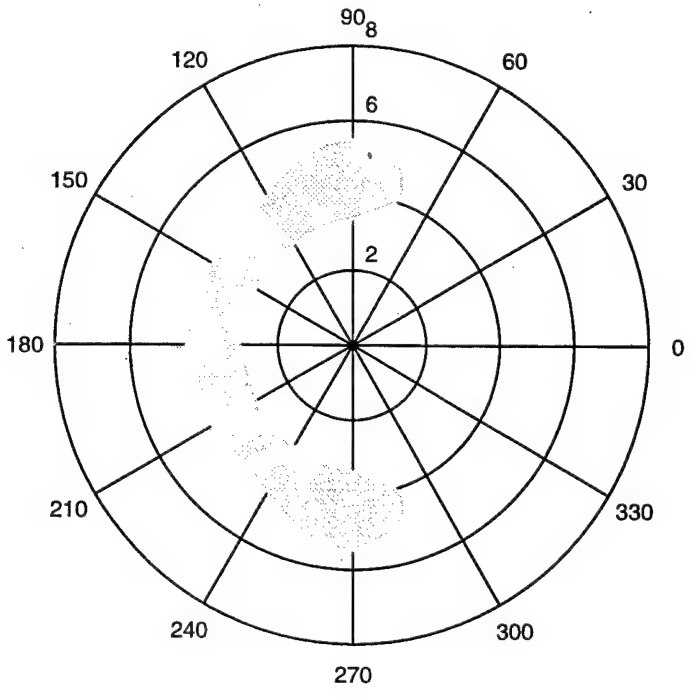

Figure 20. Sea state-polar plot, showing SOE for a submarine U=5 Knots, h=4D

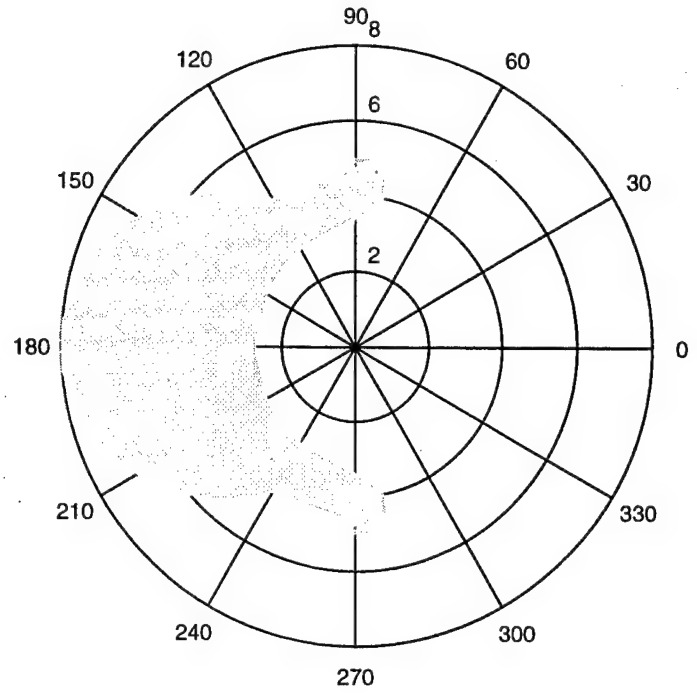

Figure 21. Sea state-polar plot, showing SOE for a submarine U=8 Knots, h=4D

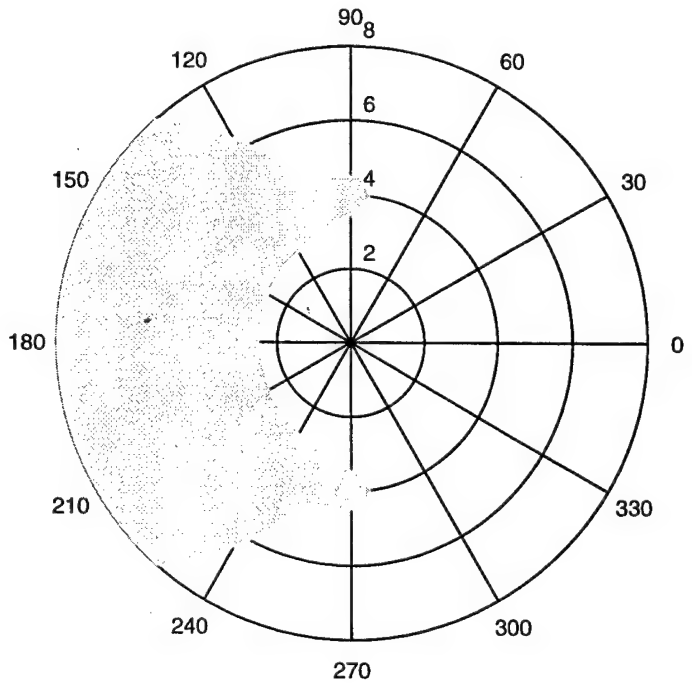

Figure 22. Sea state-polar plot, showing SOE for a submarine U=11 Knots, h=4D

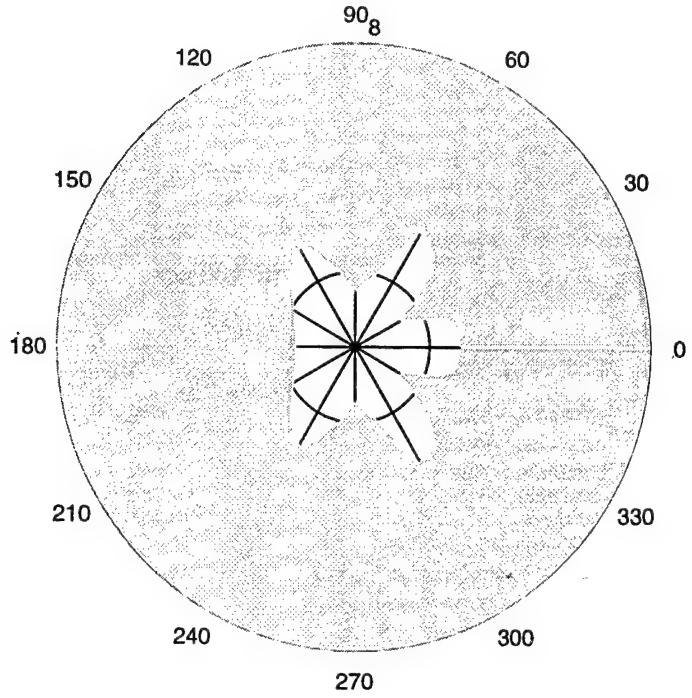

Figure 23. Sea state-polar plot, showing SOE for a submarine U=3 Knots, h=4.5D

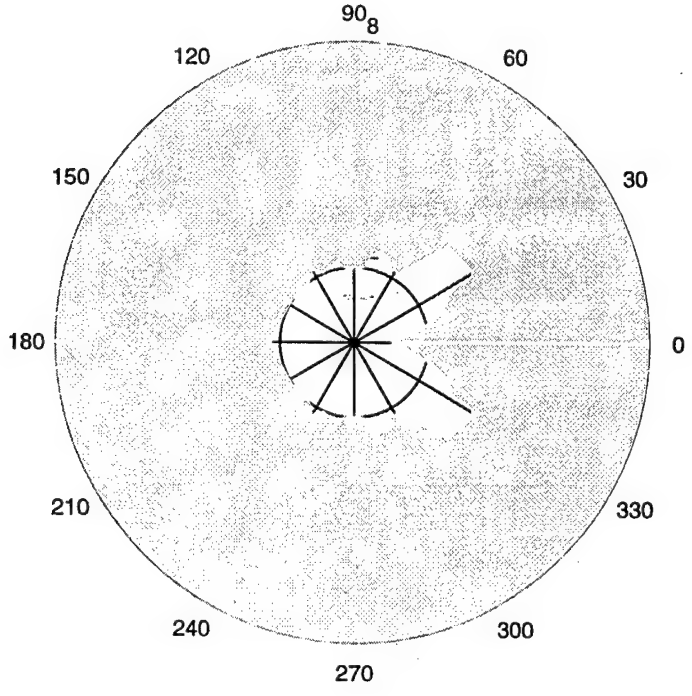

Figure 24. Sea state-polar plot, showing SOE for a submarine U=5 Knots, h=4.5D

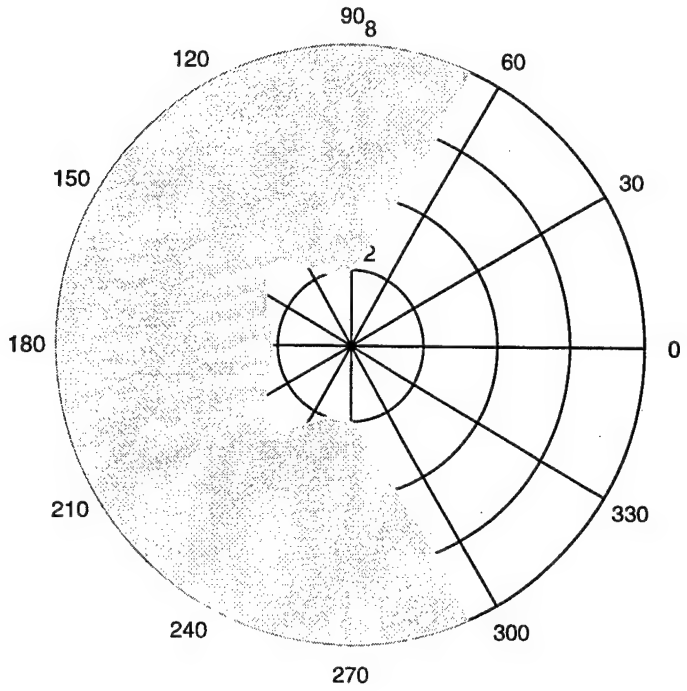

Figure 25. Sea state-polar plot, showing SOE for a submarine U=8 Knots, h=4.5D

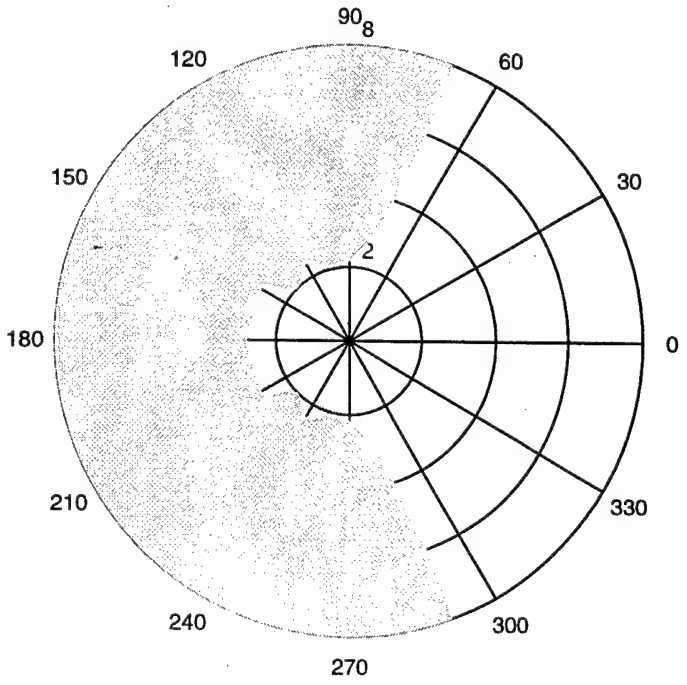

Figure 26. Sea state-polar plot, showing SOE for a submarine U=11 Knots, h=4.5D

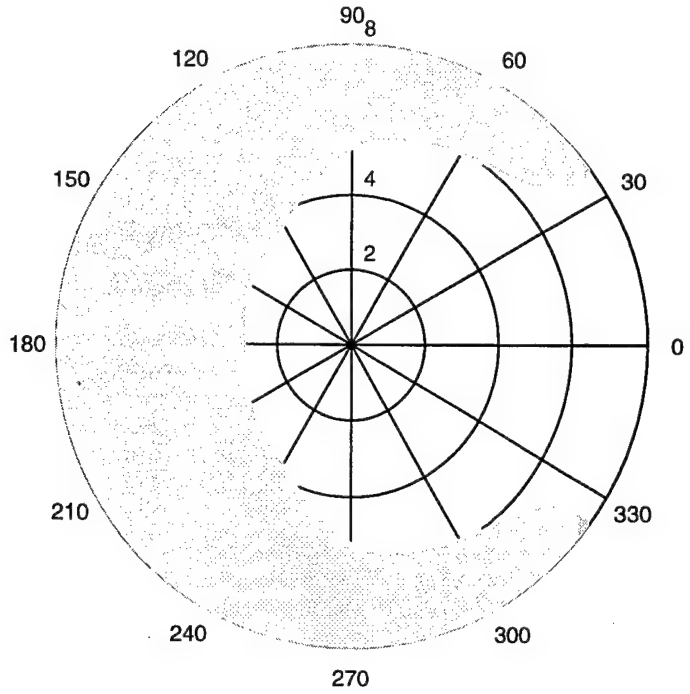

Figure 27. Sea state-polar plot, showing SOE for a submarine U=3 Knots, h=5D

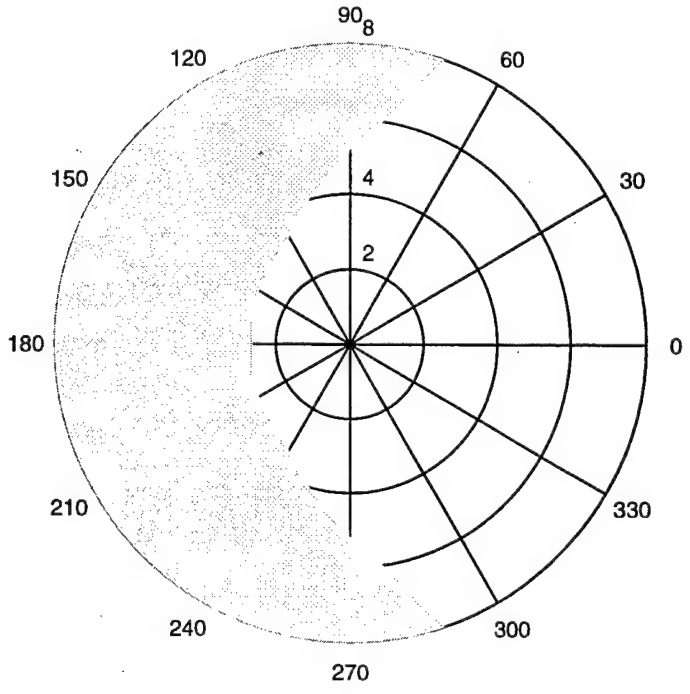

Figure 28. Sea state-polar plot, showing SOE for a submarine U=5 Knots, h=5D

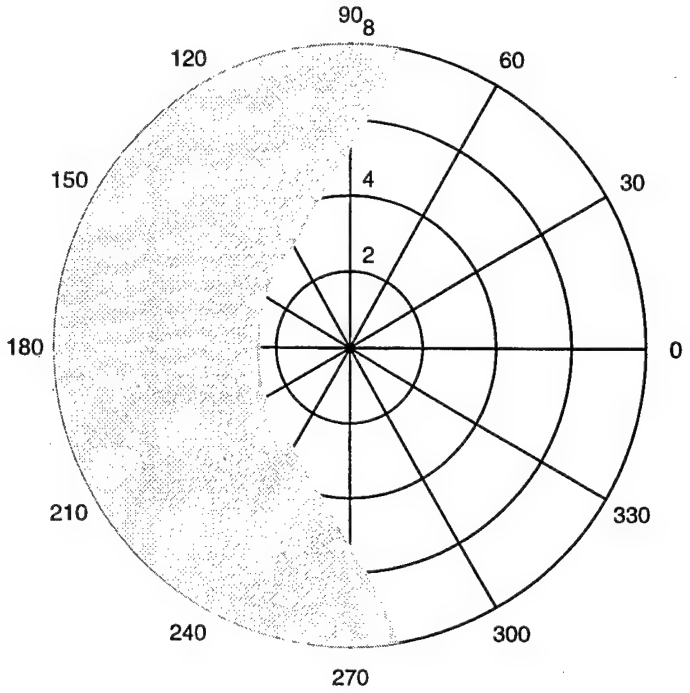

Figure 29. Sea state-polar plot, showing SOE for a submarine U=8 Knots, h=5D

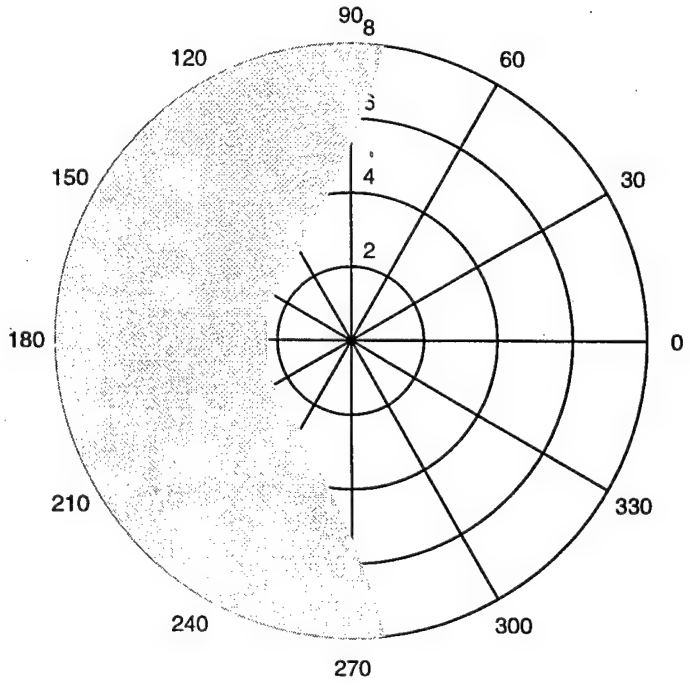

Figure 30. Sea state-polar plot, showing SOE for a submarine U=11 Knots, h=5D

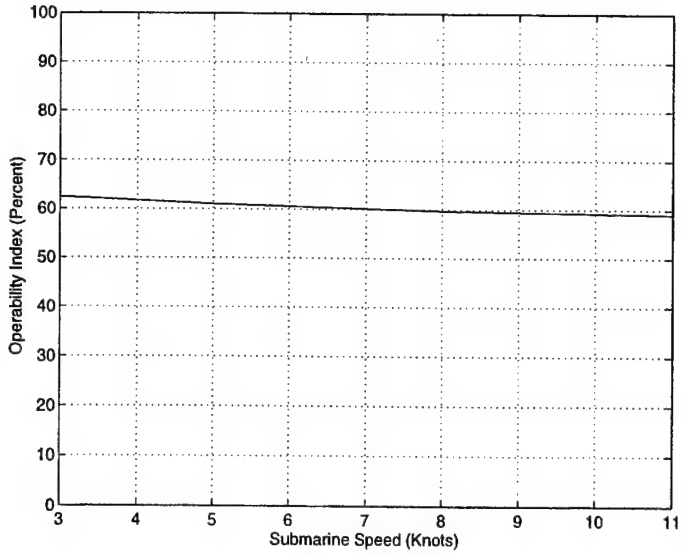

Figure 31. OI vs. Submarine Speed Plot at 2.5*D* depth

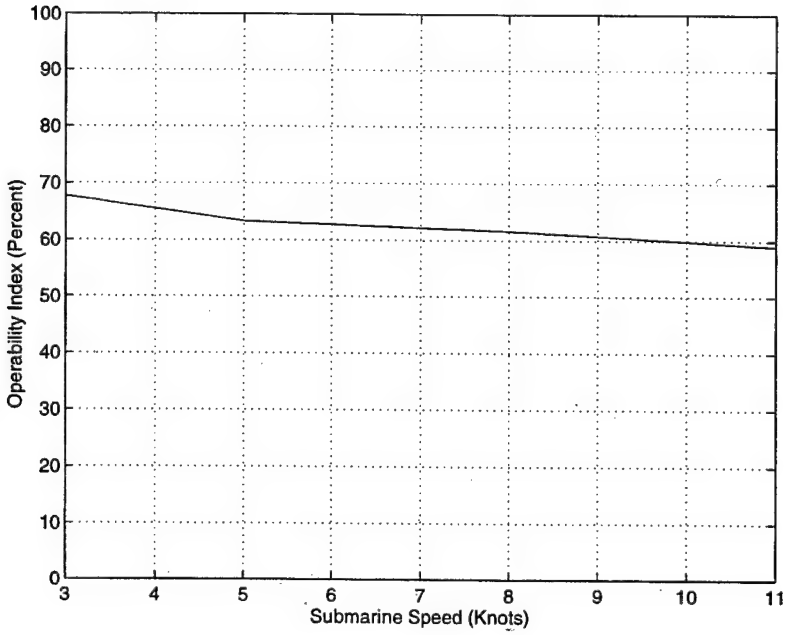

Figure 32. OI vs. Submarine Speed Plot at 3*D* depth

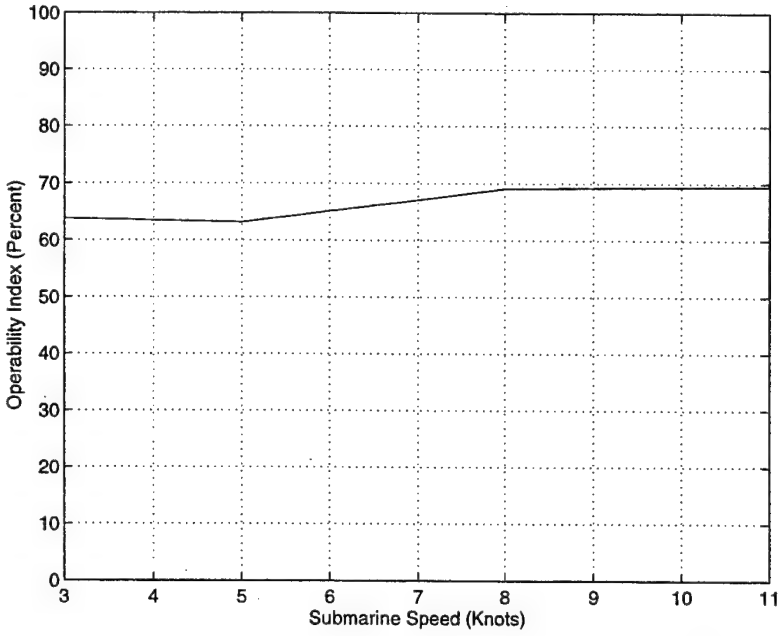

Figure 33. OI vs. Submarine Speed Plot at 3.5*D* depth

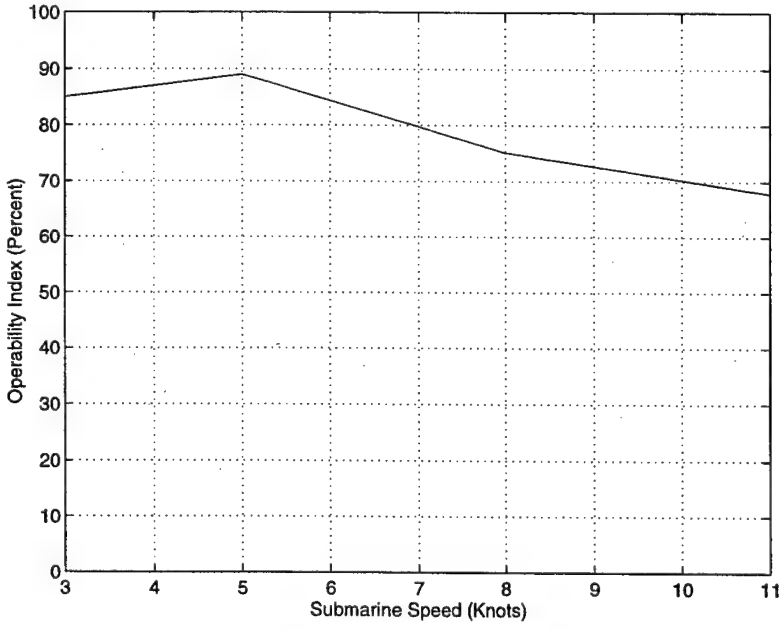

Figure 34. OI vs. Submarine Speed Plot at 4*D* depth

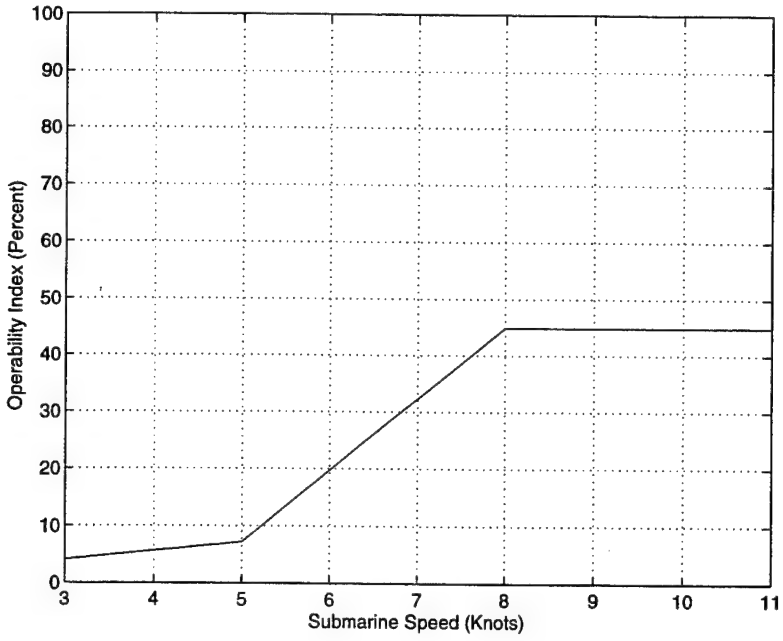

Figure 35. OI vs. Submarine Speed Plot at 4.5*D* depth

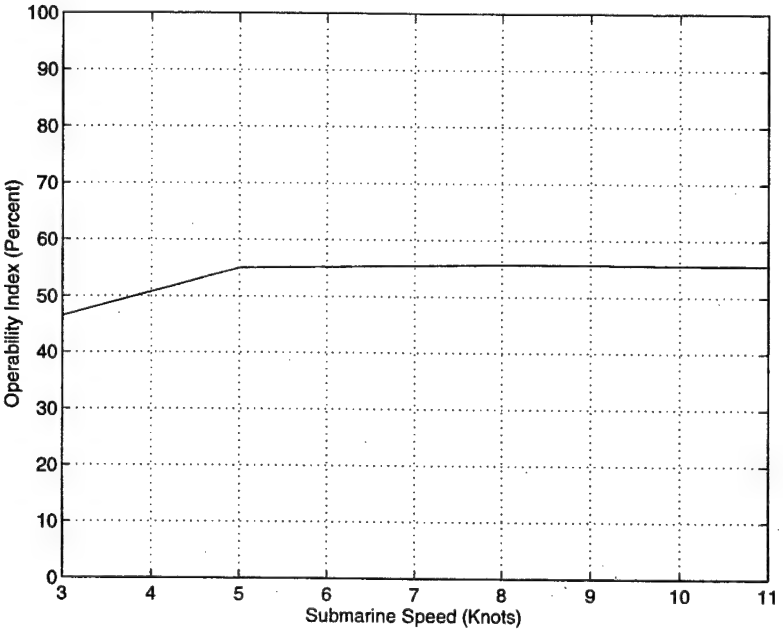

Figure 36. OI vs. Submarine Speed Plot at 5*D* depth

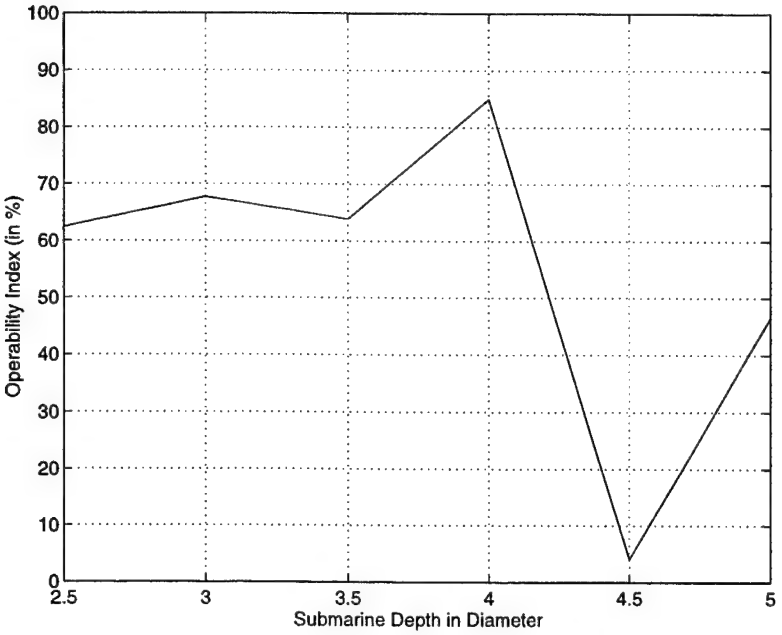

Figure 37. OI vs. Submarine Depth Plot in Submarine Diameters at 3 Knots

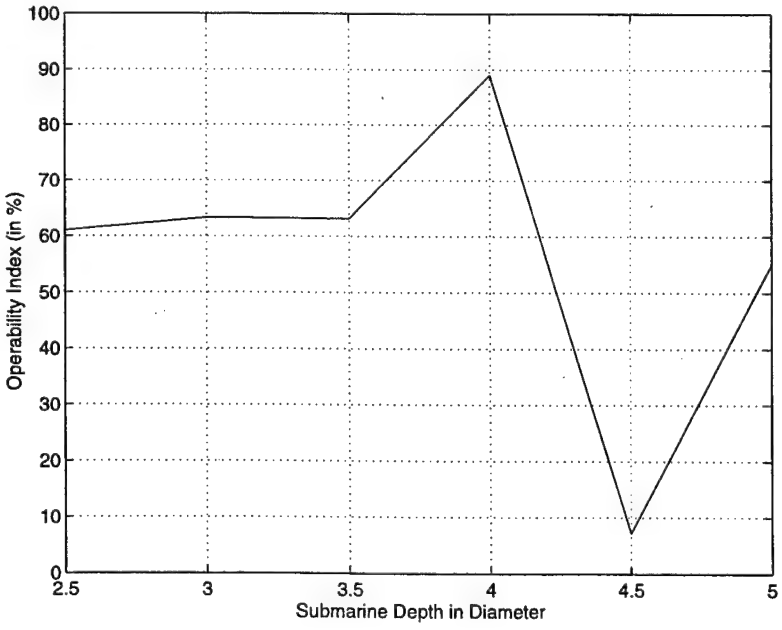

Figure 38. OI vs. Submarine Depth Plot in Submarine Diameters at 5 Knots

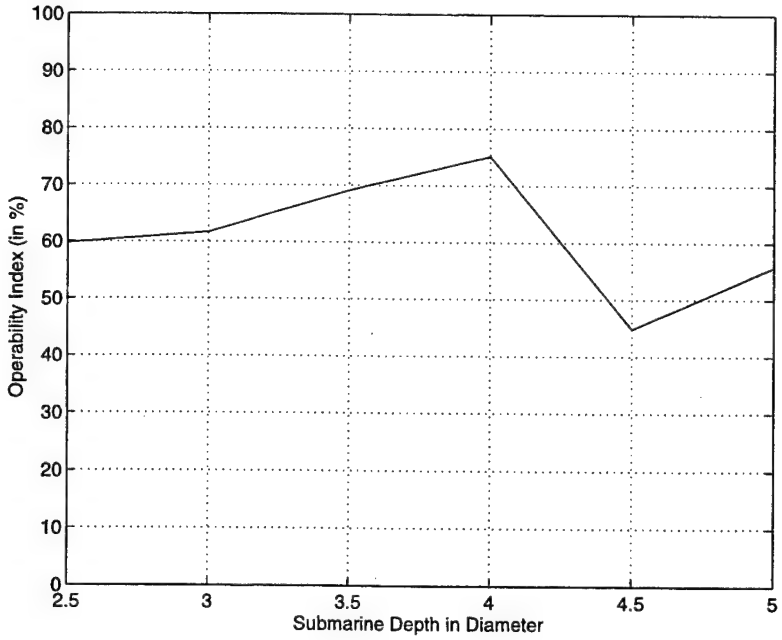

Figure 39. OI vs. Submarine Depth Plot in Submarine Diameters at 8 Knots

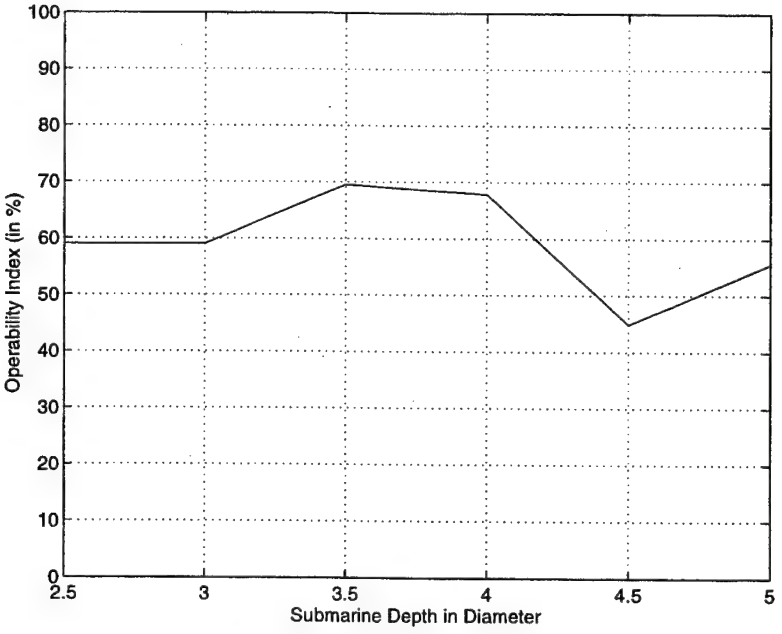

Figure 40. OI vs. Submarine Depth Plot in Submarine Diameters at 11 Knots

C. RESULTS OF SAIL BROACHING CRITERION

Typical polar plots for the sail broaching criterion event are shown in Figures 41 through 56. The operability index is presented for different speeds and operating depths in Figures 57 through 65. Based on these results we can draw the following general conclusions:

1. There does not appear to be a consistent dependence of the operability index on sea direction. Certain sea directions, however, greatly reduce the operability index for some speed/depth combinations.
2. For a given sea direction, higher sea states correspond to smaller operability indices.
3. The operability index does not vary significantly with speed or depth, and it generally increases with increasing depth..

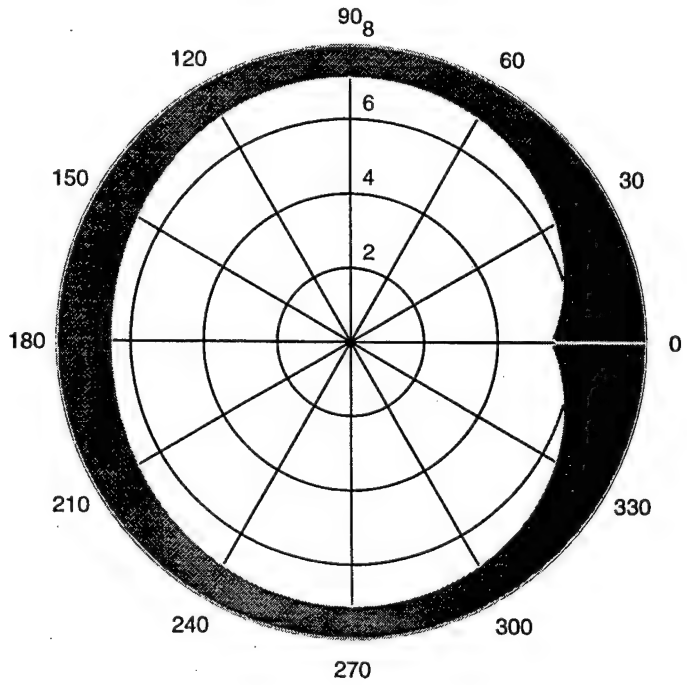

Figure 41. Sea state-polar plot, showing SOE for a submarine U=3 Knots, h=2.5D

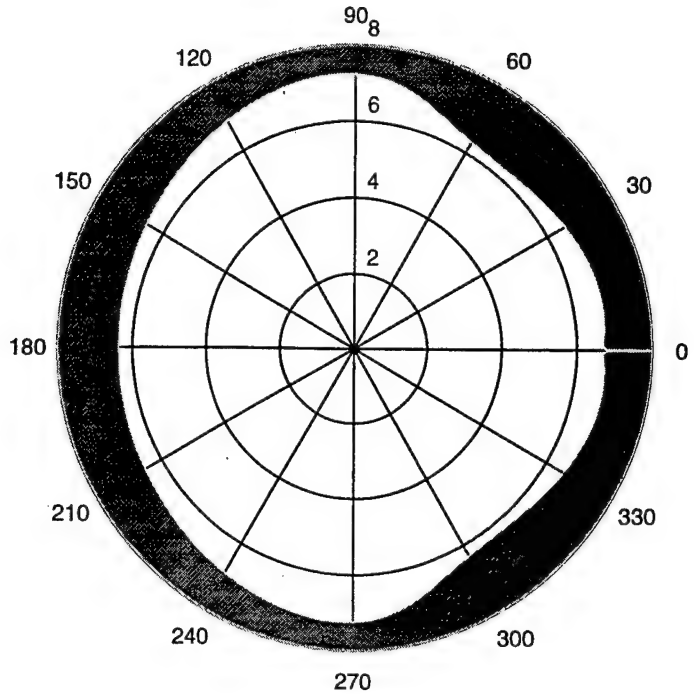

Figure 42. Sea state-polar plot, showing SOE for a submarine U=5 Knots, h=2.5D

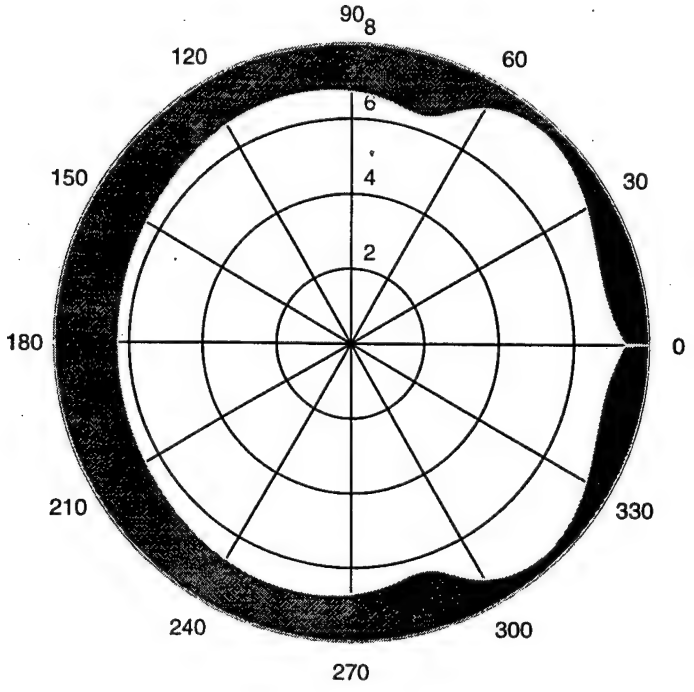

Figure 43. Sea state-polar plot, showing SOE for a submarine U=8 Knots, h=2.5D

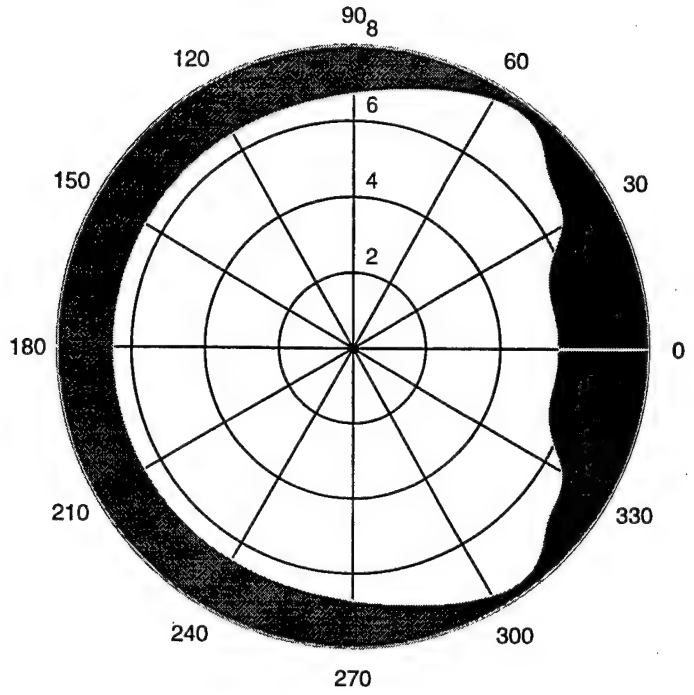

Figure 44. Sea state-polar plot, showing SOE for a submarine U=11 Knots, h=2.5D

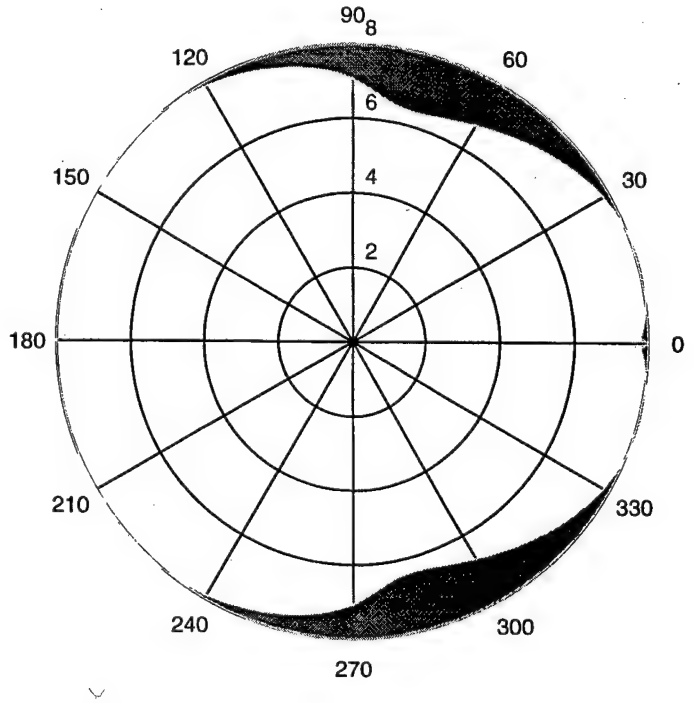

Figure 45. Sea state-polar plot, showing SOE for a submarine U=3 Knots, h=3D

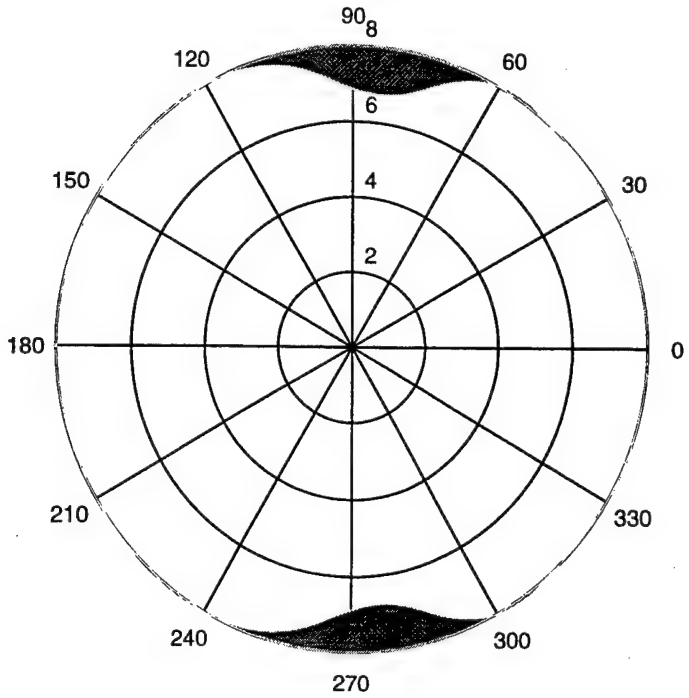

Figure 46. Sea state-polar plot, showing SOE for a submarine U=5 Knots, h=3D

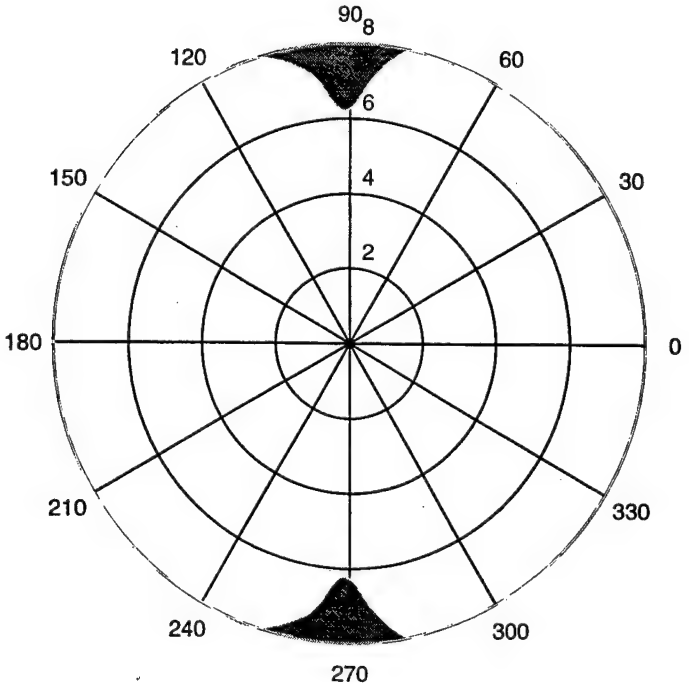

Figure 47. Sea state-polar plot, showing SOE for a submarine U=8 Knots, h=3D

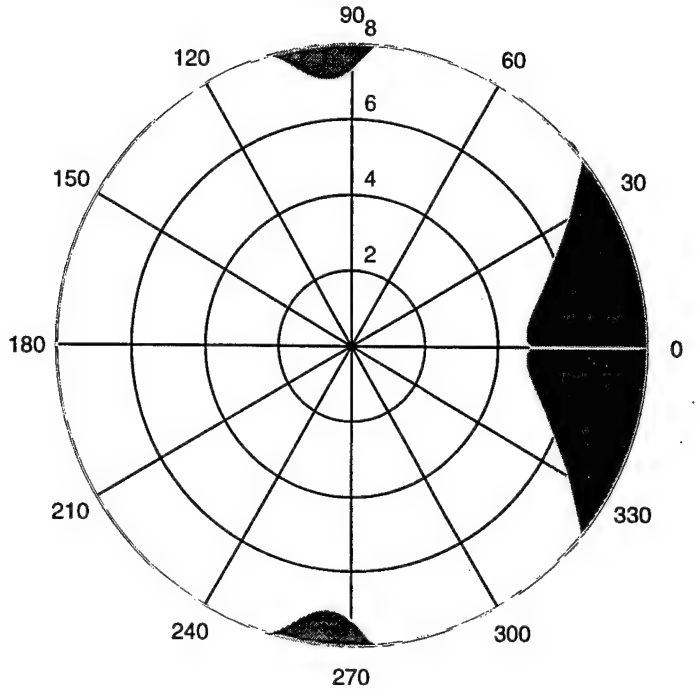

Figure 48. Sea state-polar plot, showing SOE for a submarine U=11 Knots, h=3D

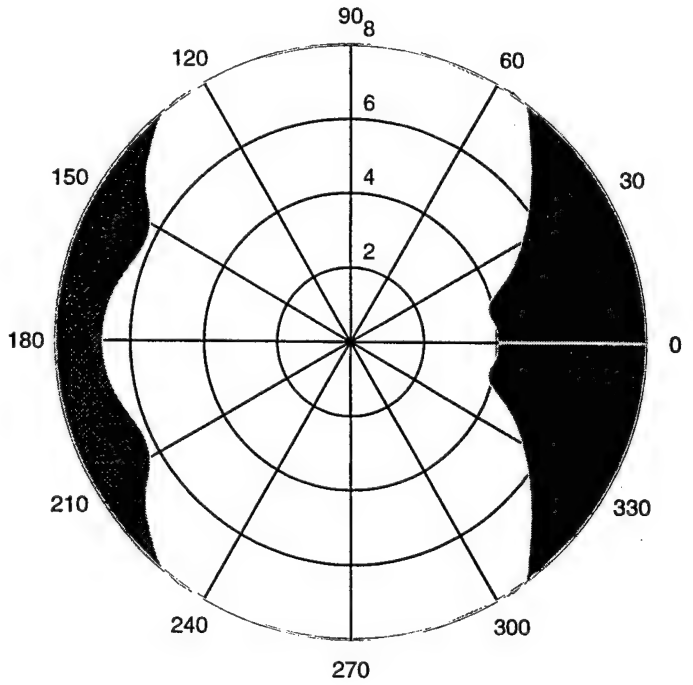

Figure 49. Sea state-polar plot, showing SOE for a submarine U=8 Knots, h=3.5D

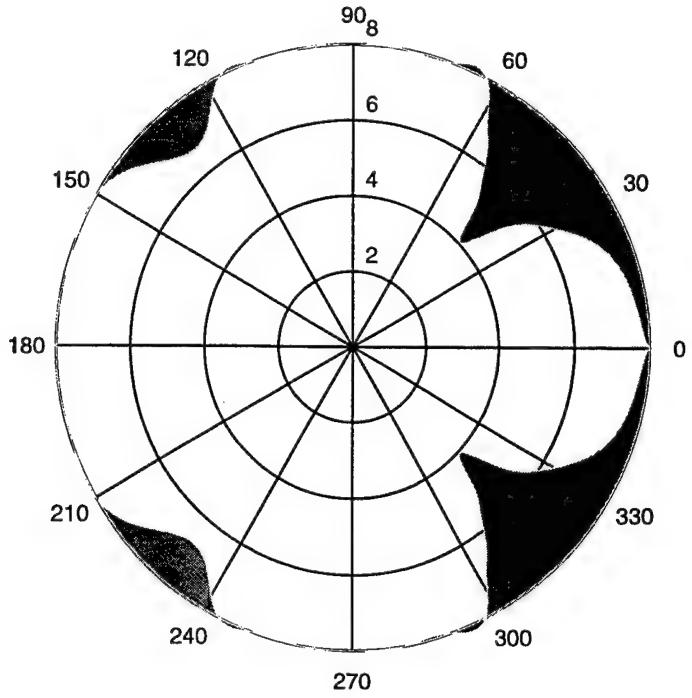

Figure 50. Sea state-polar plot, showing SOE for a submarine U=11 Knots, h=3.5D

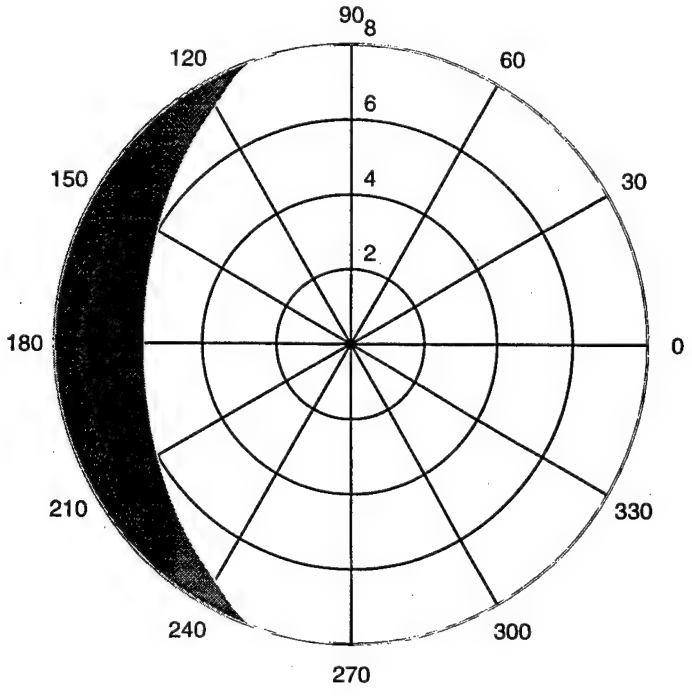

Figure 51. Sea state-polar plot, showing SOE for a submarine U=3 Knots, h=4D

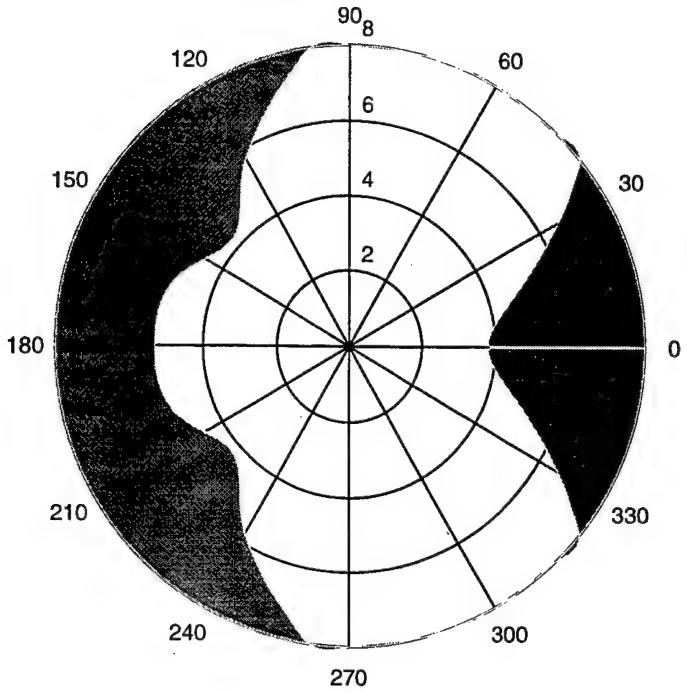

Figure 52. Sea state-polar plot, showing SOE for a submarine U=5 Knots, h=4D

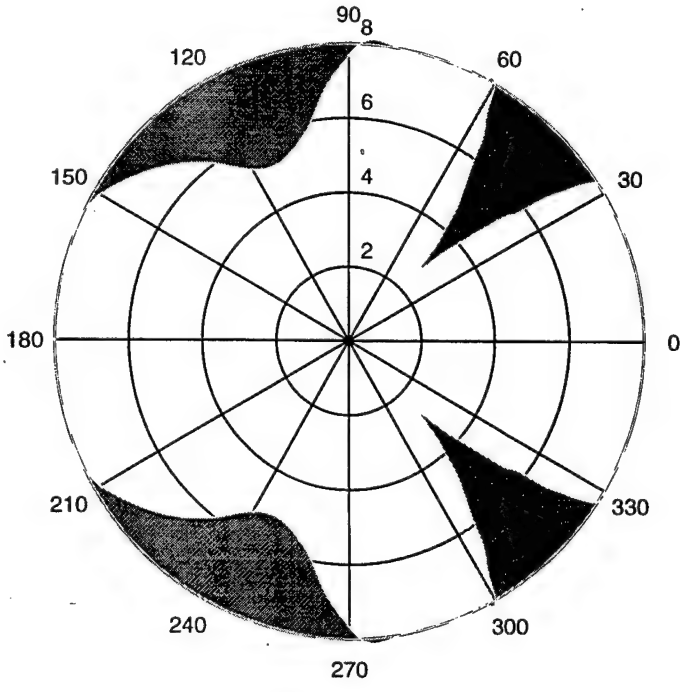

Figure 53. Sea state-polar plot, showing SOE for a submarine U=8 Knots, h=4D

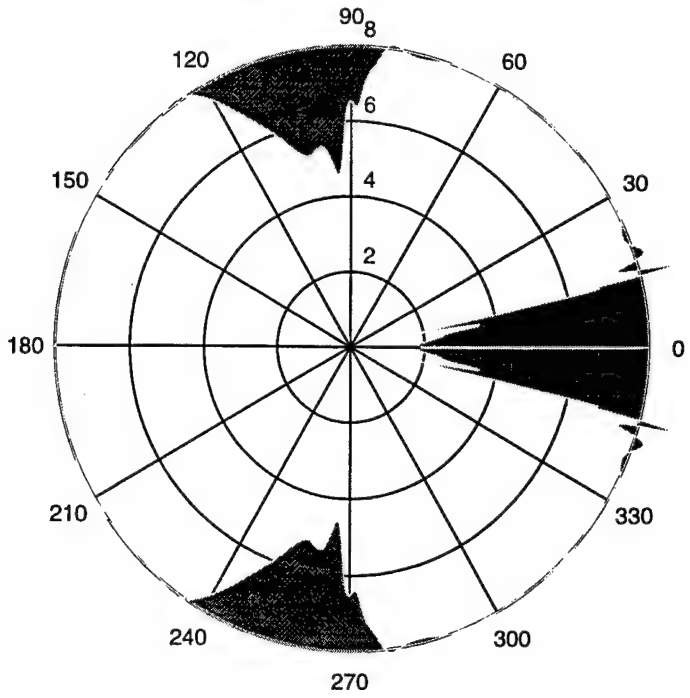

Figure 54. Sea state-polar plot, showing SOE for a submarine U=11 Knots, h=4D

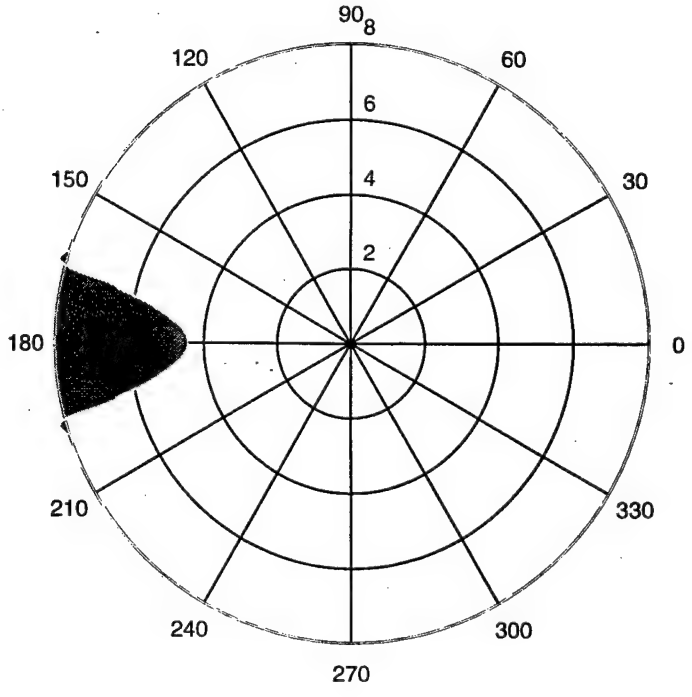

Figure 55. Sea state-polar plot, showing SOE for a submarine U=3 Knots, h=4.5D

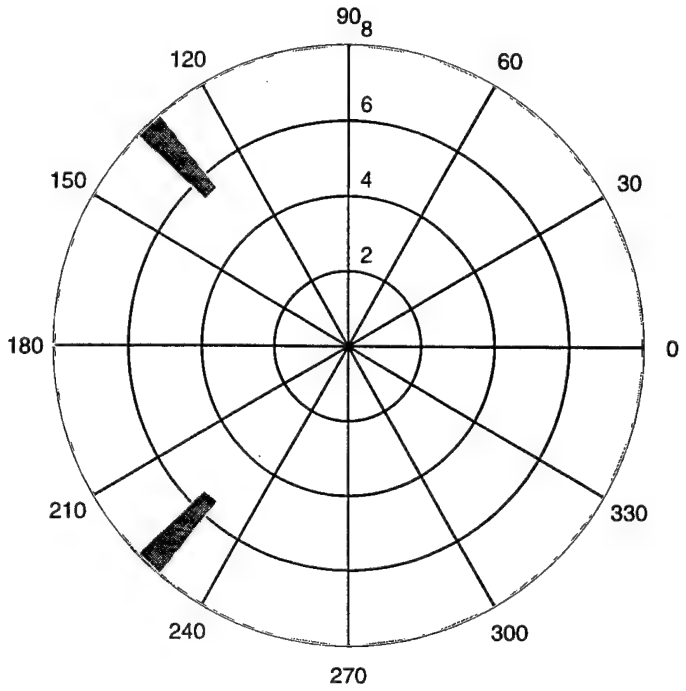

Figure 56. Sea state-polar plot, showing SOE for a submarine U=11 Knots, h=4.5D

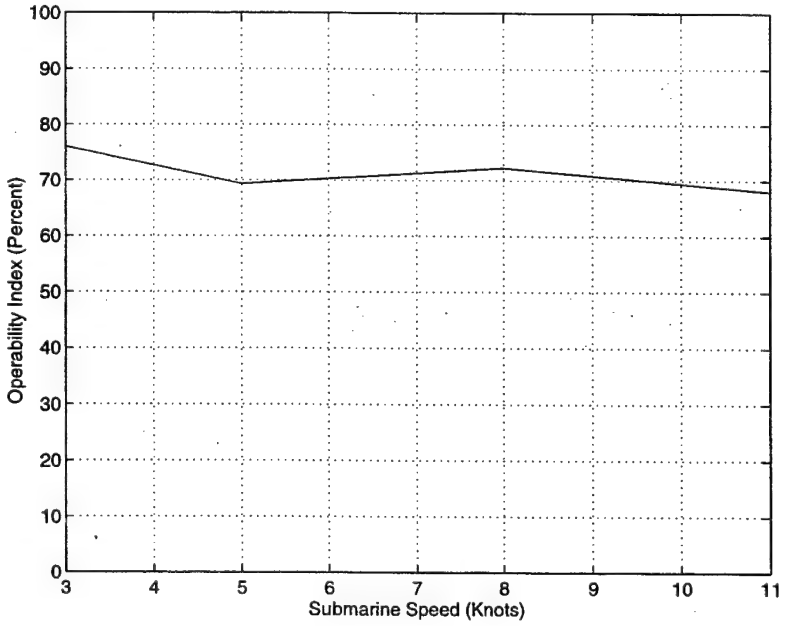

Figure 57. OI vs. Submarine Speed Plot at 2.5D depth

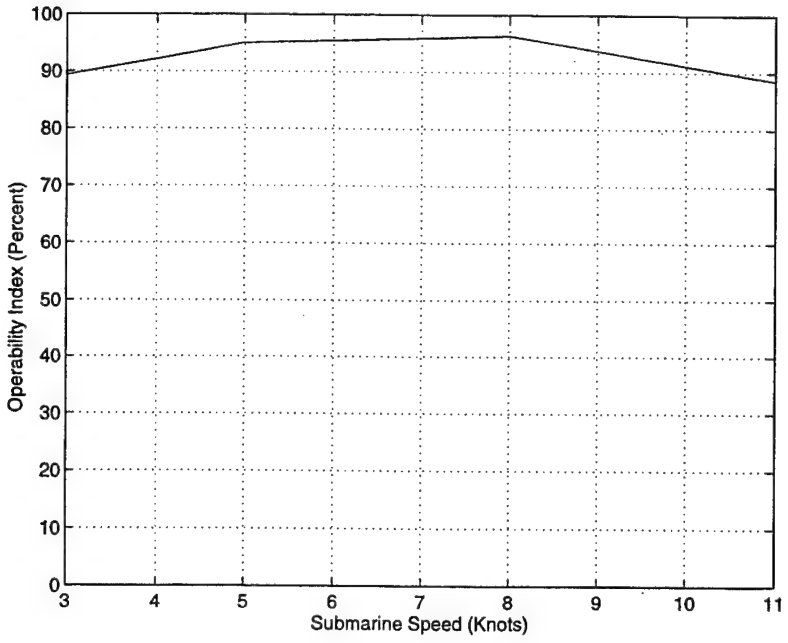

Figure 58. OI vs. Submarine Speed Plot at 3*D* depth

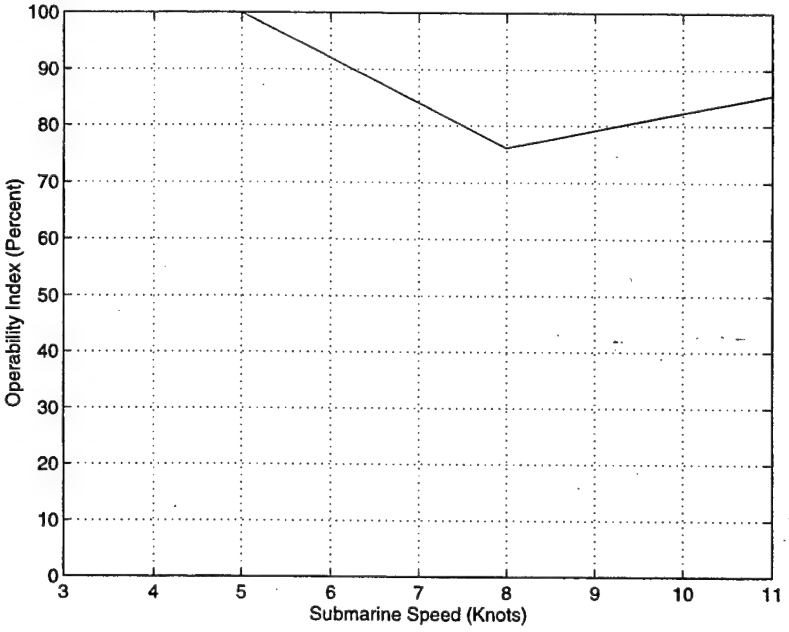

Figure 59. OI vs. Submarine Speed Plot at 3.5*D* depth

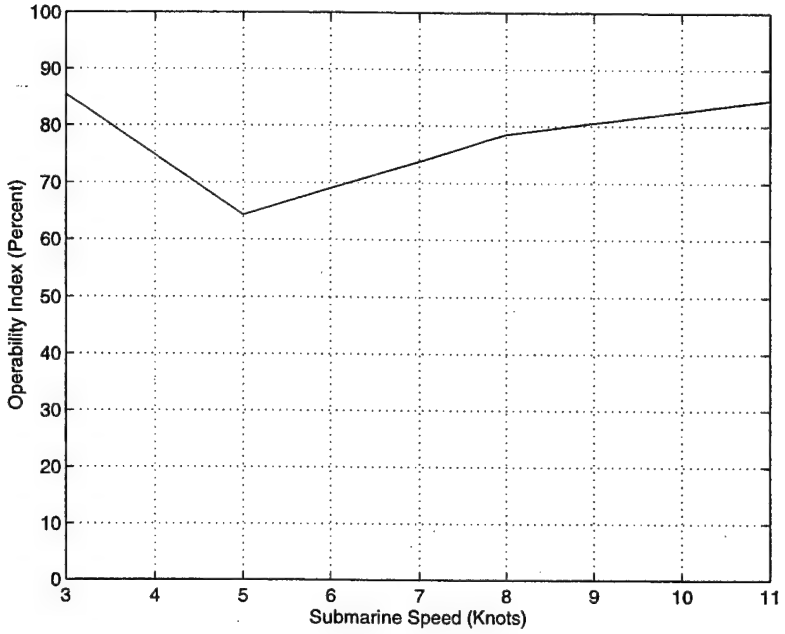

Figure 60. OI vs. Submarine Speed Plot at 4*D* depth

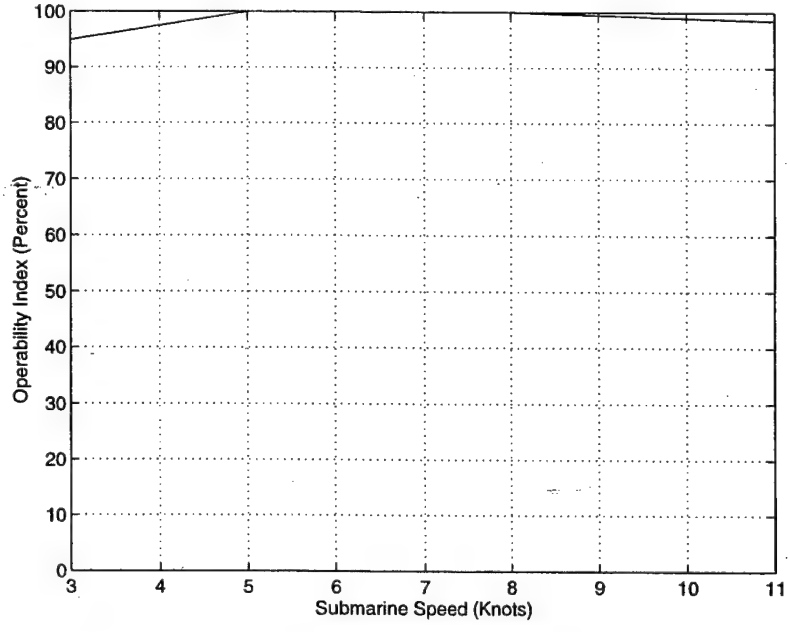

Figure 61. OI vs. Submarine Speed Plot at 4.5*D* depth

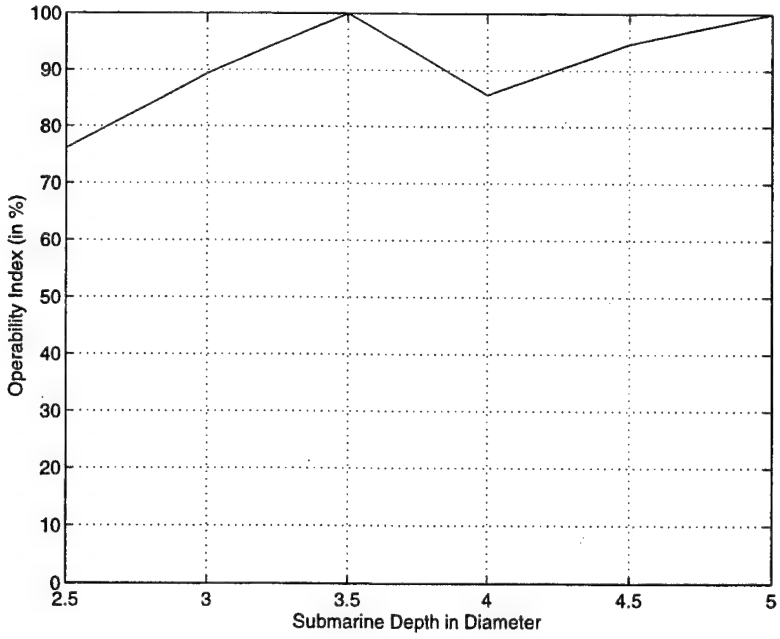

Figure 62. OI vs. Submarine Depth in Submarine Diameters at 3 Knots

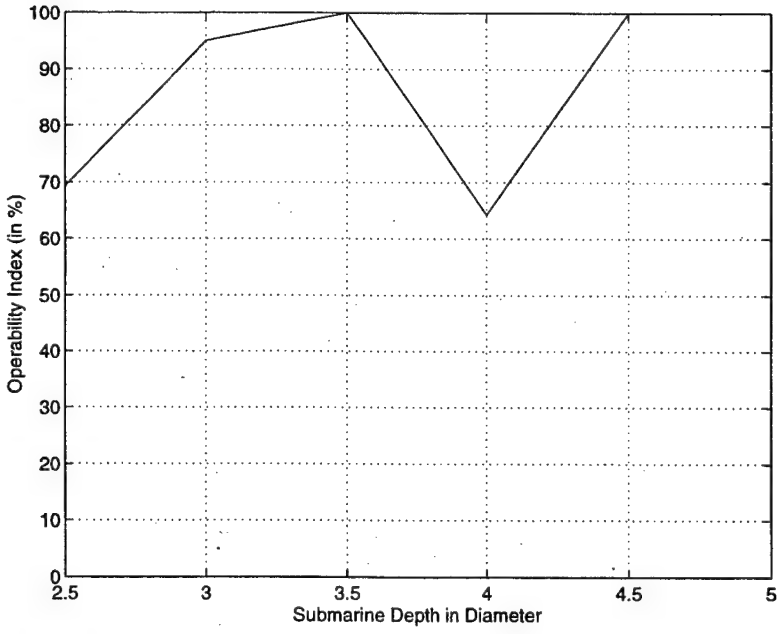

Figure 63. OI vs. Submarine Depth in Submarine Diameters at 5 Knots

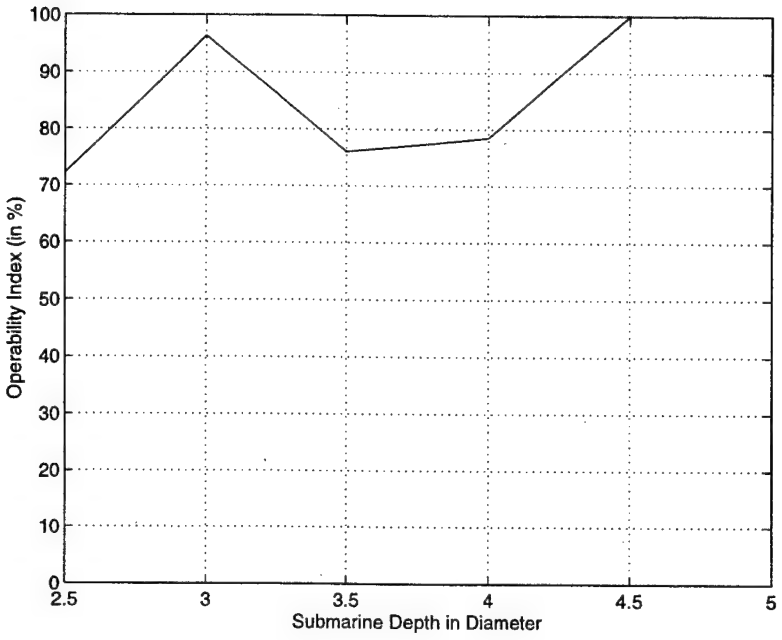

Figure 64. OI vs. Submarine Depth in Submarine Diameters at 8 Knots

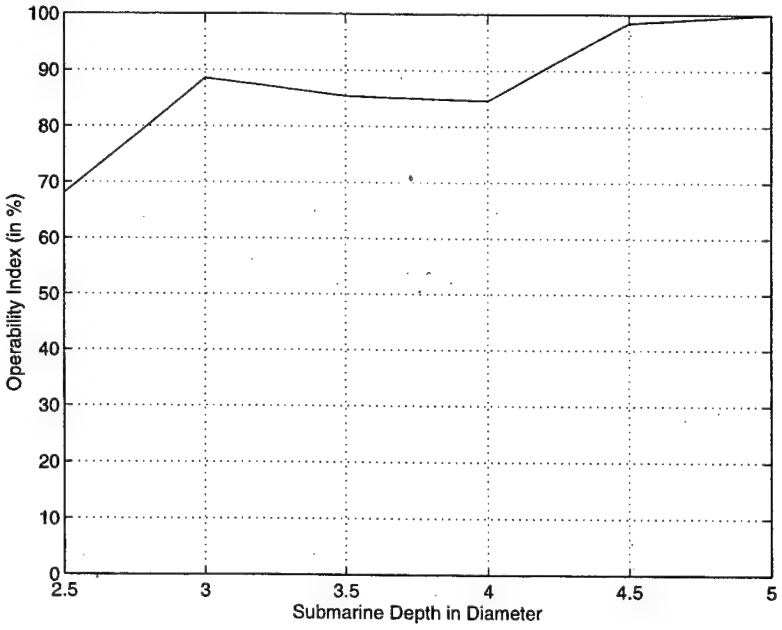

Figure 65. OI vs. Submarine Depth in Submarine Diameters at 11 Knots

D. RESULTS OF COMBINED CRITERIA

Results for both criteria combined are presented in Figures 66 through 99. The individual conclusions that were drawn previously continue to hold in this case as well. It appears that certain selections for speed and operating depth may result in higher values for the operability index. It should be mentioned, however, that this depends on the relative magnitude of the individual criteria, N_{p1} and N_{p2}. As an example, consider Figure 97. The overall operability index at 5 knots and depth 4.5 diameters appears to be less than 10%. As Figure 83 demonstrates, however, this is entirely due to the periscope submergence criterion violations. If this were of no concern in this case, the operability index would be raised to 100% as shown in Figure 61.

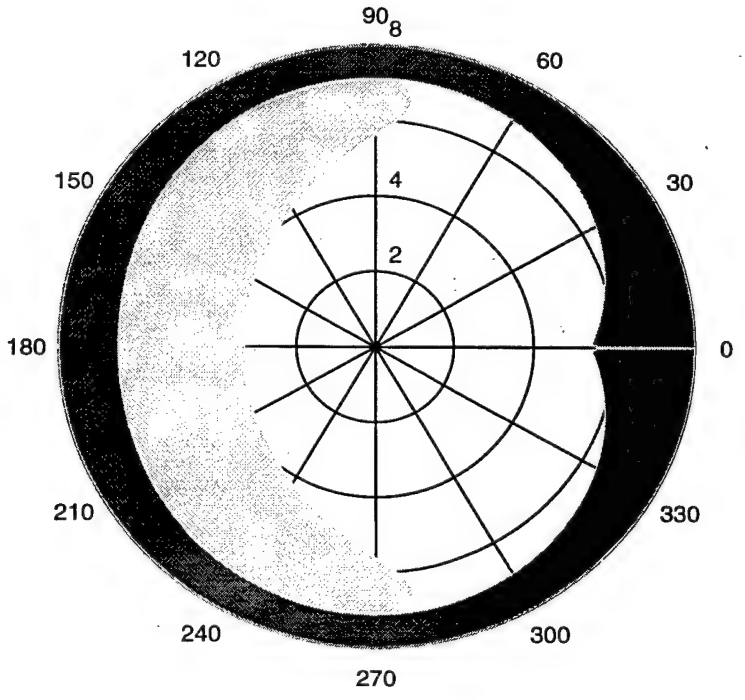

Figure 66. Sea state-polar plot, showing SOE for a submarine U=3 Knots, h=2.5D

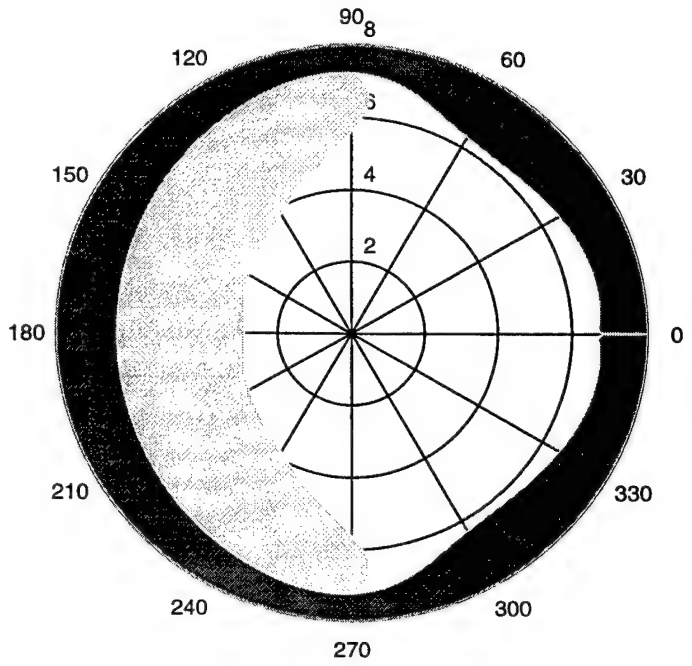

Figure 67. Sea state-polar plot, showing SOE for a submarine U=5 Knots, h=2.5D

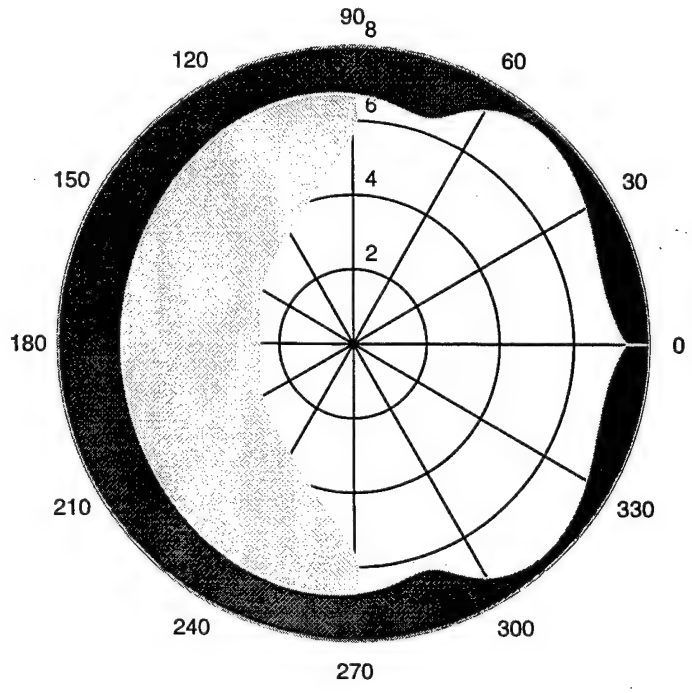

Figure 68. Sea state-polar plot, showing SOE for a submarine U=8 Knots, h=2.5D

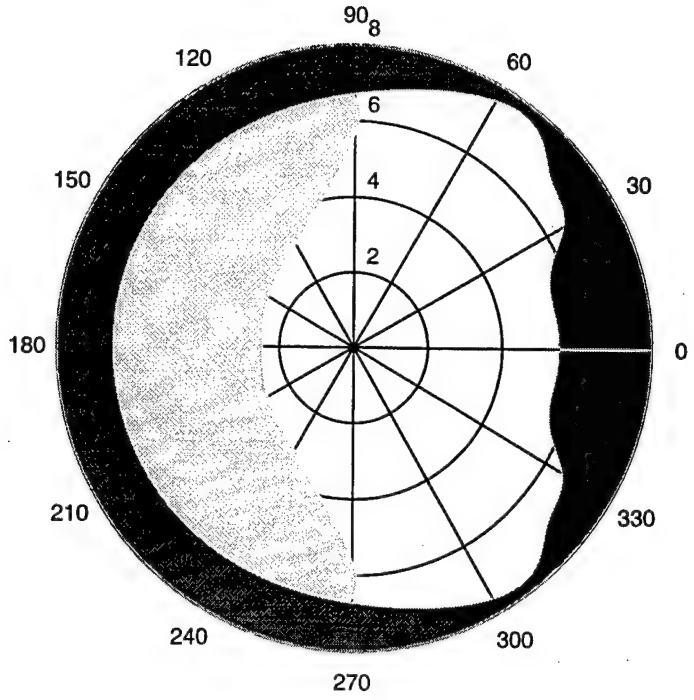

Figure 69. Sea state-polar plot, showing SOE for a submarine U=11 Knots, h=2.5D

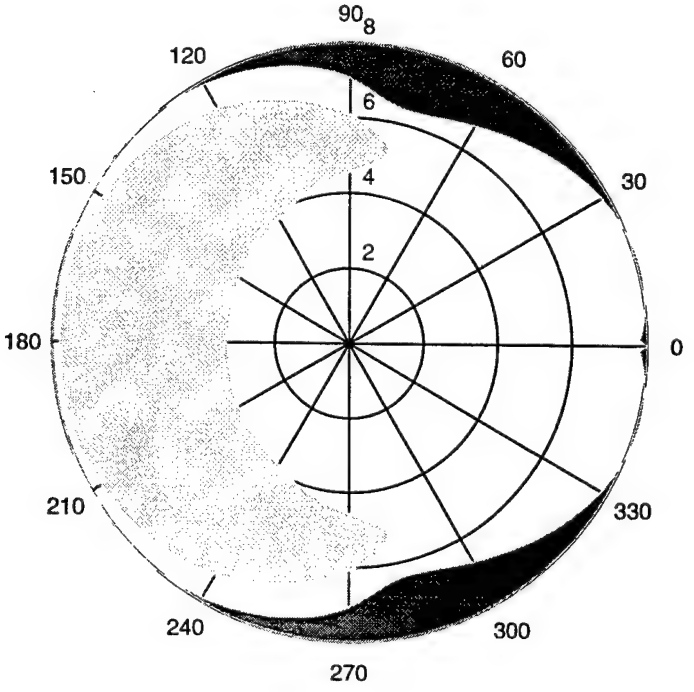

Figure 70. Sea state-polar plot, showing SOE for a submarine U=3 Knots, h=3D

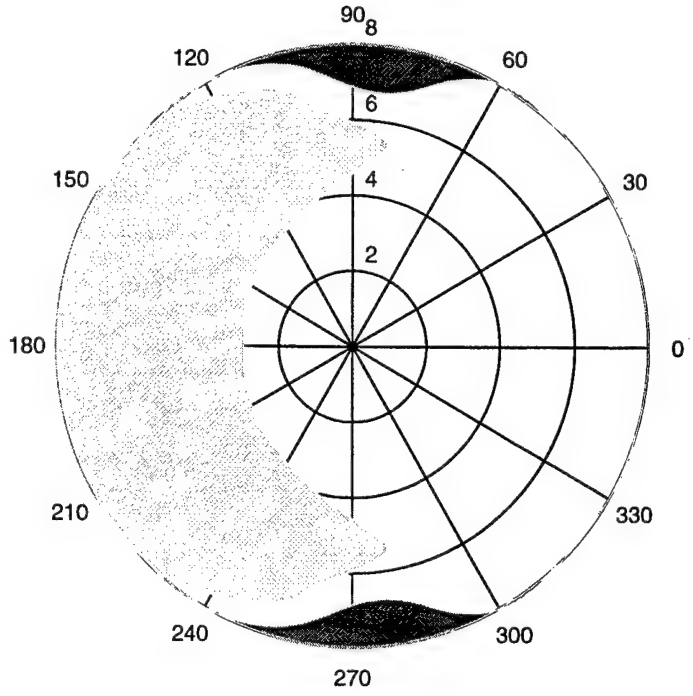

Figure 71. Sea state-polar plot, showing SOE for a submarine U=5 Knots, h=3D

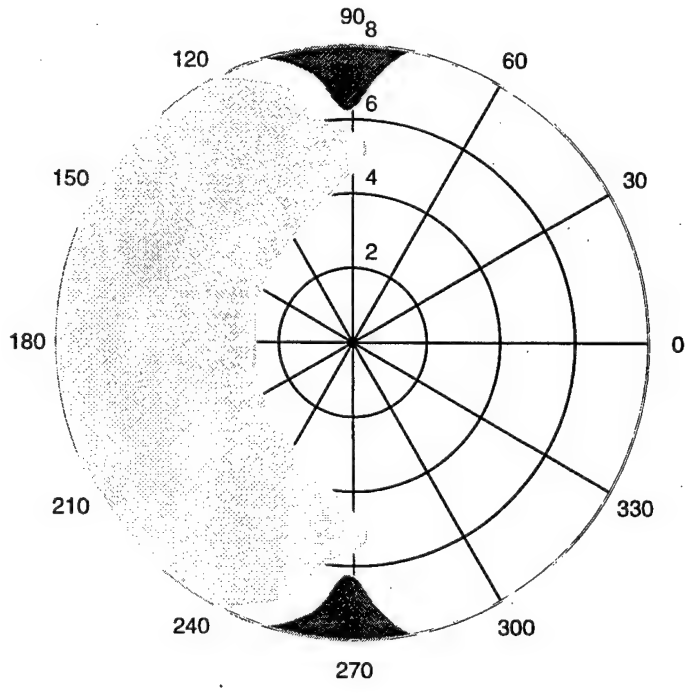

Figure 72. Sea state-polar plot, showing SOE for a submarine U=8 Knots, h=3D

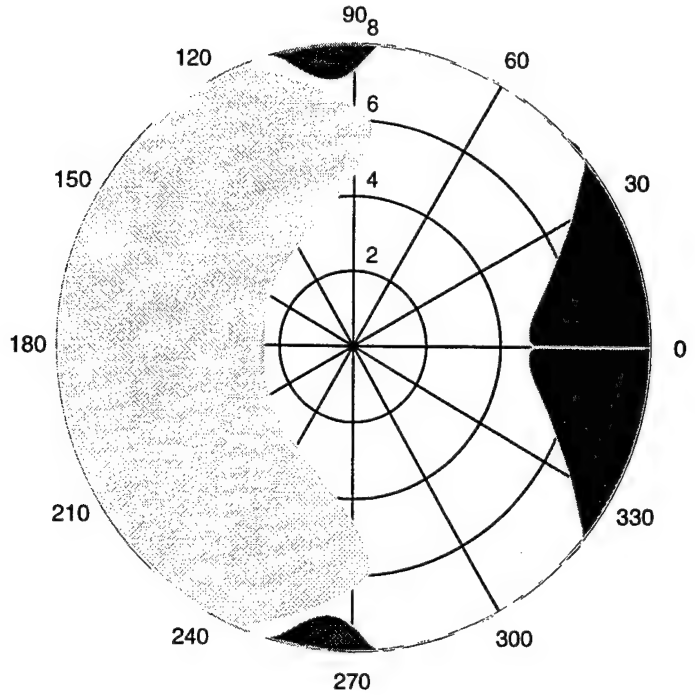

Figure 73. Sea state-polar plot, showing SOE for a submarine U=11 Knots, h=3D

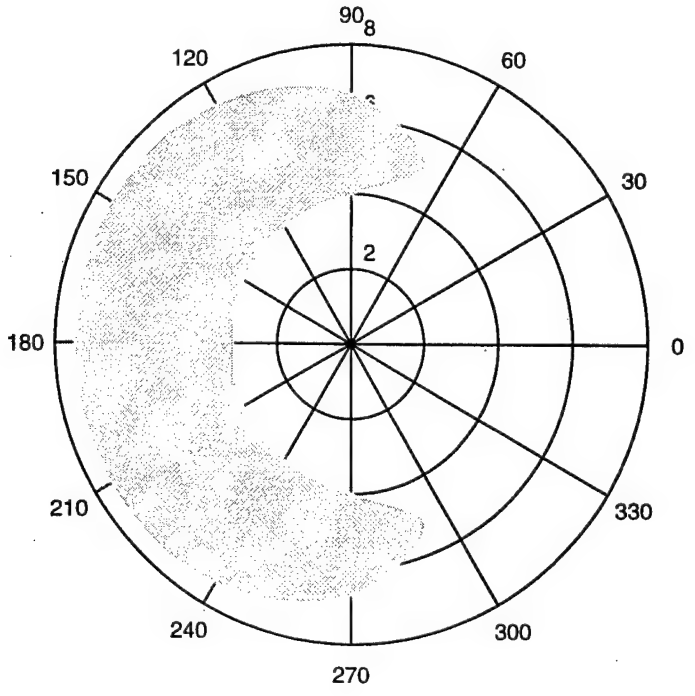

Figure 74. Sea state-polar plot, showing SOE for a submarine U=3 Knots, h=3.5D

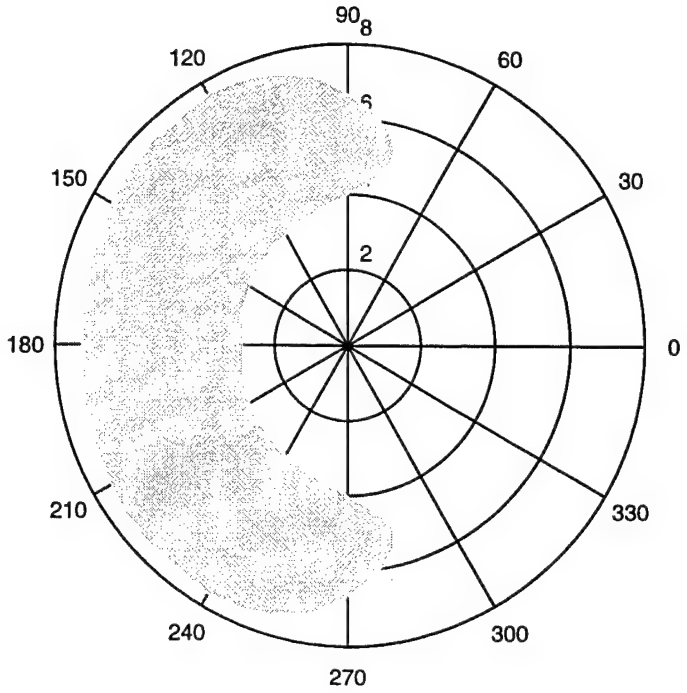

Figure 75. Sea state-polar plot, showing SOE for a submarine U=5 Knots, h=3.5D

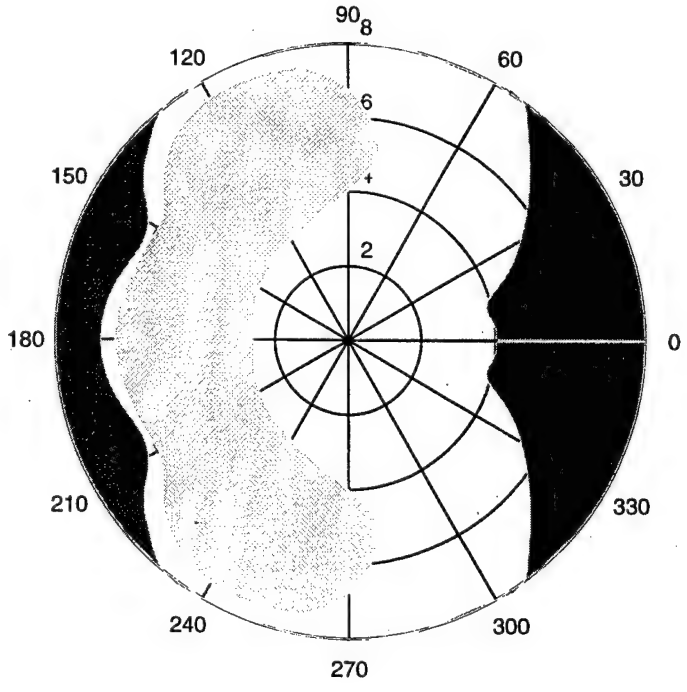

Figure 76. Sea state-polar plot, showing SOE for a submarine U=8 Knots, h=3.5D

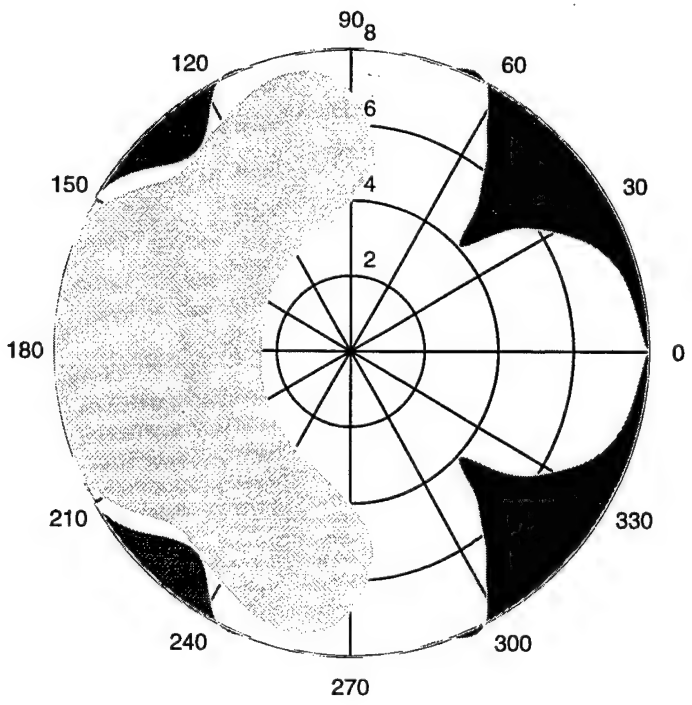

Figure 77. Sea state-polar plot, showing SOE for a submarine U=11 Knots, h=3.5D

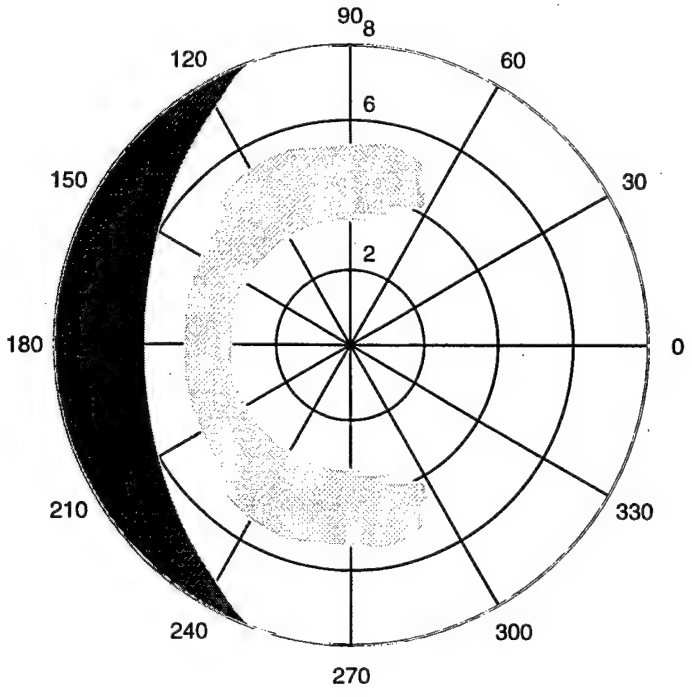

Figure 78. Sea state-polar plot, showing SOE for a submarine U=3 Knots, h=4D

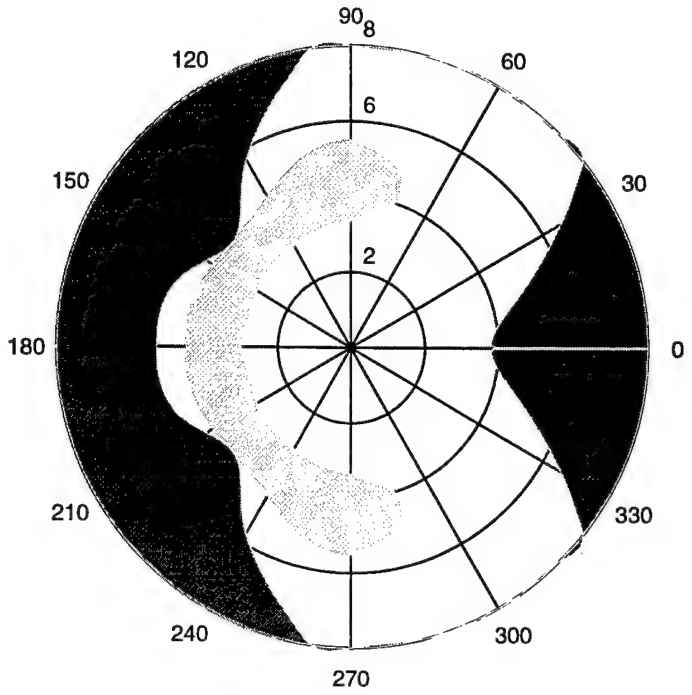

Figure 79. Sea state-polar plot, showing SOE for a submarine U=5 Knots, h=4D

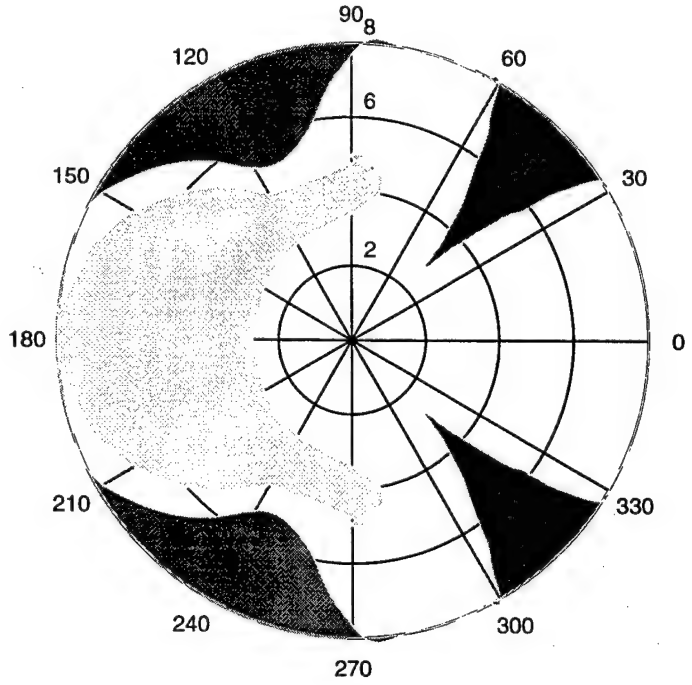

Figure 80. Sea state-polar plot, showing SOE for a submarine U=8 Knots, h=4D

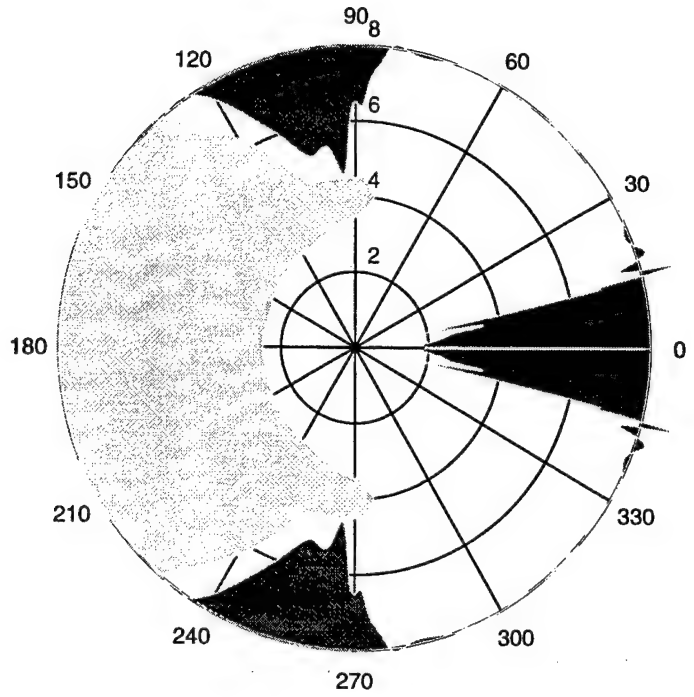

Figure 81. Sea state-polar plot, showing SOE for a submarine U=11 Knots, h=4D

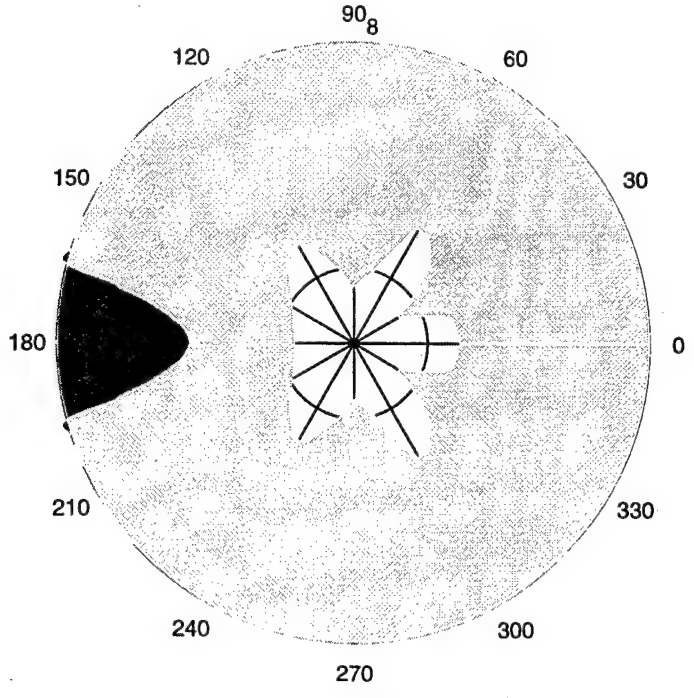

Figure 82. Sea state-polar plot, showing SOE for a submarine U=3 Knots, h=4.5D

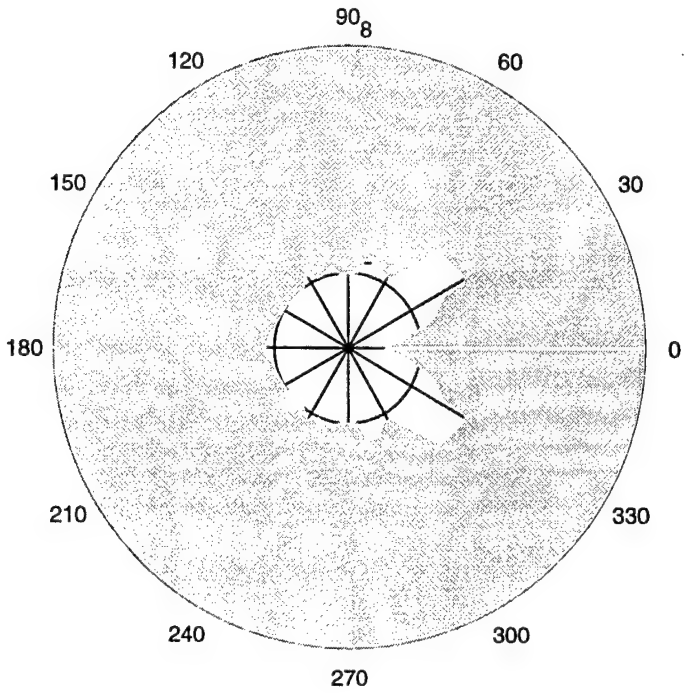

Figure 83. Sea state-polar plot, showing SOE for a submarine U=5 Knots, h=4.5D

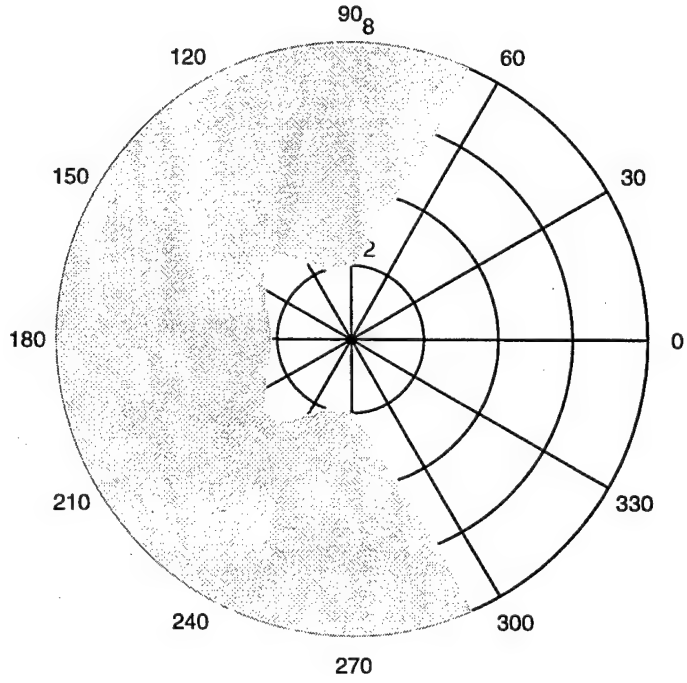

Figure 84. Sea state-polar plot, showing SOE for a submarine U=8 Knots, h=4.5D

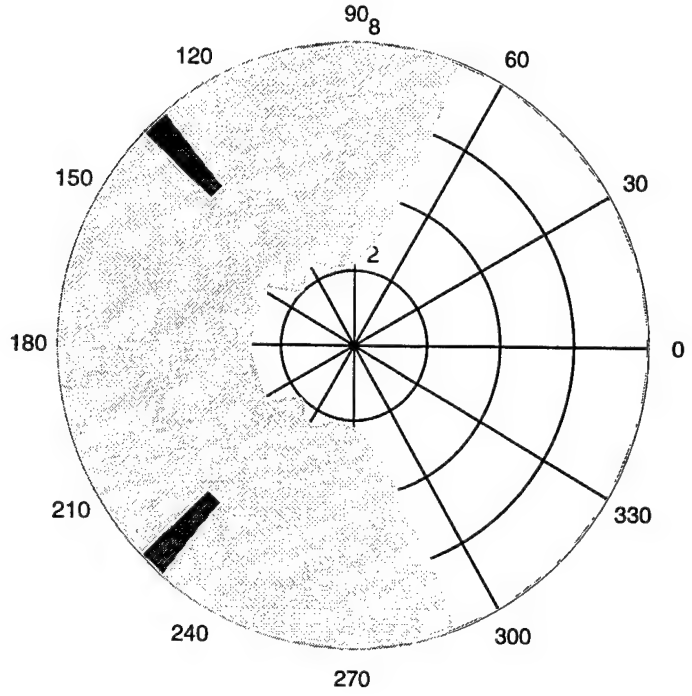

Figure 85. Sea state-polar plot, showing SOE for a submarine U=11 Knots, h=4.5D

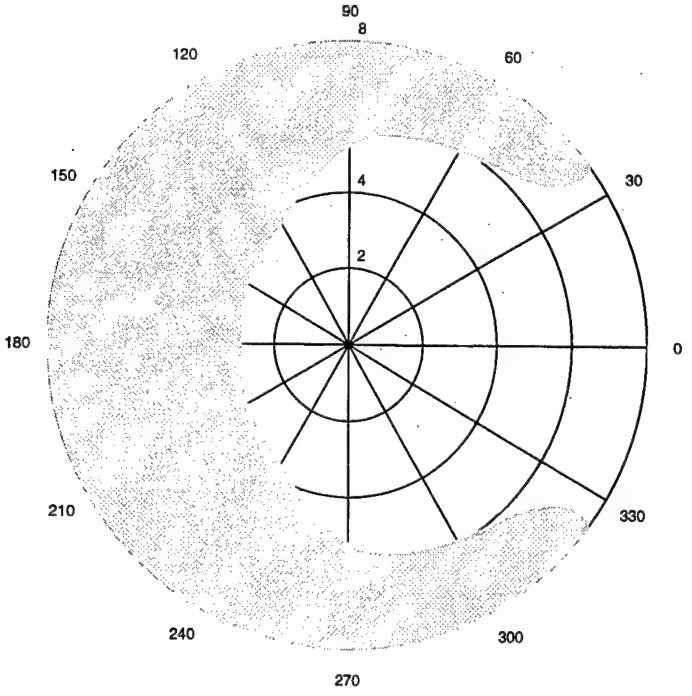

Figure 86. Sea state-polar plot, showing SOE for a submarine U=3 Knots, h=5D

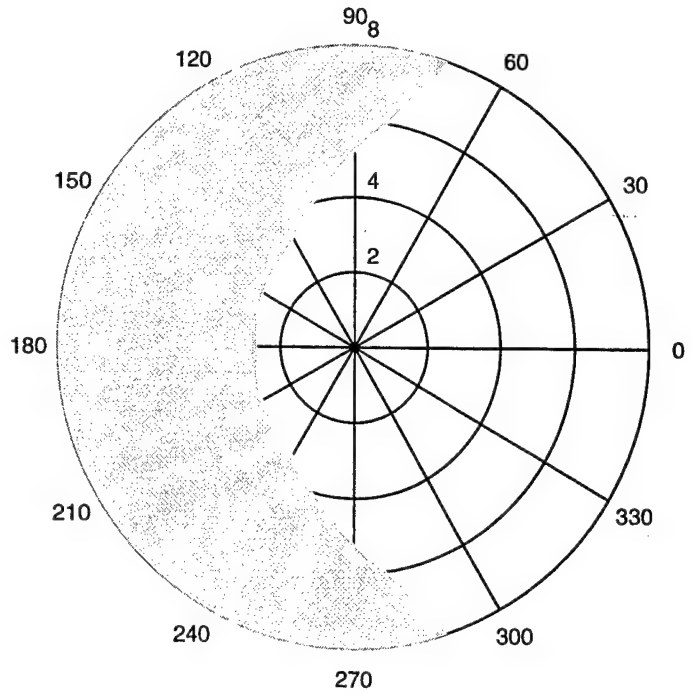

Figure 87. Sea state-polar plot, showing SOE for a submarine U=5 Knots, h=5D

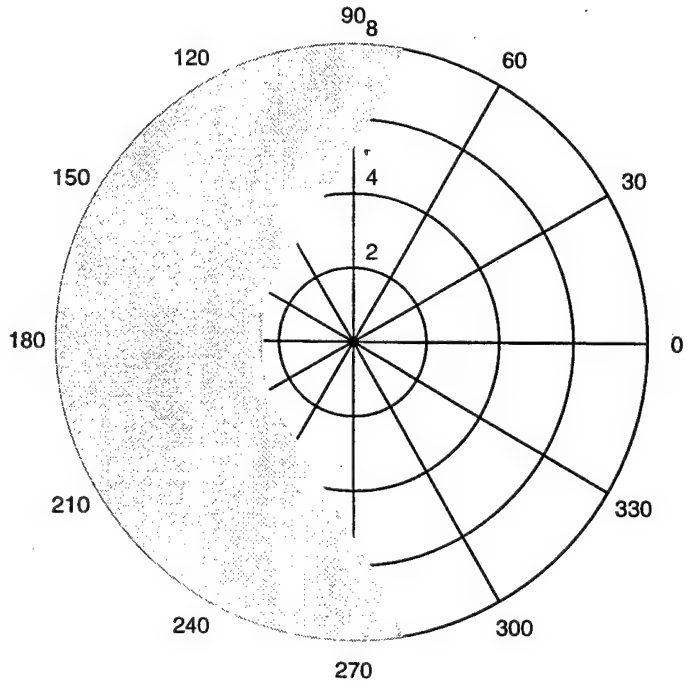

Figure 88. Sea state-polar plot, showing SOE for a submarine U=8 Knots, h=5D

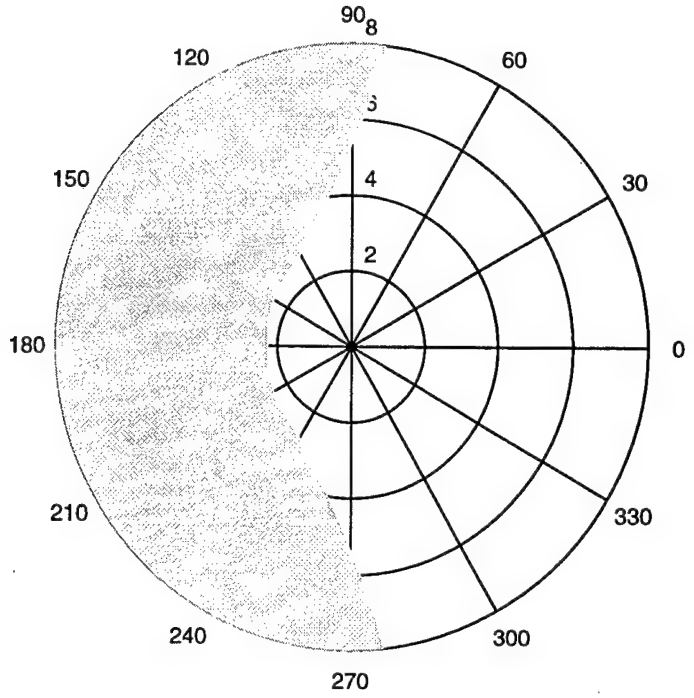

Figure 89. Sea state-polar plot, showing SOE for a submarine U=11 Knots, h=5D

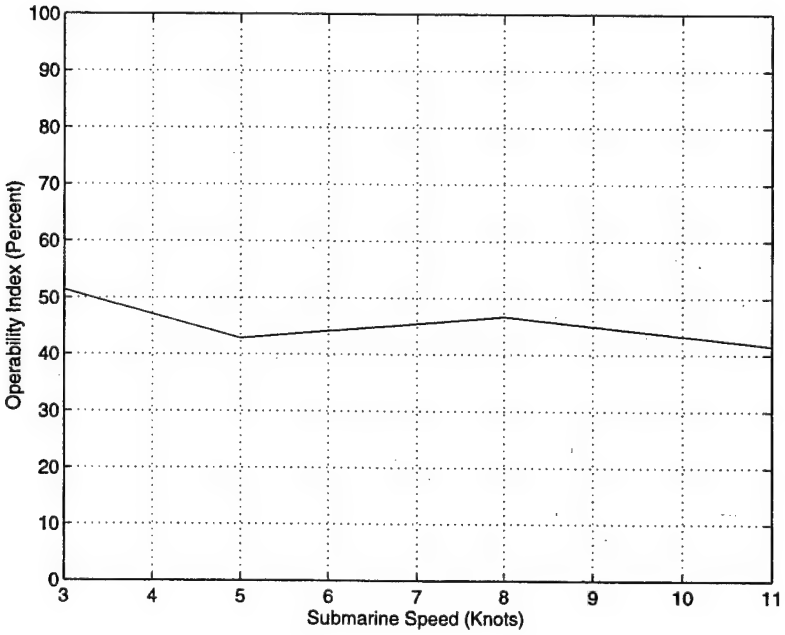

Figure 90. OI vs. Submarine Speed Plot at 2.5D depth

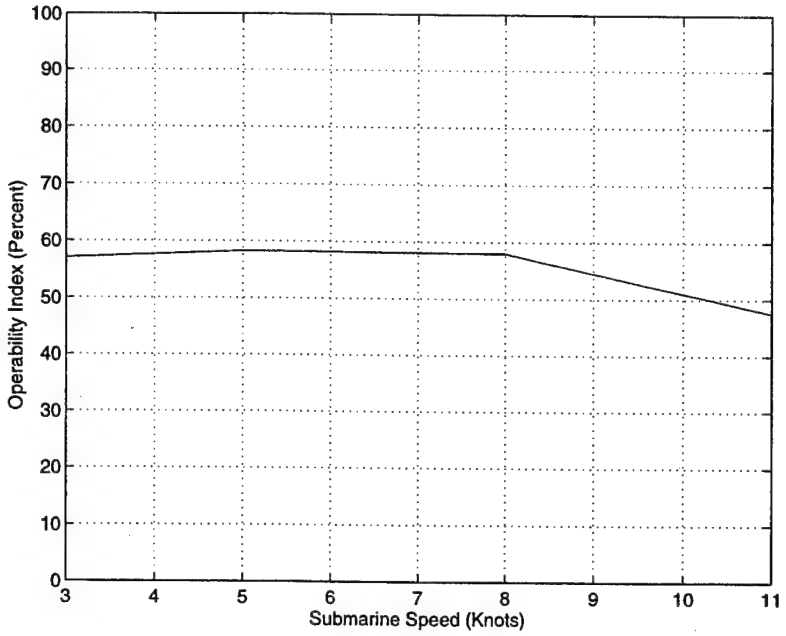

Figure 91. OI vs. Submarine Speed Plot at 3*D* depth

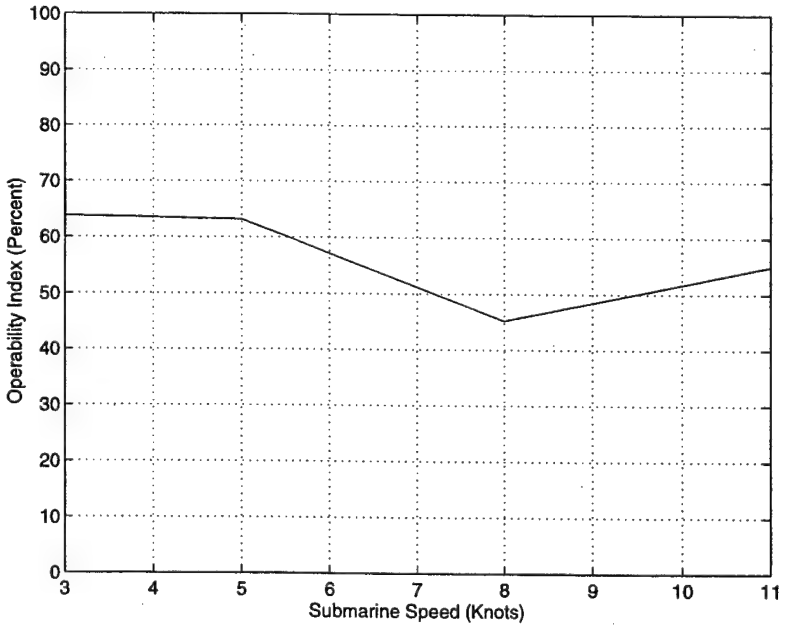

Figure 92. OI vs. Submarine Speed Plot at 3.5*D* depth

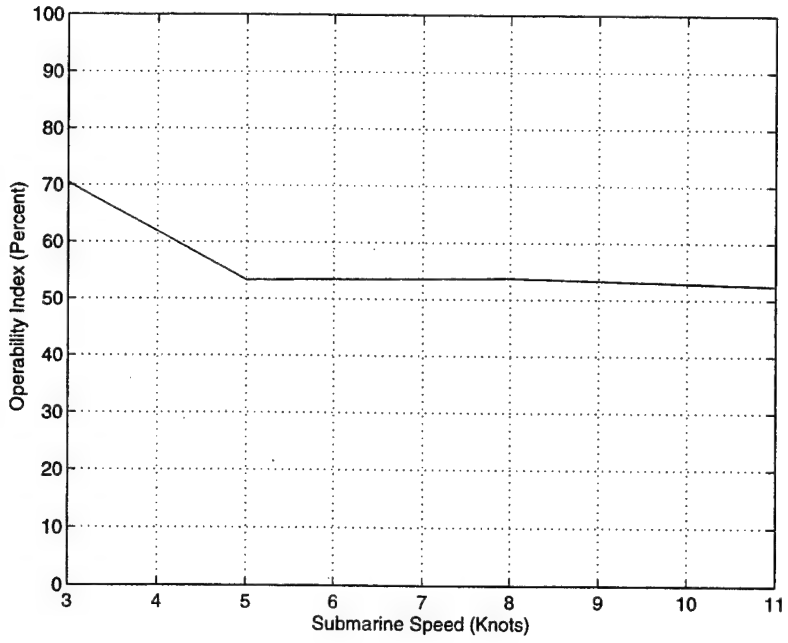

Figure 93. OI vs. Submarine Speed Plot at 4*D* depth

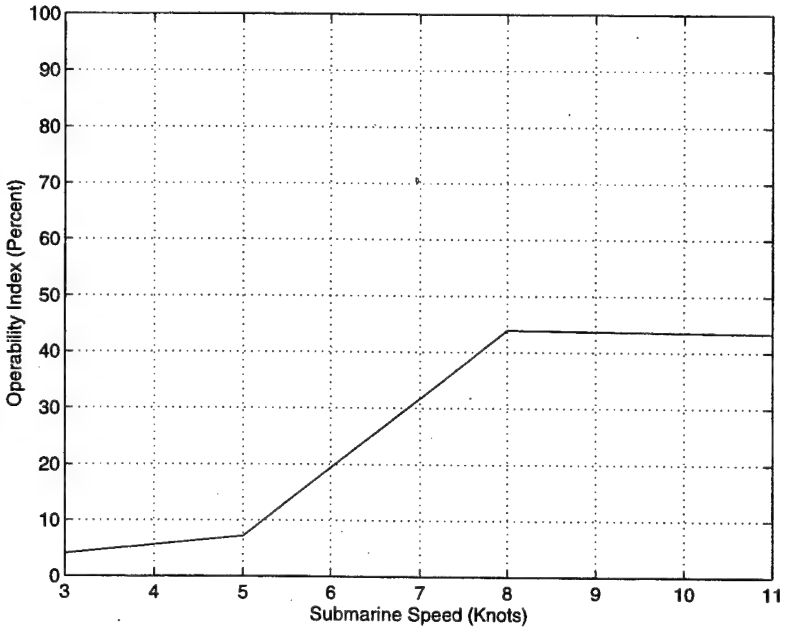

Figure 94. OI vs. Submarine Speed Plot at 4.5*D* depth

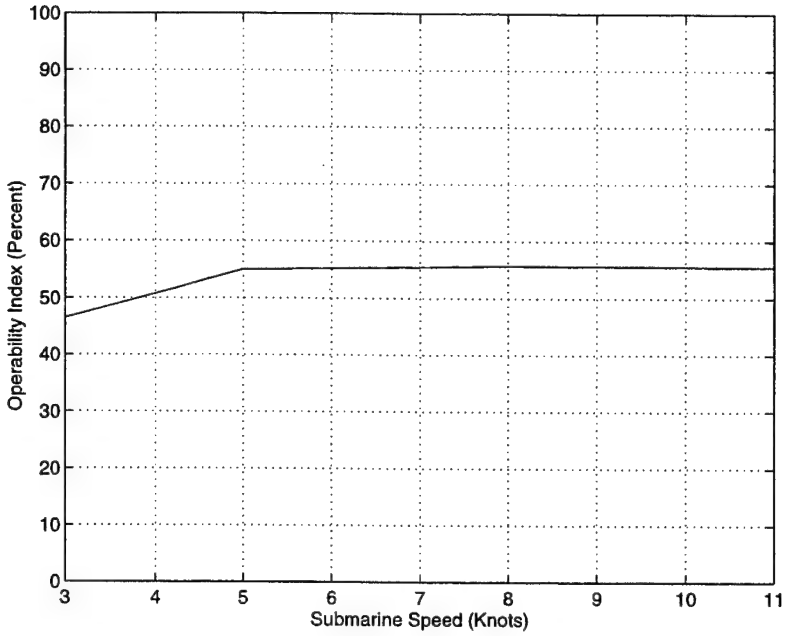

Figure 95. OI vs. Submarine Speed Plot at 5*D* depth

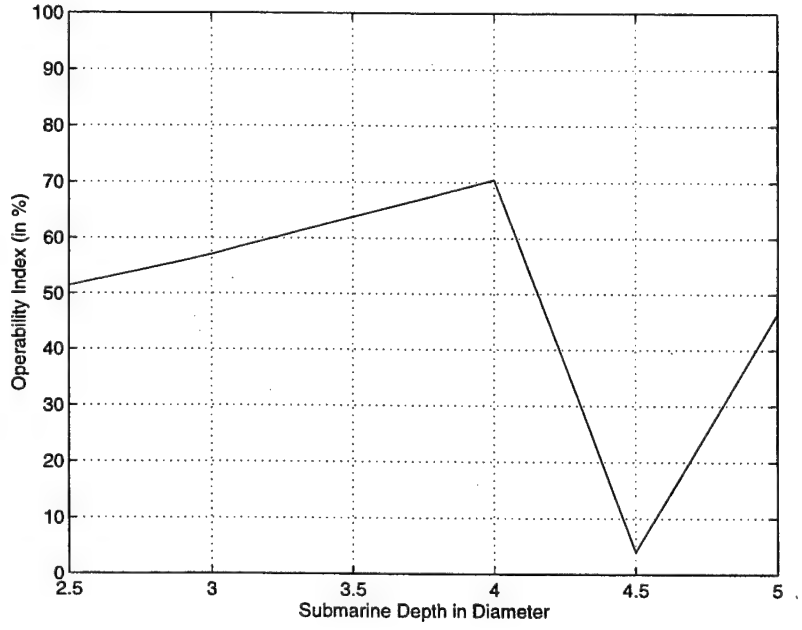

Figure 96. OI vs. Submarine Depth in Submarine Diameters at 3 Knots

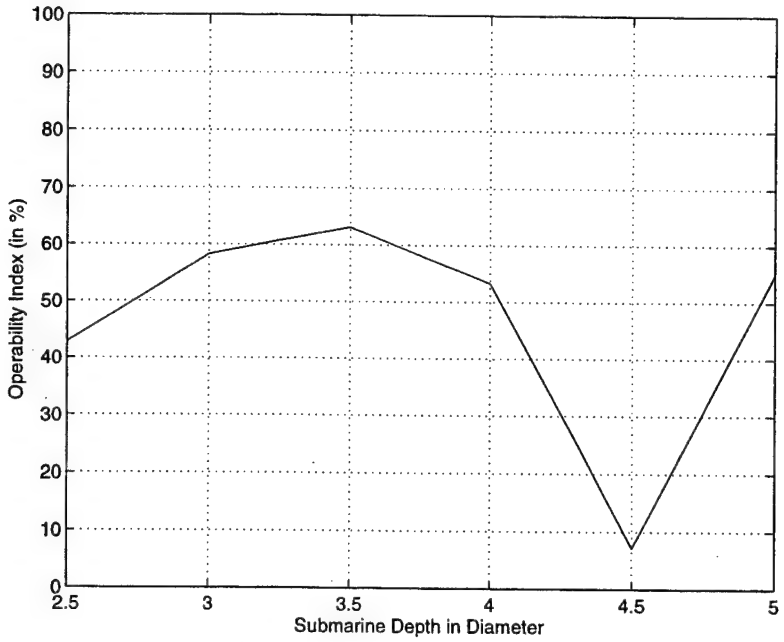

Figure 97. OI vs. Submarine Depth in Submarine Diameters at 5 Knots

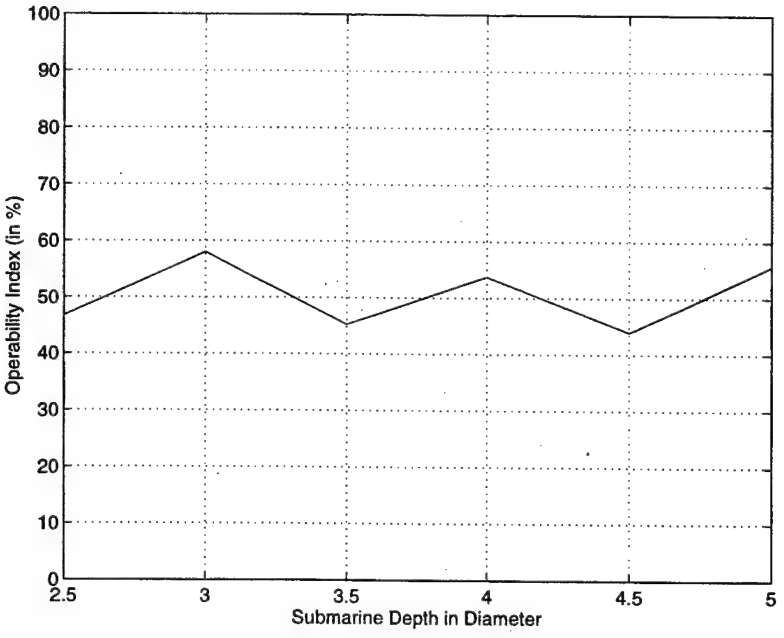

Figure 98. OI vs. Submarine Depth in Submarine Diameters at 8 Knots

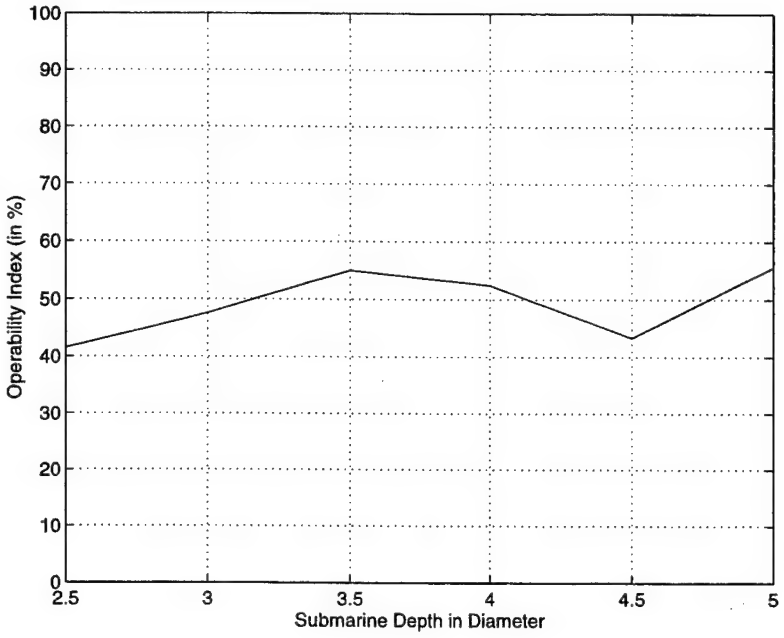

Figure 99. OI vs. Submarine Depth in Submarine Diameters at 11 Knots

IV. SHALLOW WATER RESULTS

In this chapter we present results for shallow water operations; i.e., for finite water depth beneath the keel. Shallow water corrections are implemented in the software package as described in [Ref. 3]. The results are presented in terms of the two criteria used in deep water, periscope submergence and sail broaching as well as for an additional criterion which quantifies the probability of collision between the boat and the sea bed. This is calculated based on the absolute vertical motion at either the bow or the stern and the clearance from the sea bed at the appropriate motion point. All results are presented for a standard depth between keel and free surface of three diameters.

A. RESULTS OF PERISCOPE SUBMERGENCE CRITERION

Figures 100 through 108 present the results for the periscope submergence criterion. Each polar plot is for a given depth beneath the keel and for four forward speeds, namely three, five, eight, and eleven knots. Figure 109 shows the operability index in percentage normalized with respect to its deep water value, as a function of both speed and shallow depth. The percent change in the operability index is calculated by subtracting the shallow water value from the deep water value and dividing by the deep water index. Therefore, positive values show that the operability in shallow water is smaller compared to deep water. It can be seen that the operability index does not change much and it does not follow a consistent trend. For certain speeds it decreases in shallow water, while for other speeds, it increases and then starts to decrease. The numerical values are quite small and the shape of the polar plots does not change significantly for different water depths. It appears, therefore, that the operability index with regards to periscope submergence remains essentially the same for deep and shallow waters.

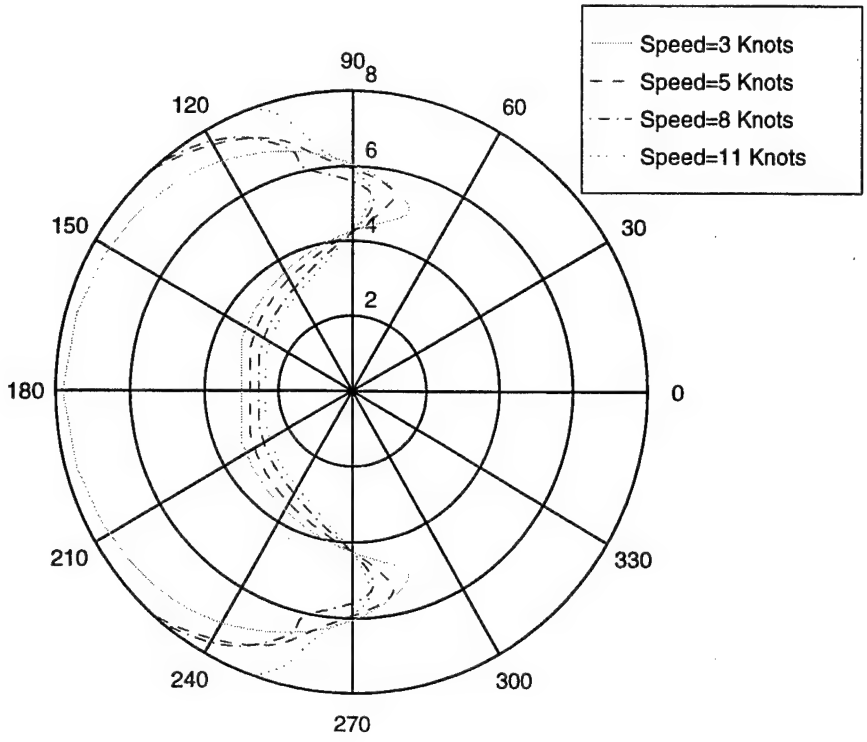

Figure 100. Sea state-polar plot, showing SOE for different U's and $5D$ Water Depth

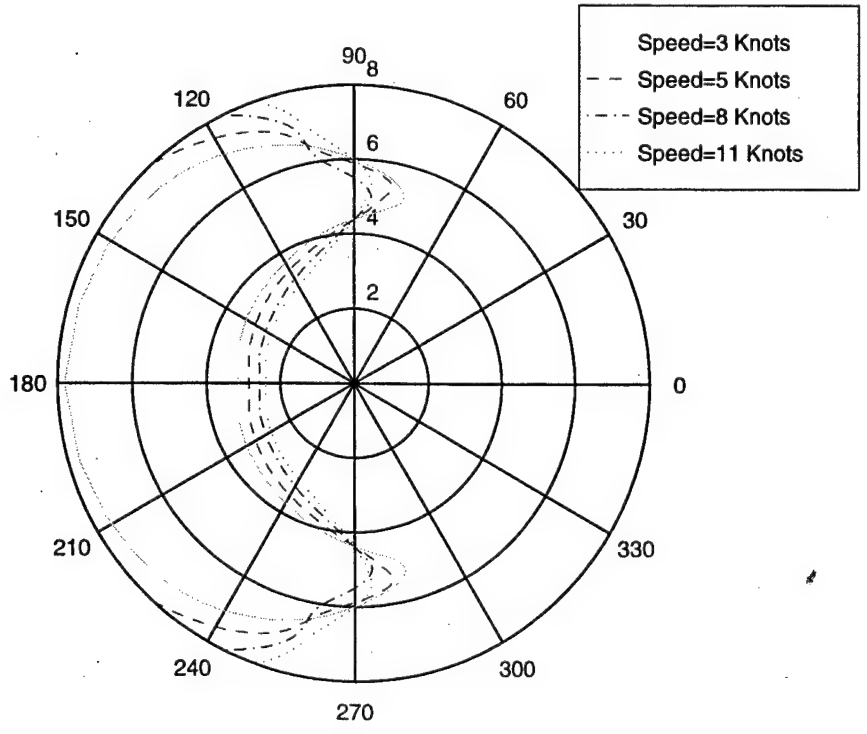

Figure 101. Sea state-polar plot, showing SOE for different U's and $6D$ Water Depth

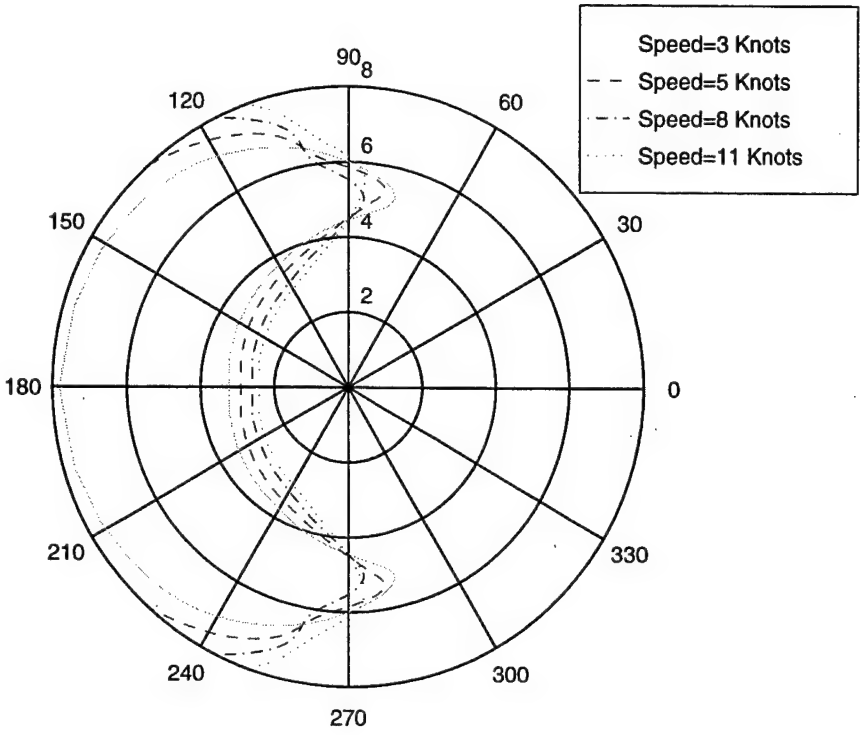

Figure 102. Sea state-polar plot, showing SOE for different U's and 7D Water Depth

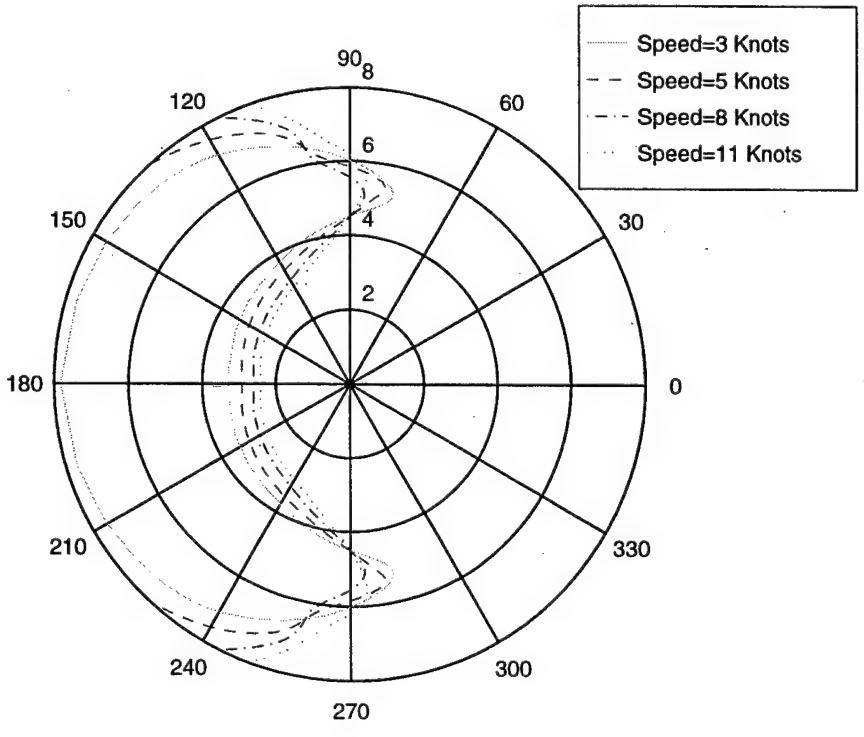

Figure 103. Sea state-polar plot, showing SOE for different U's and 8D Water Depth

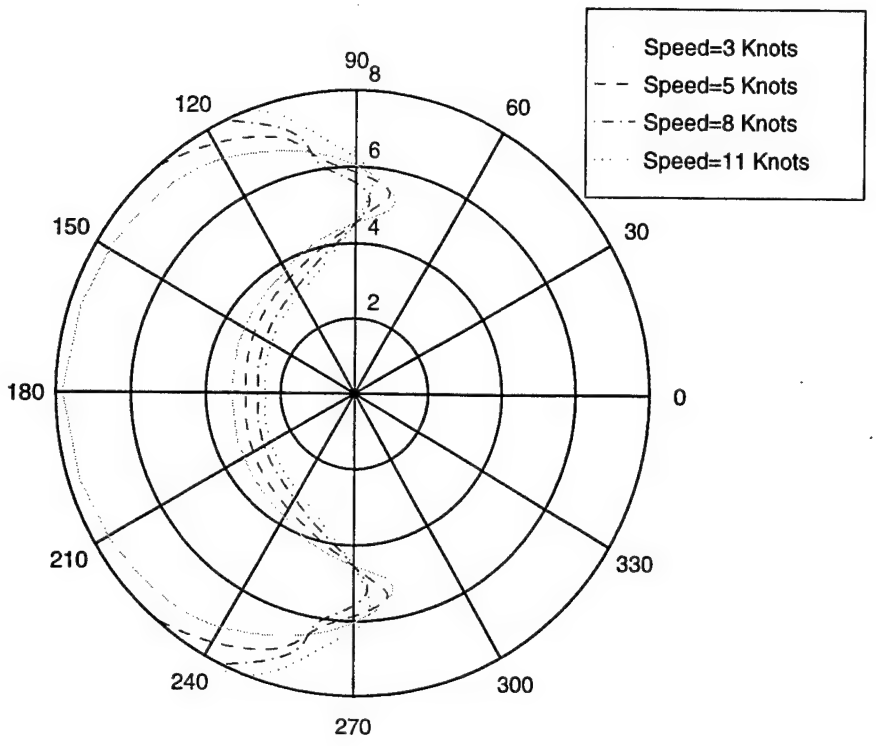

Figure 104. Sea state-polar plot, showing SOE for different U's and 10D Water Depth

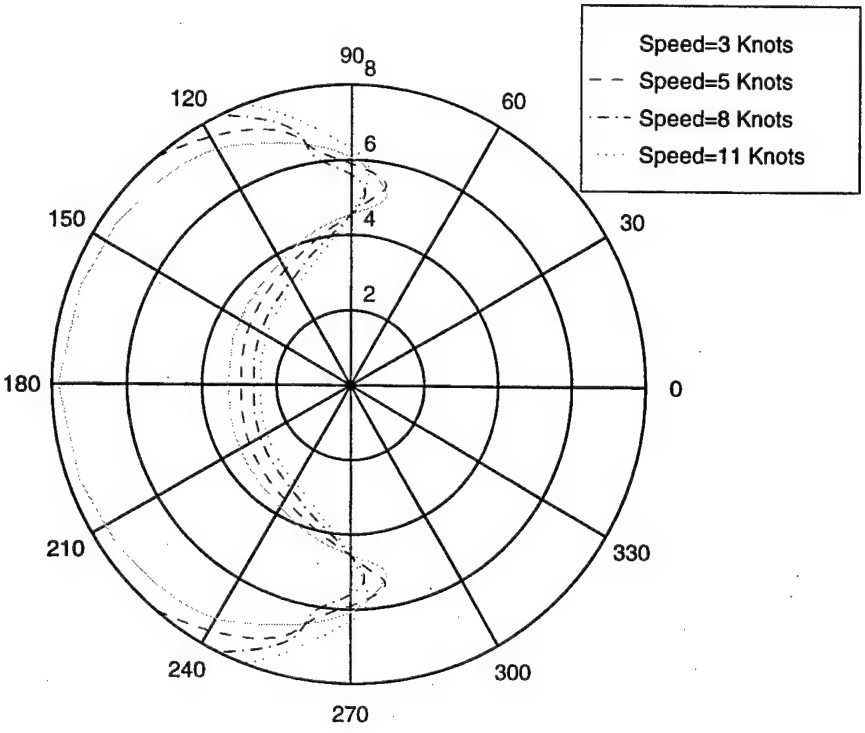

Figure 105. Sea state-polar plot, showing SOE for different U's and 15D Water Depth

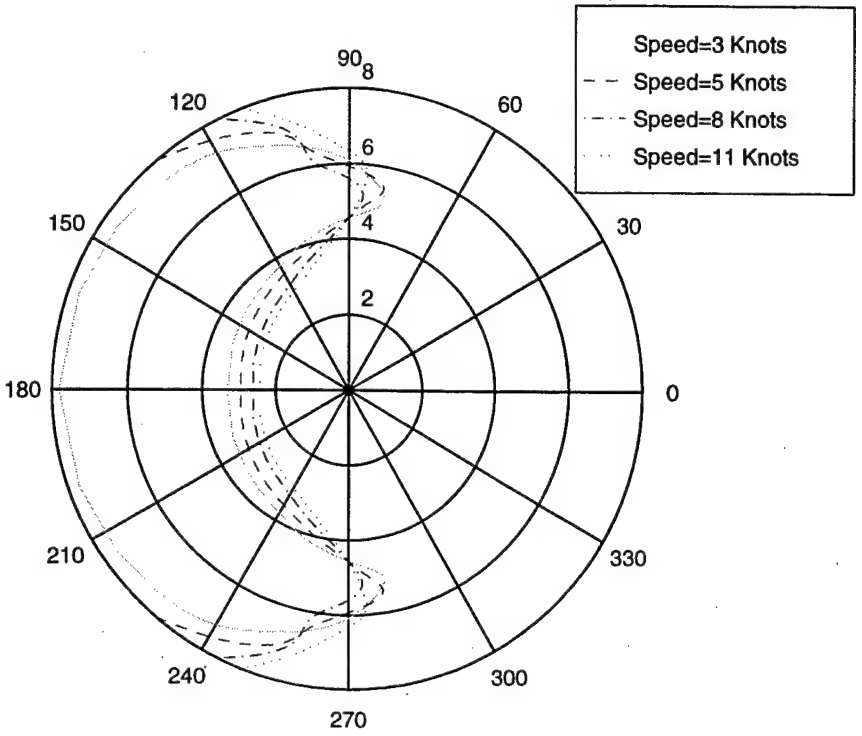

Figure 106. Sea state-polar plot, showing SOE for different U's and 20D Water Depth

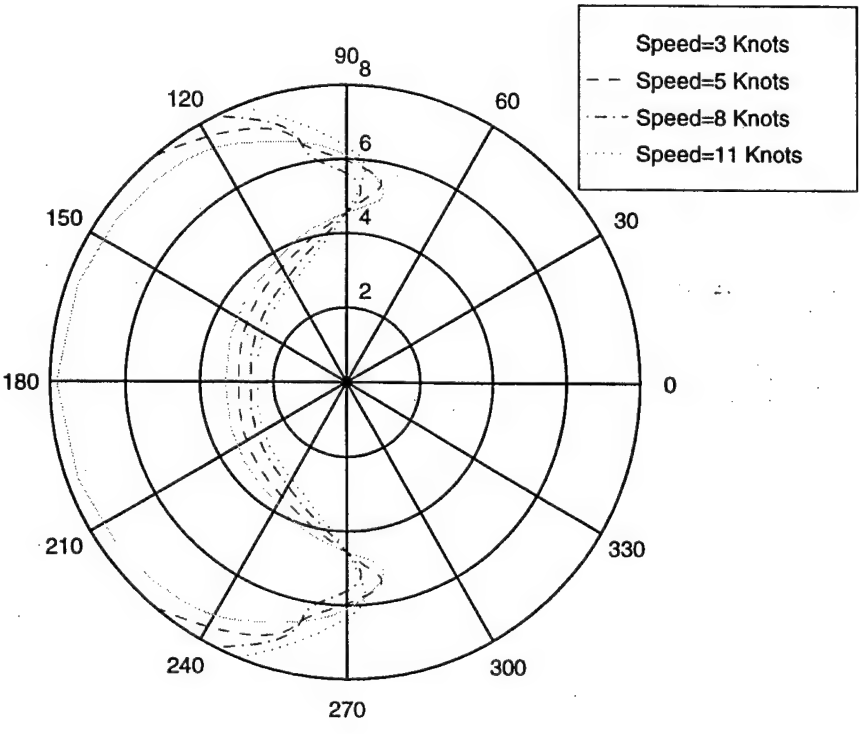

Figure 107. Sea state-polar plot, showing SOE for different U's and 30D Water Depth

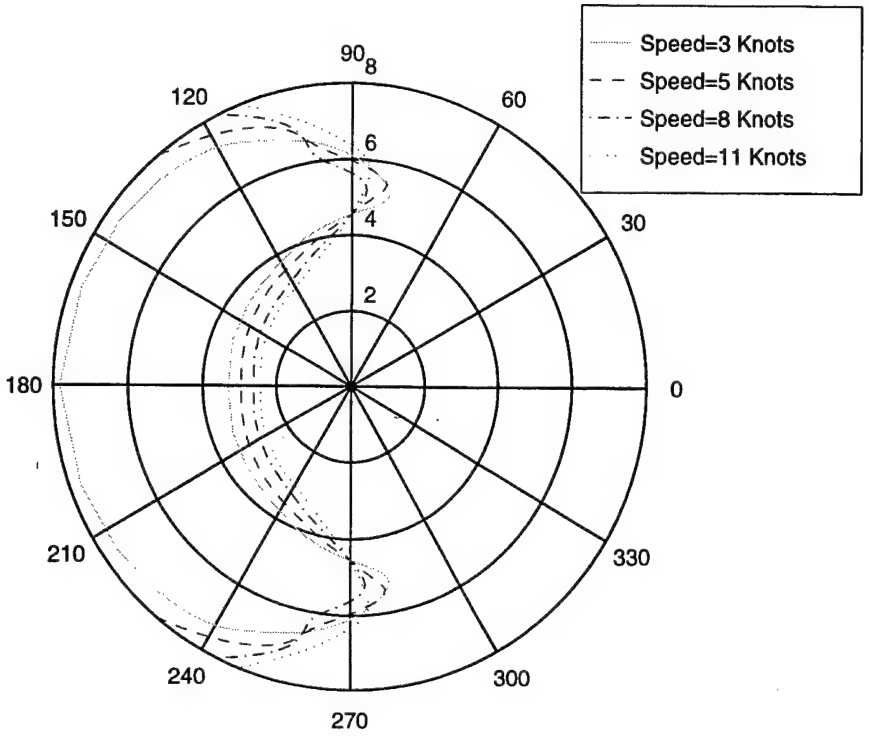

Figure 108. Sea state-polar plot, showing SOE for different U's and 40D Water Depth

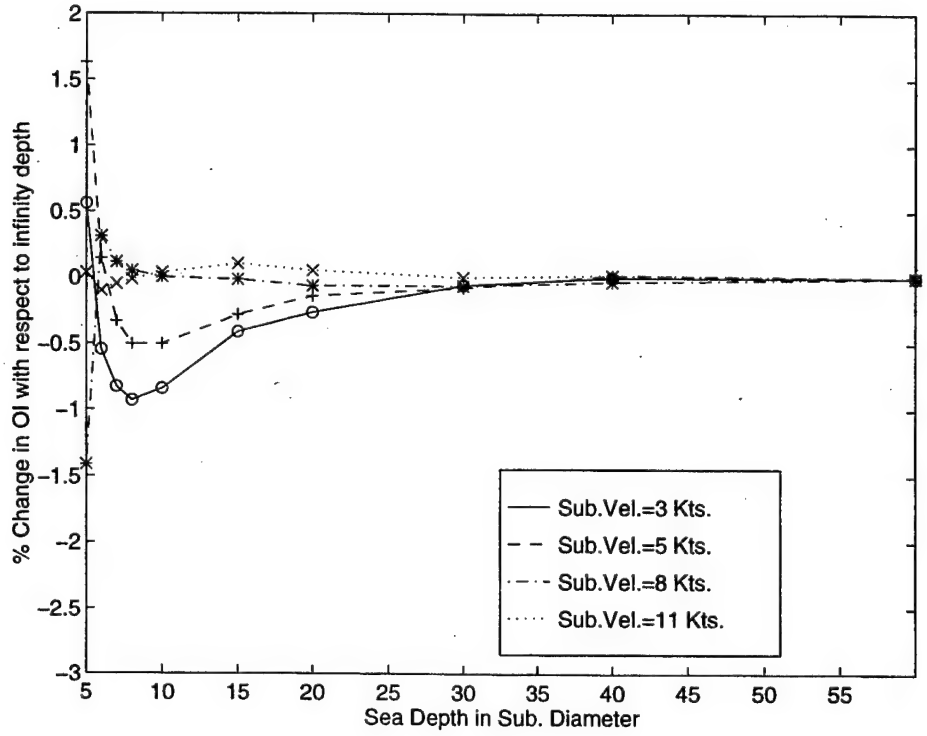

Figure 109. Change in OI with respect to infinite depth vs. Water Depth

B. RESULTS OF SAIL BROACHING CRITERION

Results for the sail broaching criterion are presented in Figures 110 through 118. The same parameters as for periscope submergence were used here as well. The percent change in the operability index is shown in Figure 119. Here it seems that water depth has a more important effect on both the value of the operability index and the shape of the polar plots. In general, the operability index is decreasing as the water depth becomes smaller.

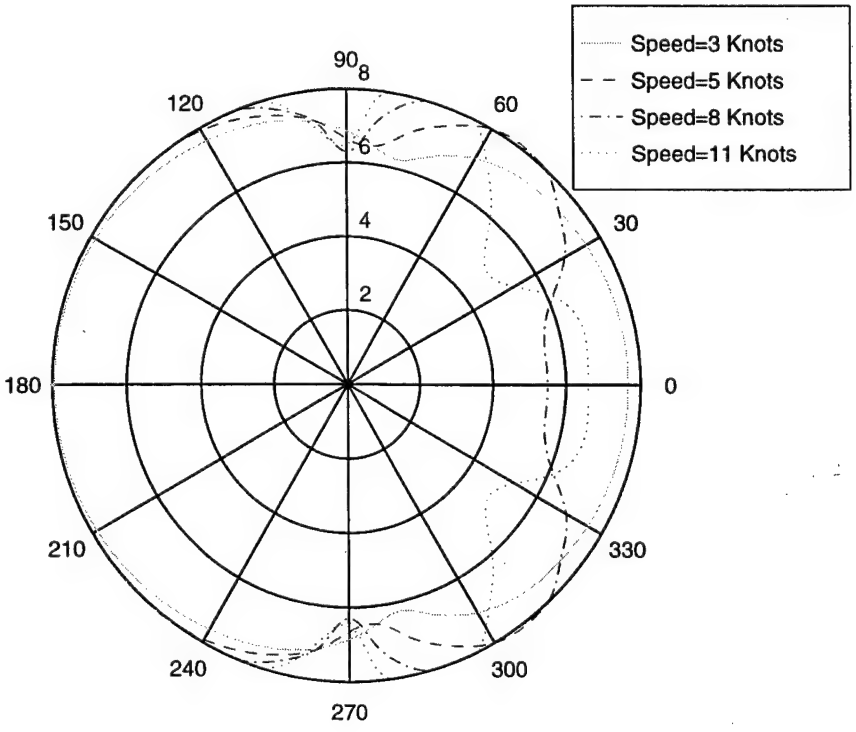

Figure 110. Sea state-polar plot, showing SOE for different *U*'s and 5*D* Water Depth

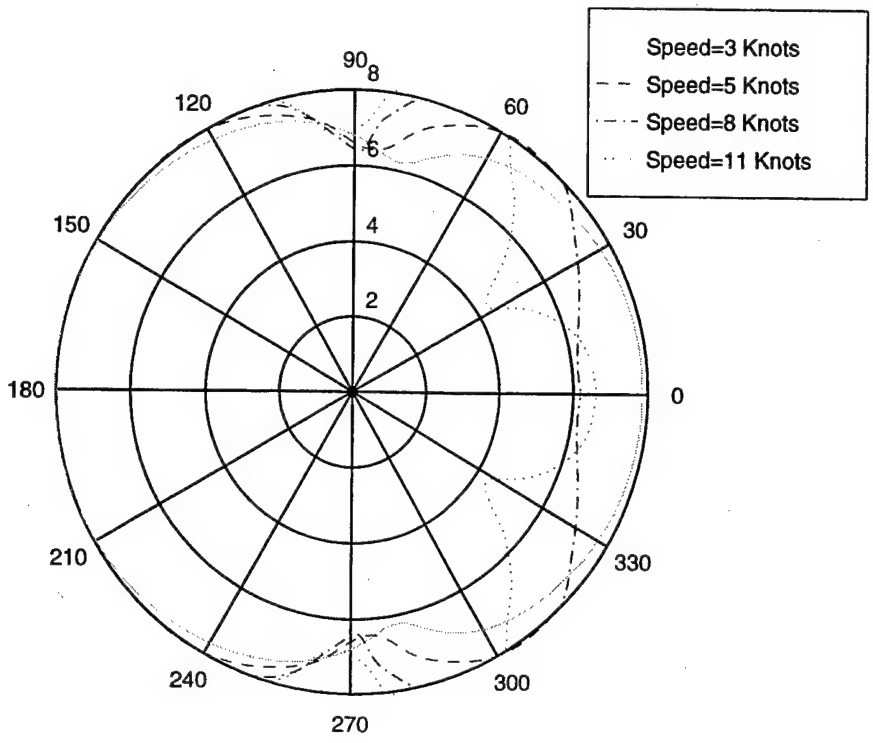

Figure 111. Sea state-polar plot, showing SOE for different U's and $6D$ Water Depth

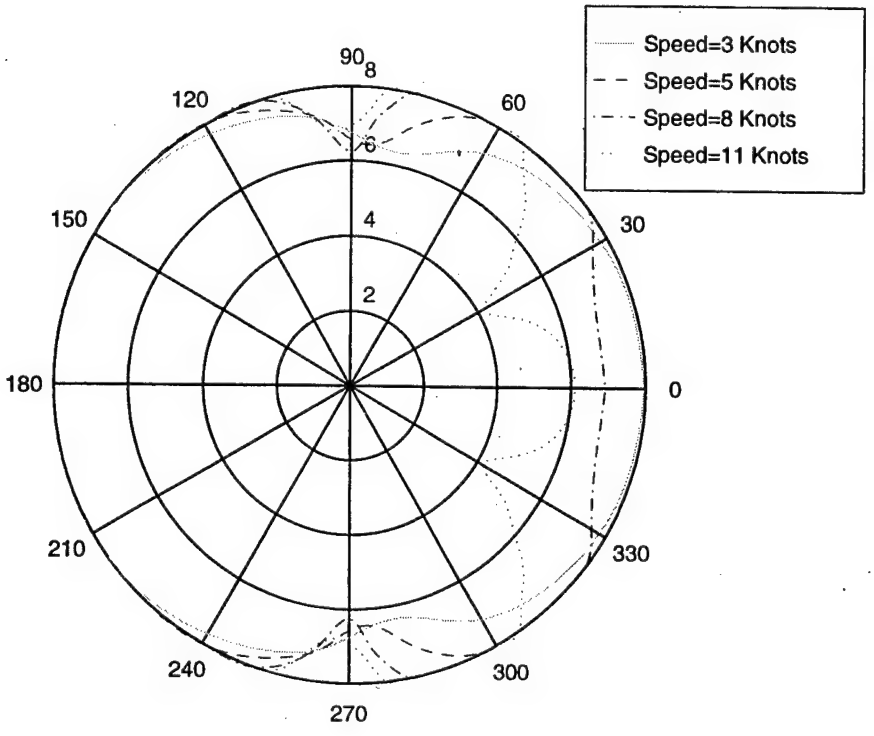

Figure 112. Sea state-polar plot, showing SOE for different U's and $7D$ Water Depth

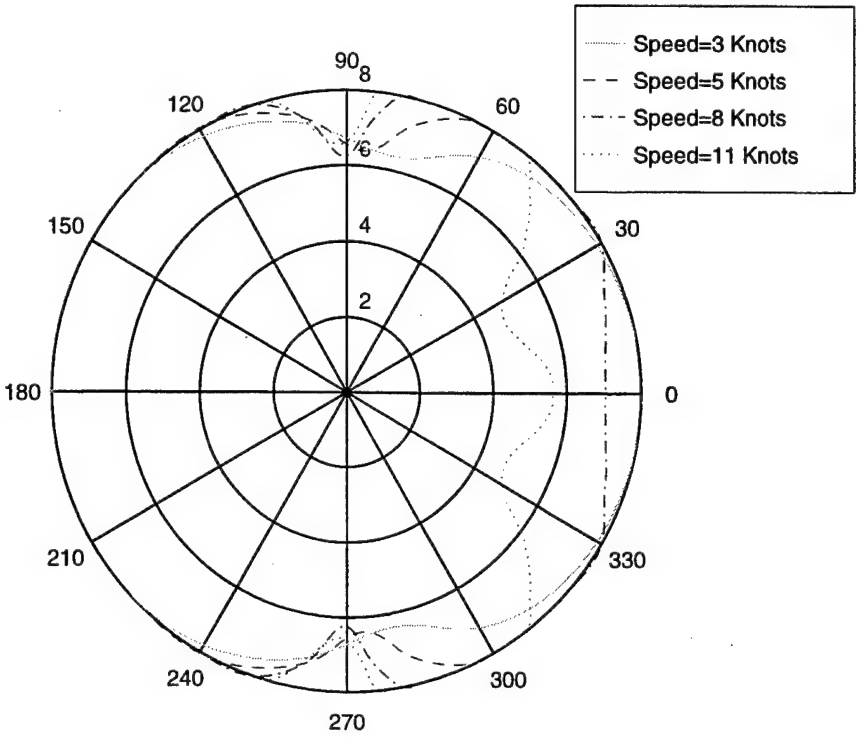

Figure 113. Sea state-polar plot, showing SOE for different *U*'s and 8*D* Water Depth

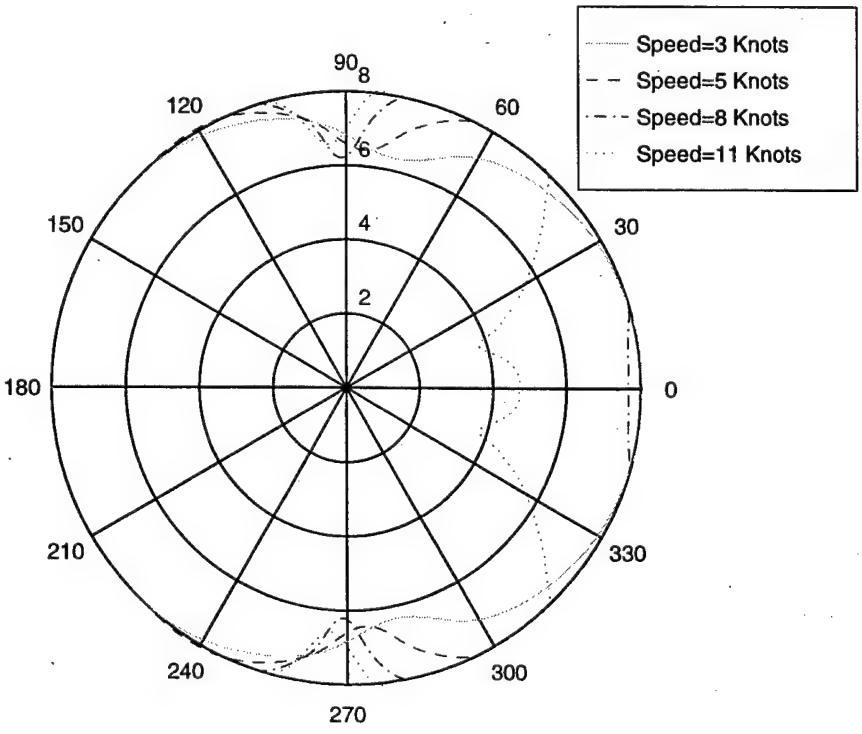

Figure 114. Sea state-polar plot, showing SOE for different *U*'s and 10*D* Water Depth

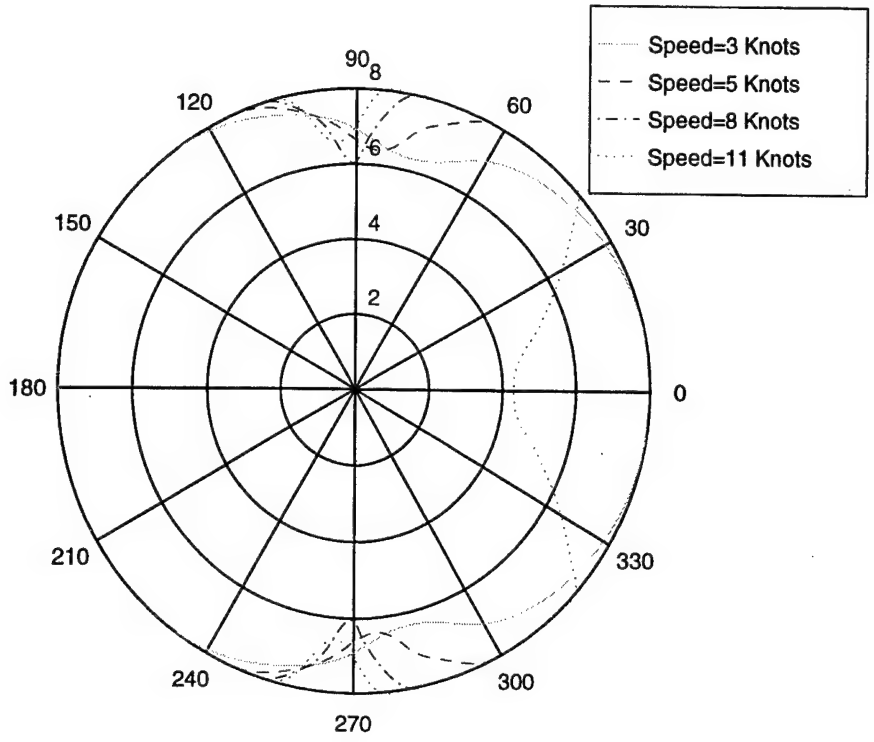

Figure 115. Sea state-polar plot, showing SOE for different U's and 15D Water Depth

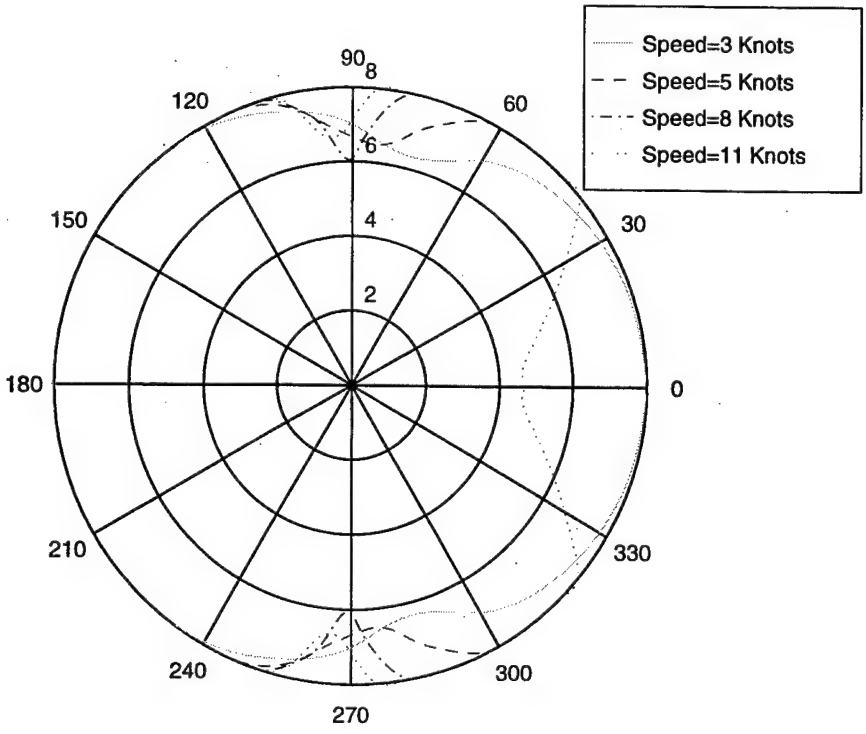

Figure 116. Sea state-polar plot, showing SOE for different U's and 20D Water Depth

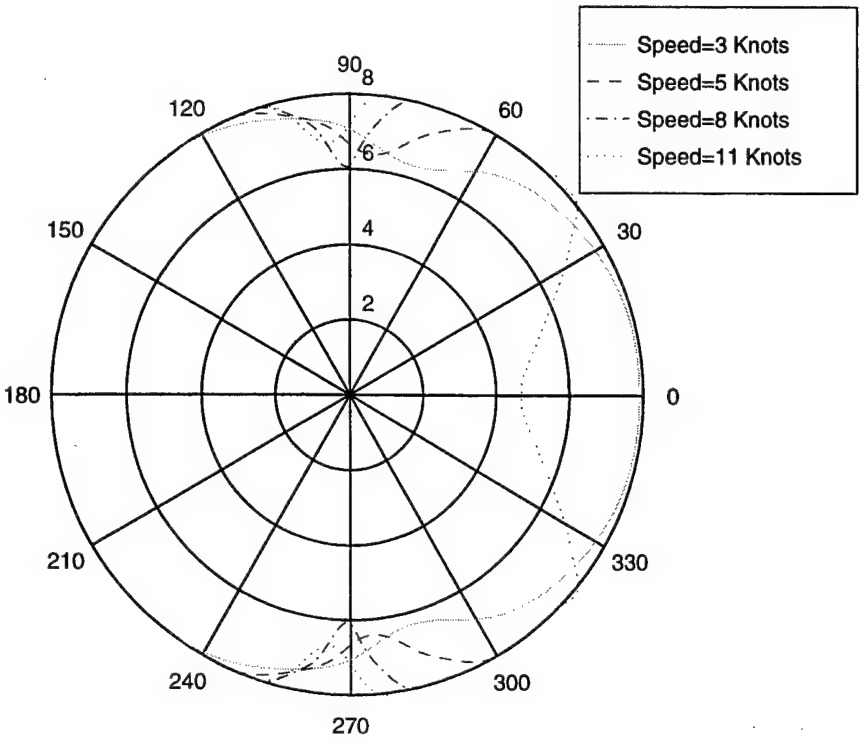

Figure 117. Sea state-polar plot, showing SOE for different *U*'s and 30*D* Water Depth

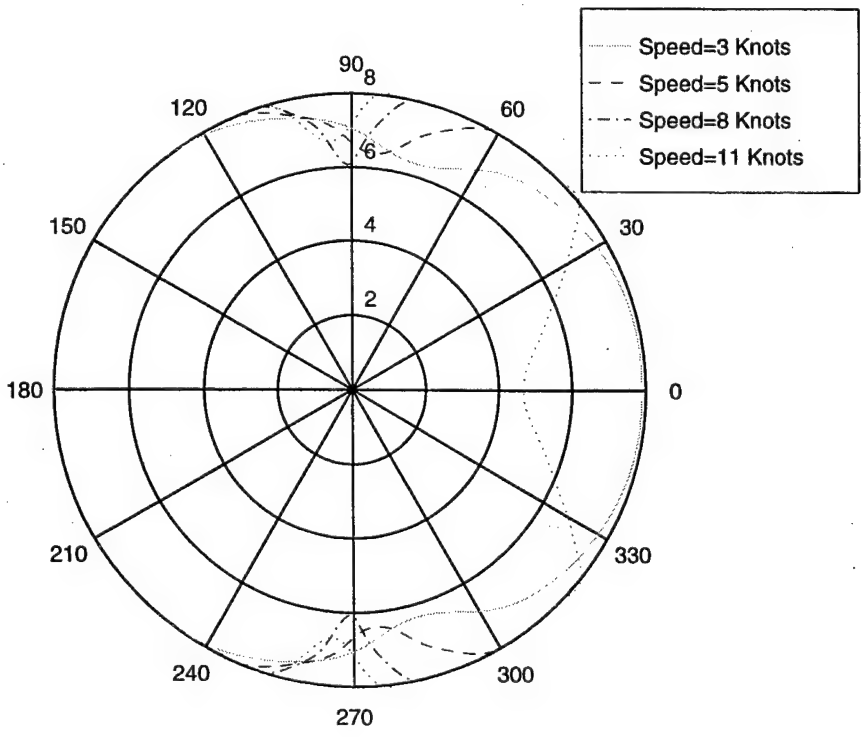

Figure 118. Sea state-polar plot, showing SOE for different *U*'s and 40*D* Water Depth

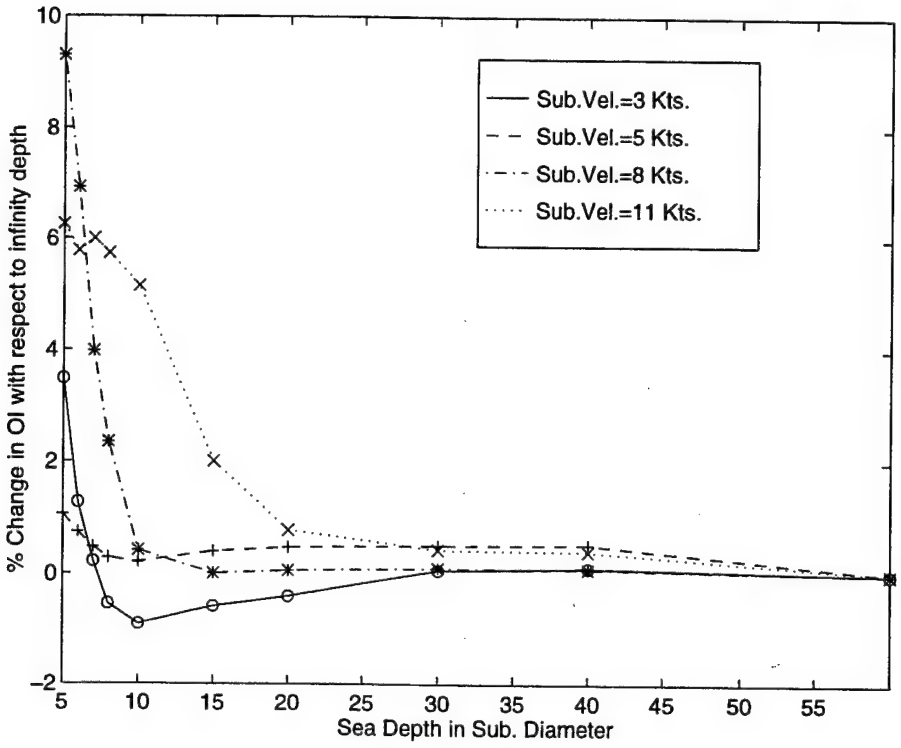

Figure 119. Change in OI with respect to infinite depth vs. Water Depth

C. RESULTS OF COLLISION CRITERION

Results for the sea-bed collision criterion are summarized in Figures 120 through 125. The operability index is shown in Figure 126. As expected, the operability index decreases with decreasing water depth. The shape of the polar plots, i.e., specific sea state and sea direction combinations, also varies significantly with water depth.

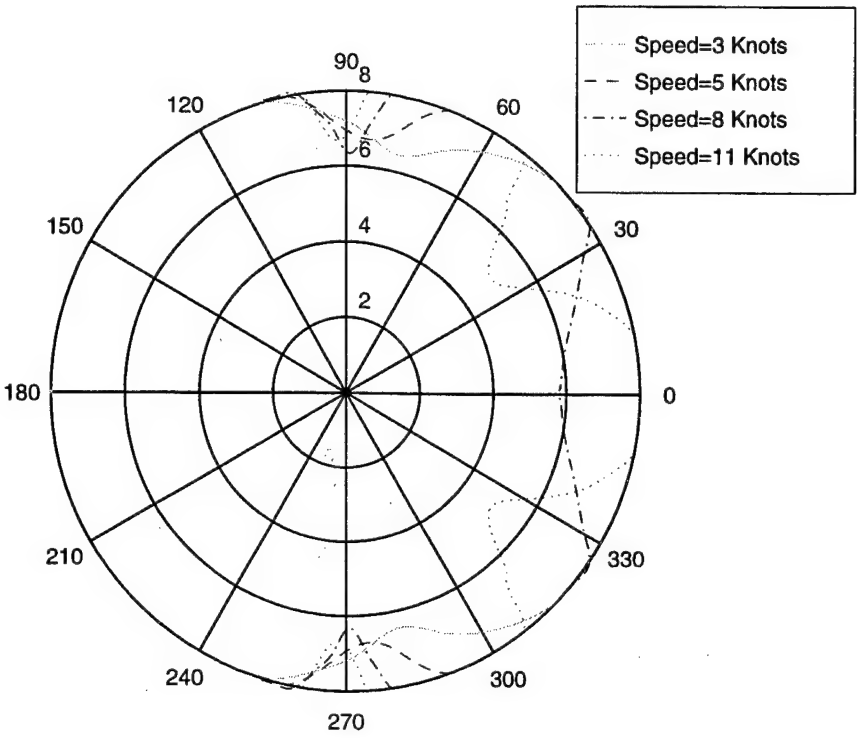

Figure 120. Sea state-polar plot, showing SOE for different U's and $5D$ Water Depth

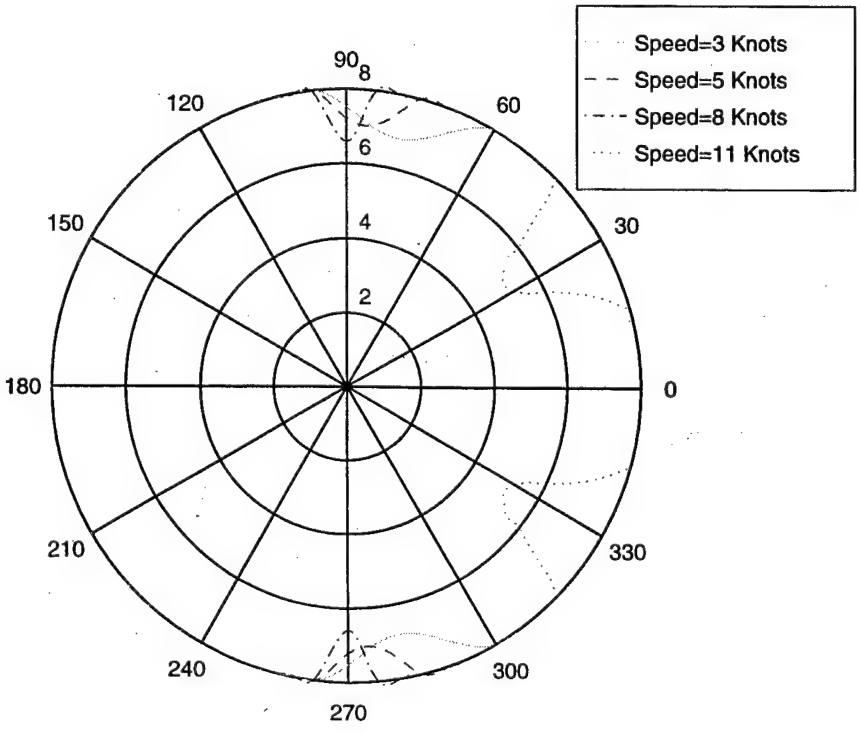

Figure 121. Sea state-polar plot, showing SOE for different U's and $6D$ Water Depth

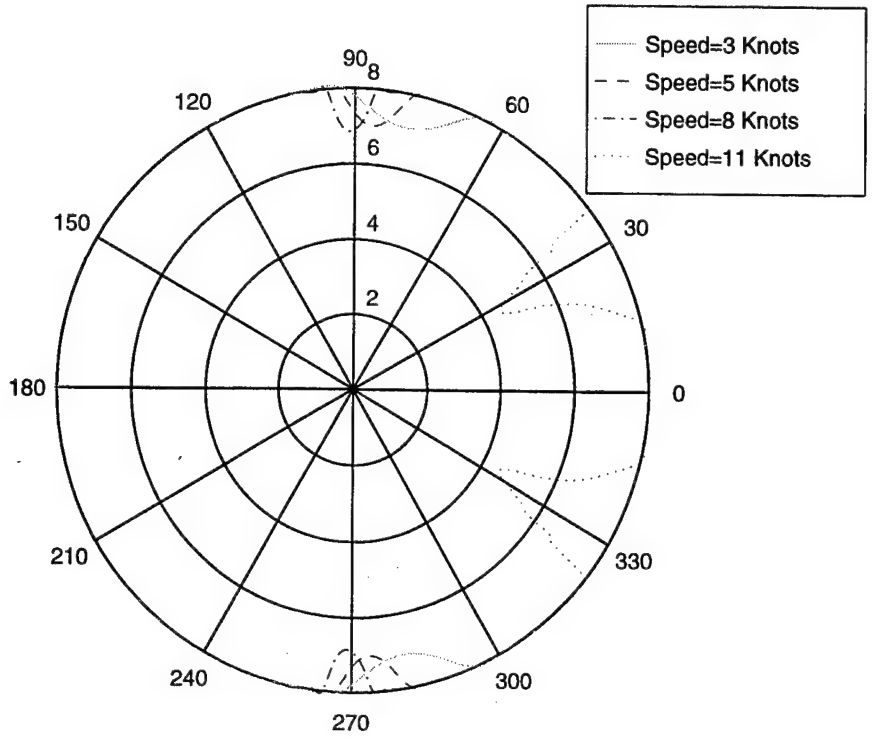

Figure 122. Sea state-polar plot, showing SOE for different U's and $7D$ Water Depth

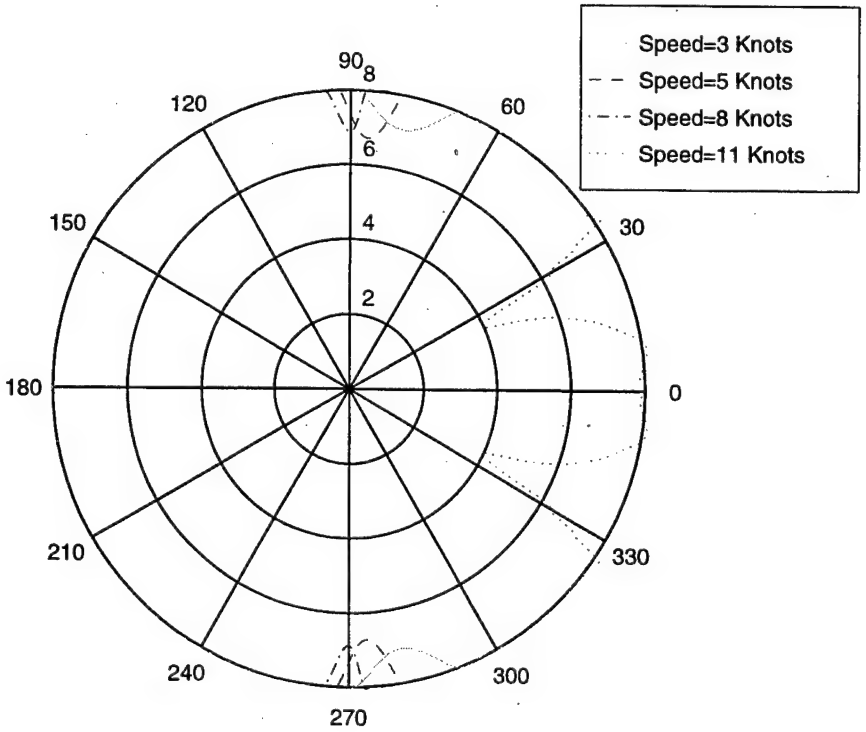

Figure 123. Sea state-polar plot, showing SOE for different U's and $8D$ Water Depth

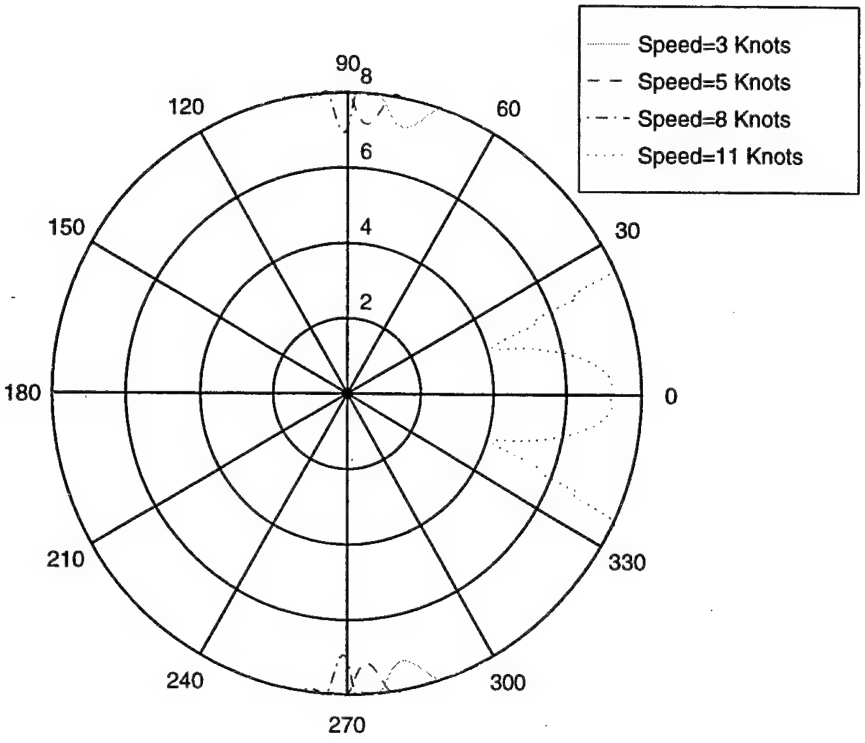

Figure 124. Sea state-polar plot, showing SOE for different U's and 10D Water Depth

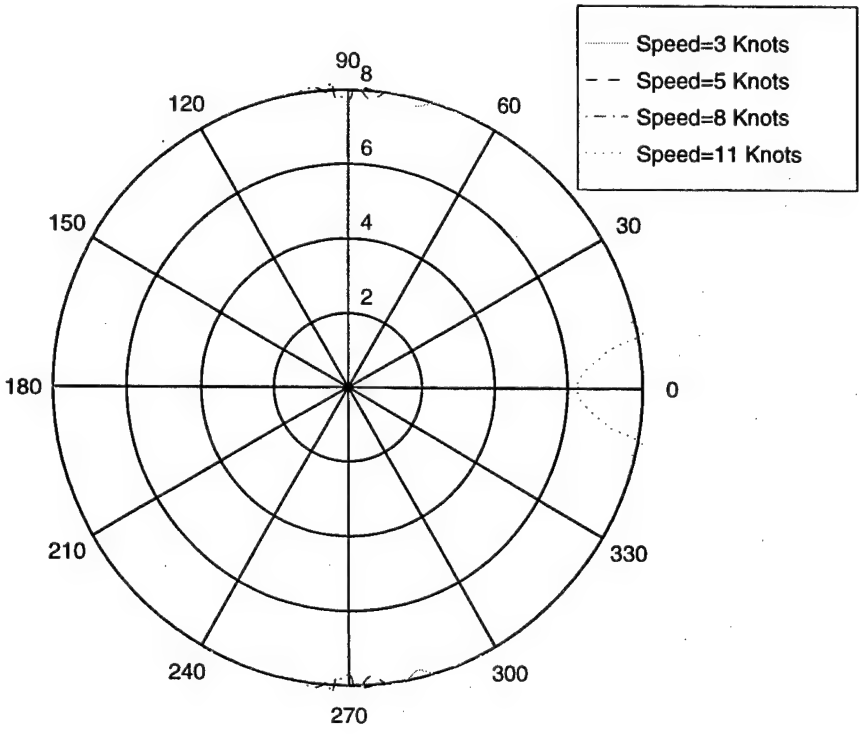

Figure 125. Sea state-polar plot, showing SOE for different U's and 15D Water Depth

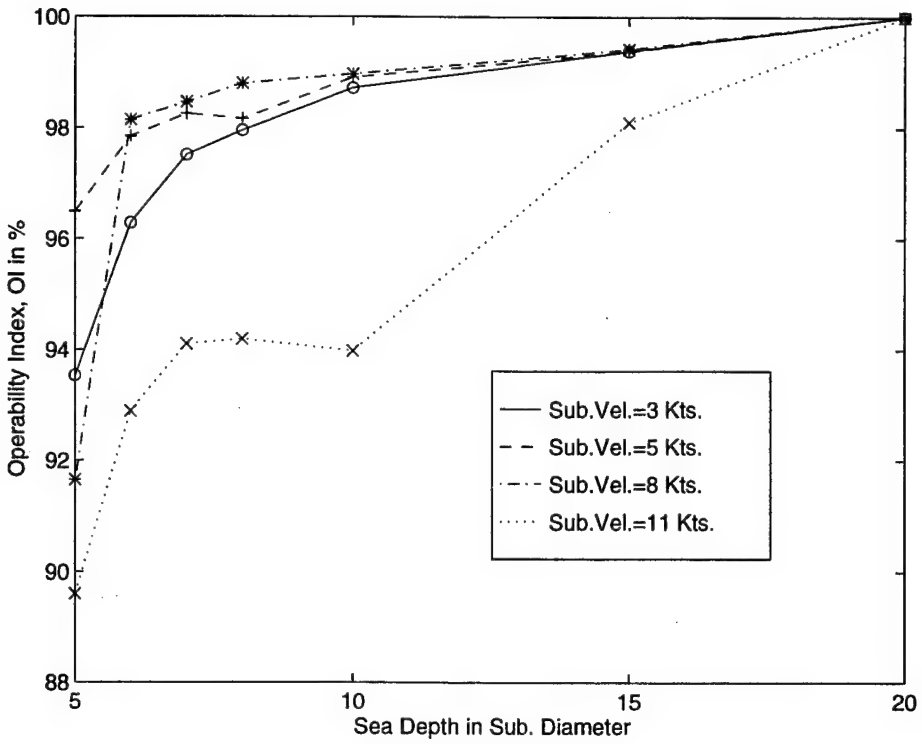

Figure 126. OI vs. Water Depth

D. RESULTS OF COMBINED CRITERIA

Results for all three criteria combined are presented in Figures 127 through 162. Lighter shades correspond to the periscope submergence criterion while the darkest shades correspond to the collision criterion. It can be seen that, in general, the sail broaching criterion dominates the collision criterion for the parameters selected; i.e., one occurrence per hour for sail broaching and one occurrence per two hours for collision. Should different values for the parameters had been selected, the collision criterion might dominate instead. The total change in the operability index is shown in Figure 163. It can be seen that, in general, the operability index is decreasing for decreasing water depth. Shallow water effects seem to be insignificant for depths exceeding 30 submarine diameters.

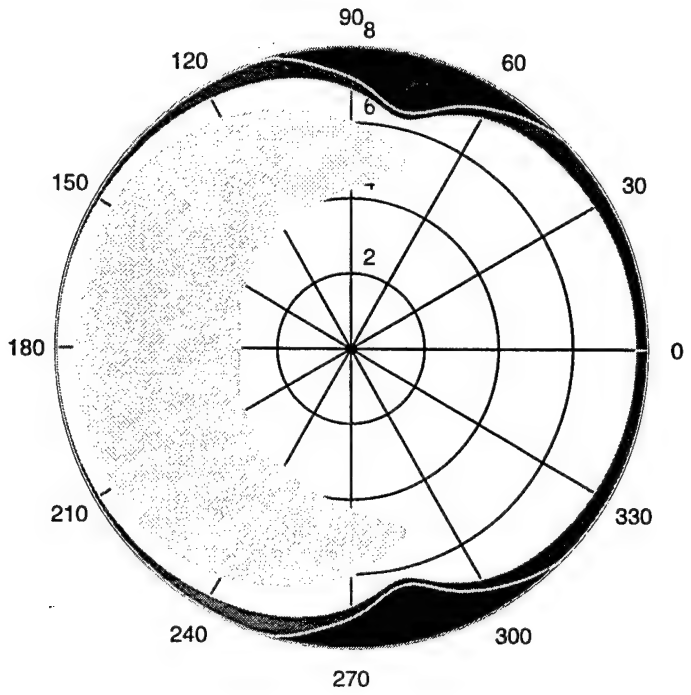

Figure 127. Sea state-polar plot, showing SOE for U=3 Knots and 5D Water Depth

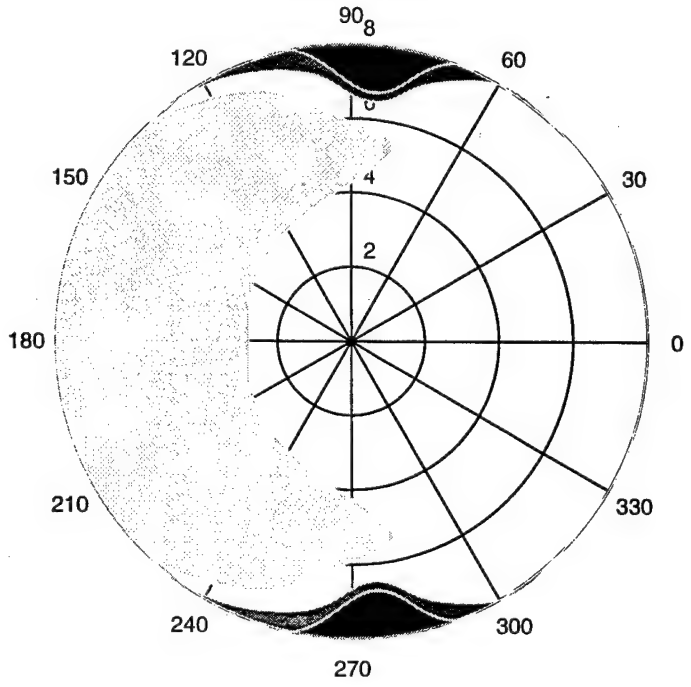

Figure 128. Sea state-polar plot, showing SOE for U=5 Knots and 5D Water Depth

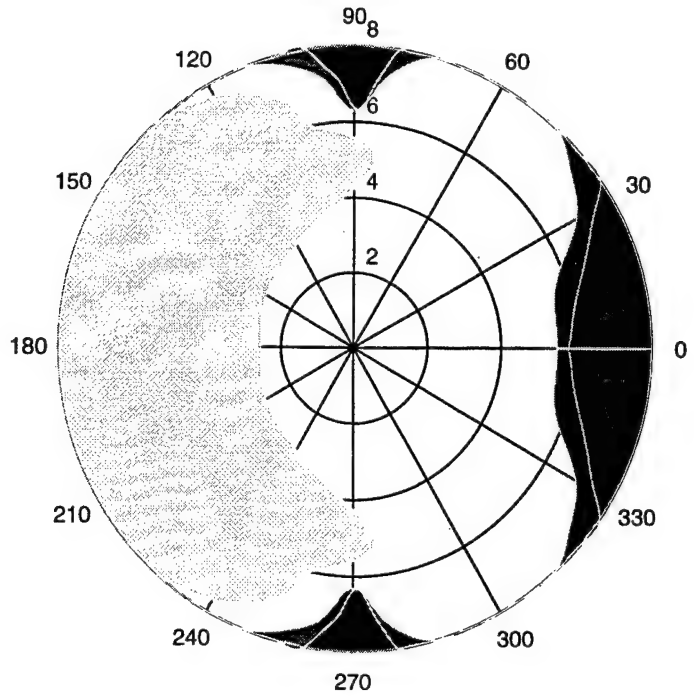

Figure 129. Sea state-polar plot, showing SOE for U=8 Knots and 5D Water Depth

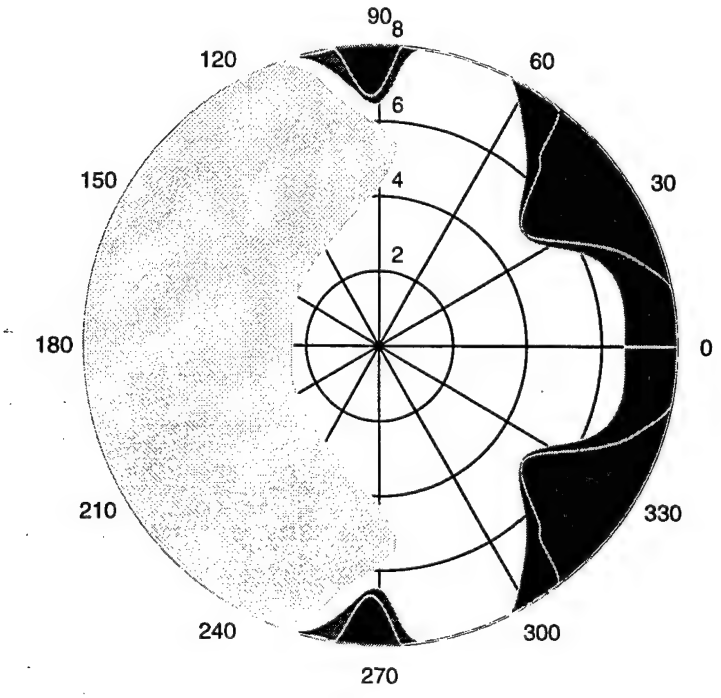

Figure 130. Sea state-polar plot, showing SOE for U=11 Knots and 5D Water Depth

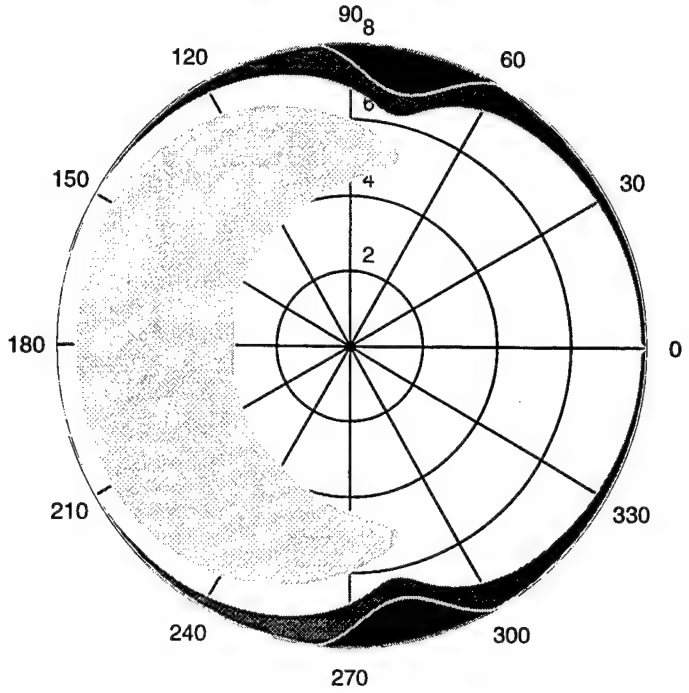

Figure 131. Sea state-polar plot, showing SOE for U=3 Knots and 6D Water Depth

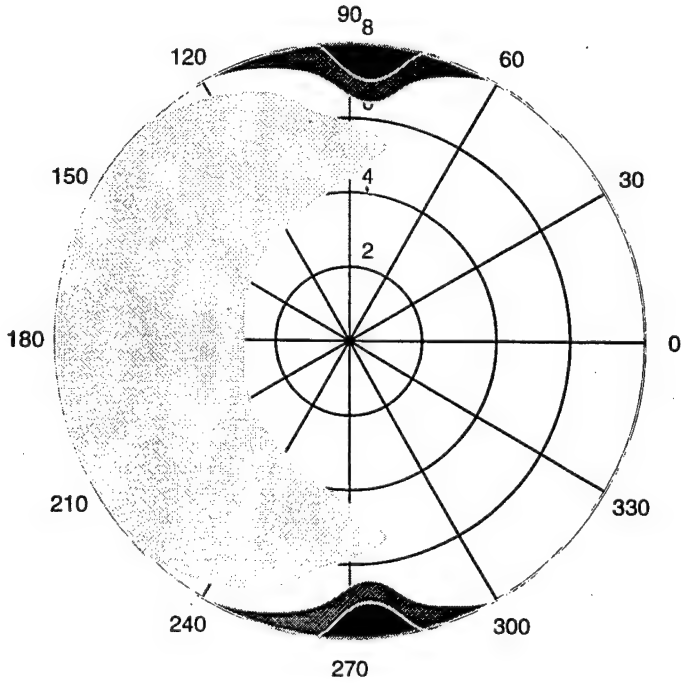

Figure 132. Sea state-polar plot, showing SOE for U=5 Knots and 6D Water Depth

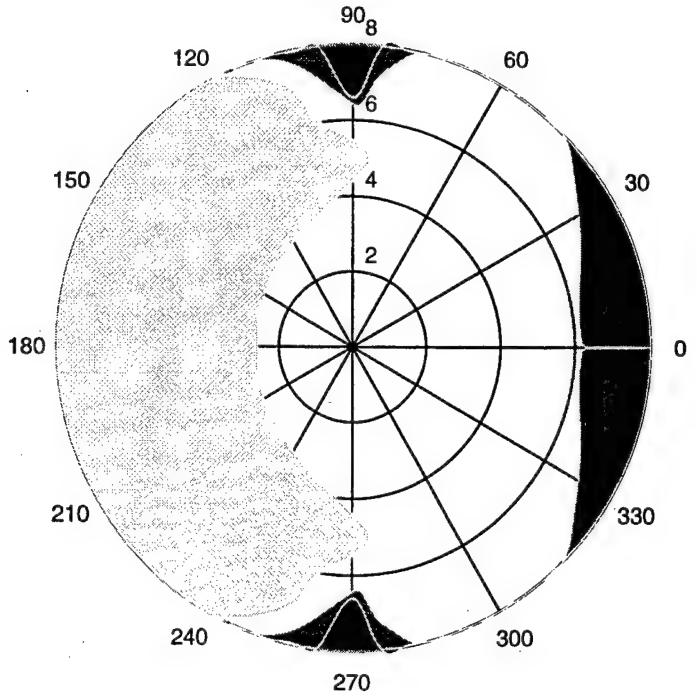

Figure 133. Sea state-polar plot, showing SOE for U=8 Knots and 6D Water Depth

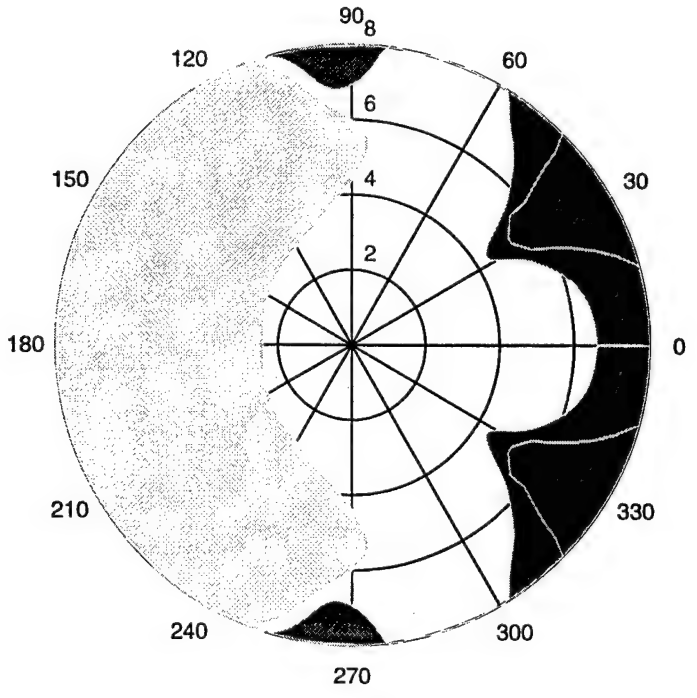

Figure 134. Sea state-polar plot, showing SOE for U=11 Knots and 6D Water Depth

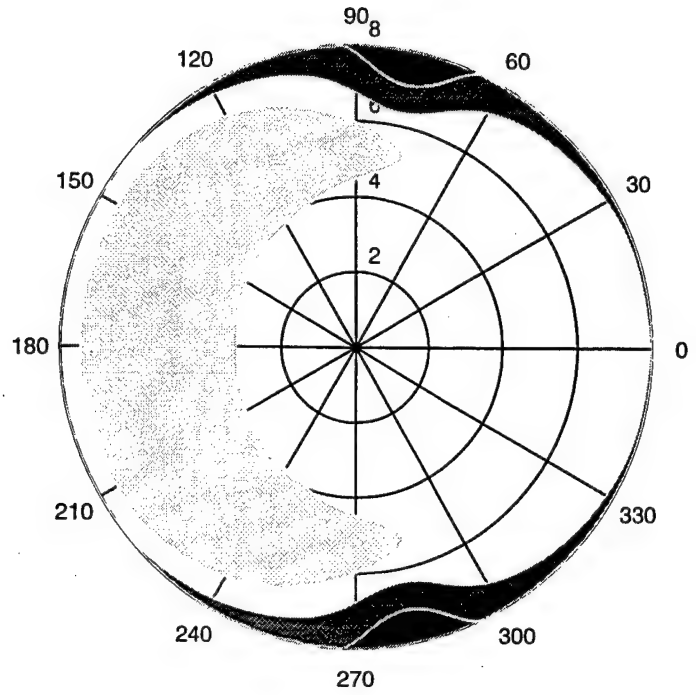

Figure 135. Sea state-polar plot, showing SOE for U=3 Knots and 7D Water Depth

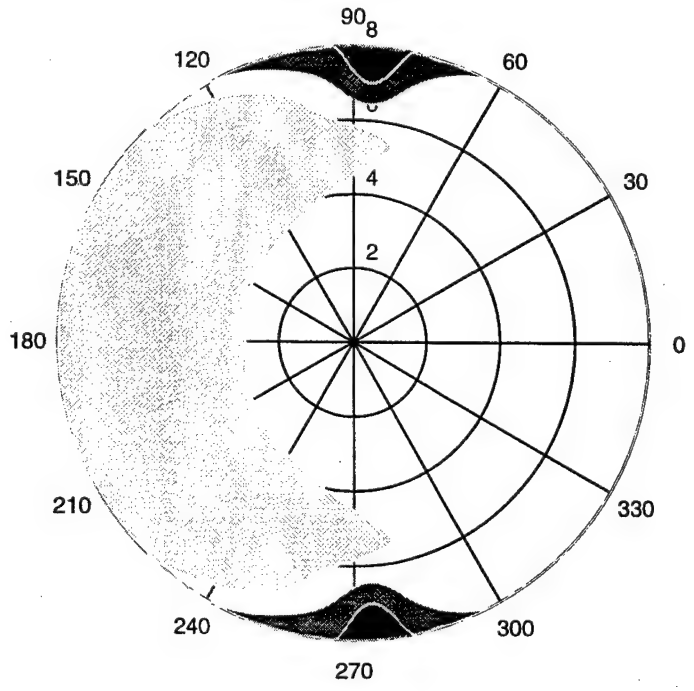

Figure 136. Sea state-polar plot, showing SOE for U=5 Knots and 7D Water Depth

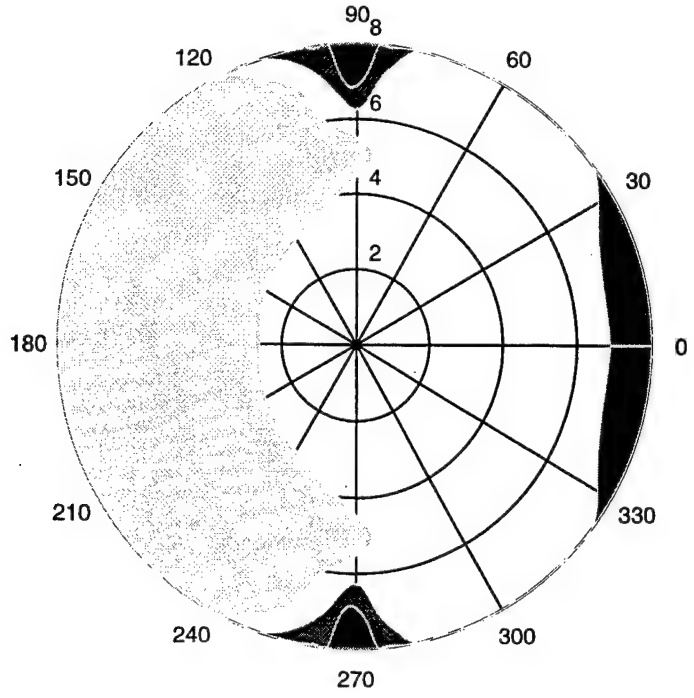

Figure 137. Sea state-polar plot, showing SOE for U=8 Knots and 7D Water Depth

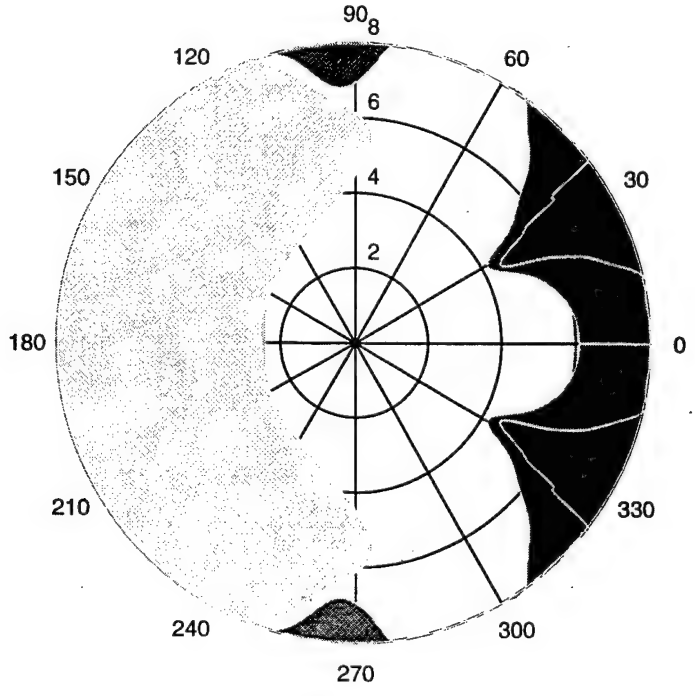

Figure 138. Sea state-polar plot, showing SOE for U=11 Knots and 7D Water Depth

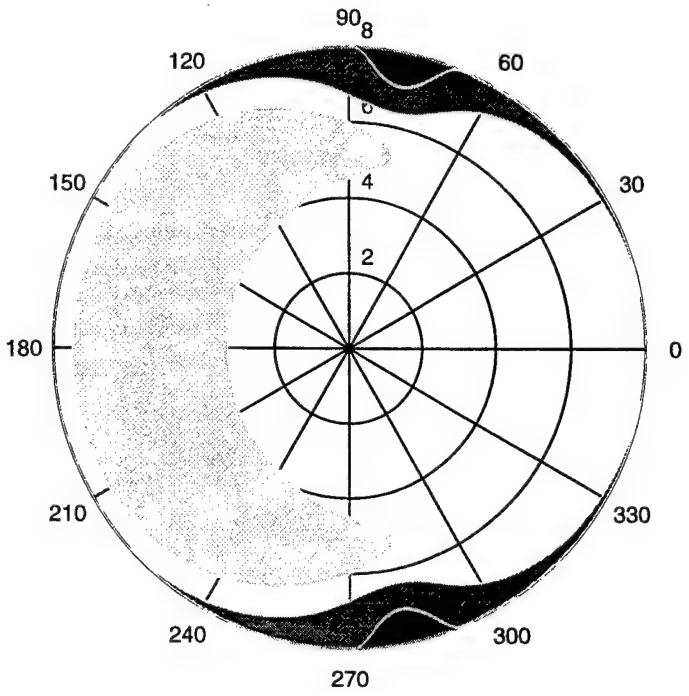

Figure 139. Sea state-polar plot, showing SOE for U=3 Knots and 8D Water Depth

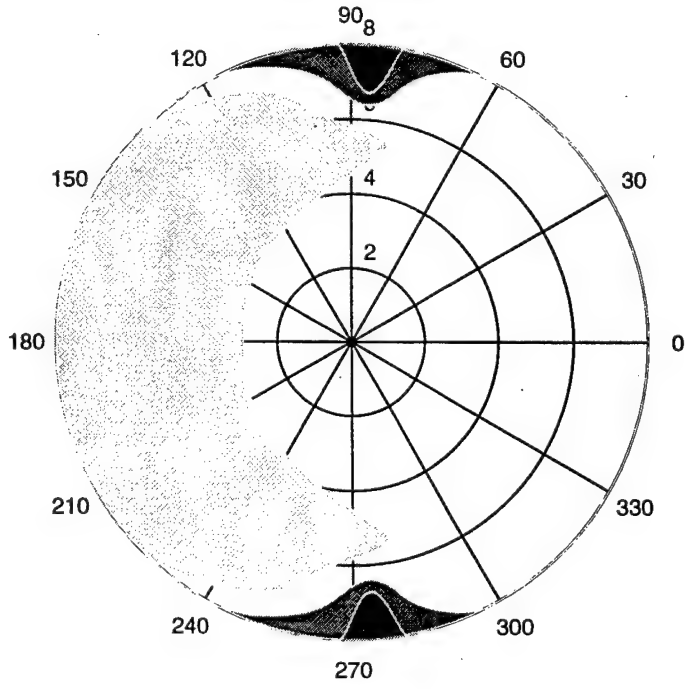

Figure 140. Sea state-polar plot, showing SOE for U=5 Knots and 8D Water Depth

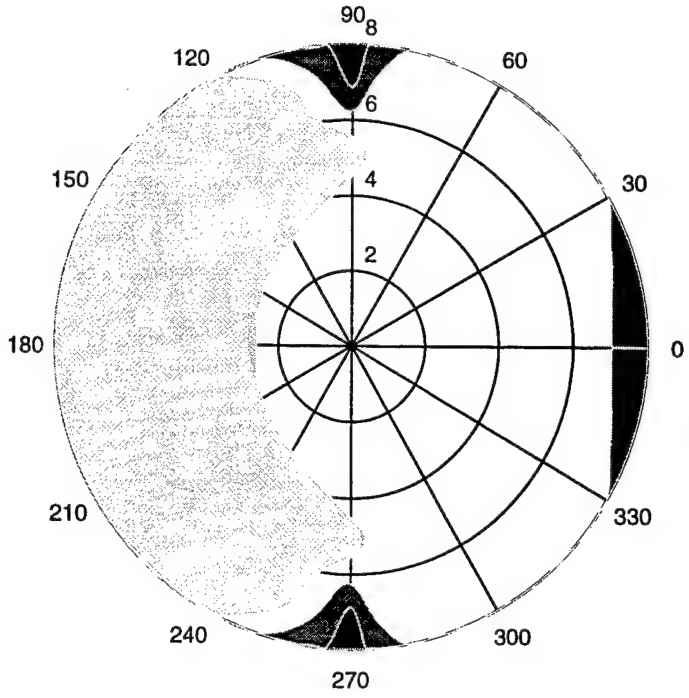

Figure 141. Sea state-polar plot, showing SOE for U=8 Knots and 8D Water Depth

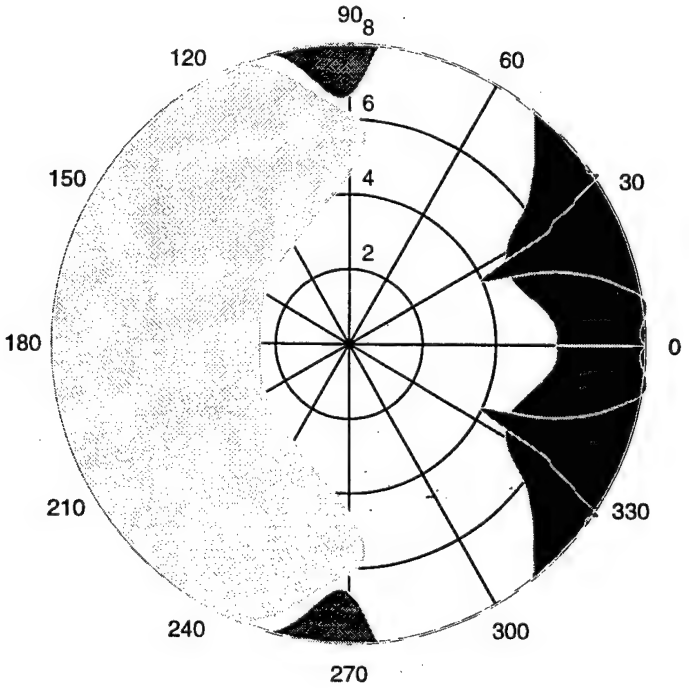

Figure 142. Sea state-polar plot, showing SOE for U=11 Knots and 8D Water Depth

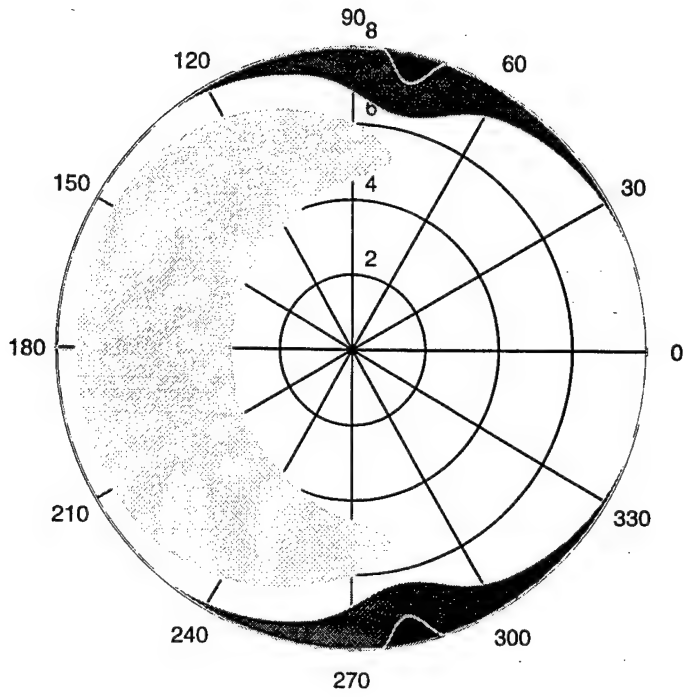

Figure 143. Sea state-polar plot, showing SOE for U=3 Knots and 10D Water Depth

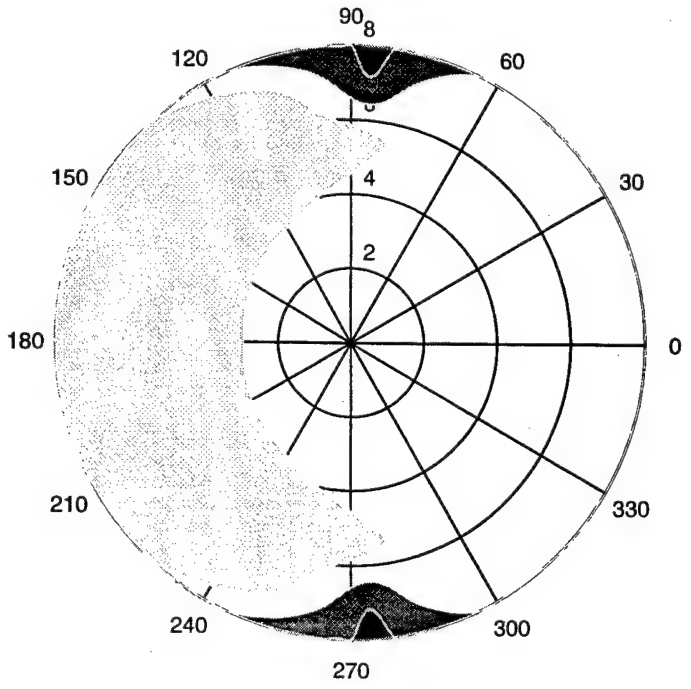

Figure 144. Sea state-polar plot, showing SOE for U=5 Knots and 10D Water Depth

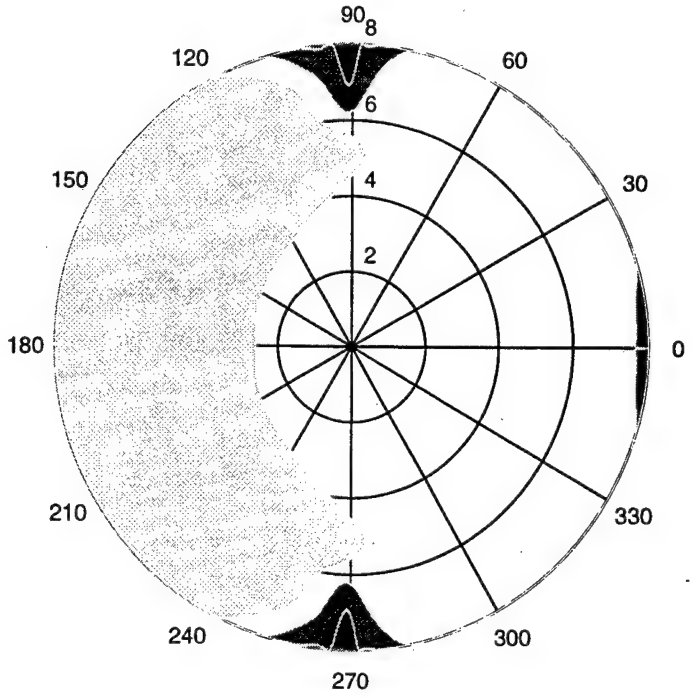

Figure 145. Sea state-polar plot, showing SOE for U=8 Knots and 10D Water Depth

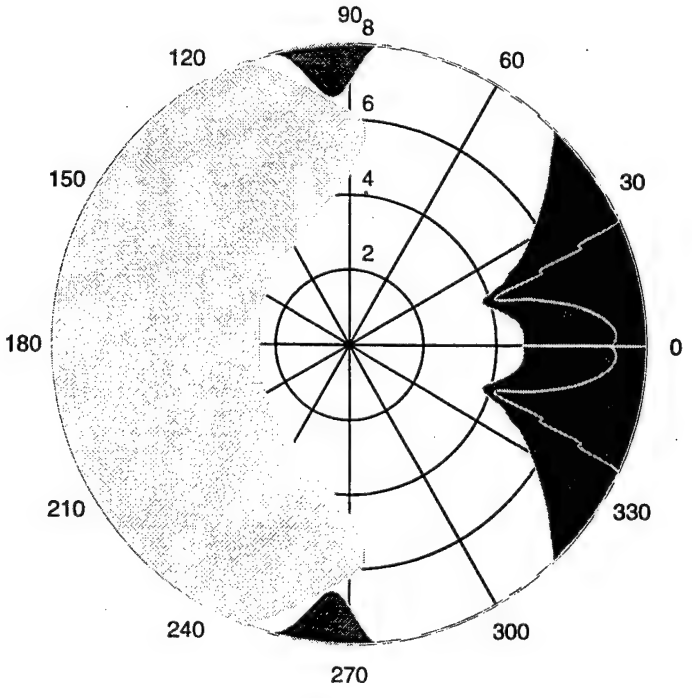

Figure 146. Sea state-polar plot, showing SOE for U=11 Knots and 10D Water Depth

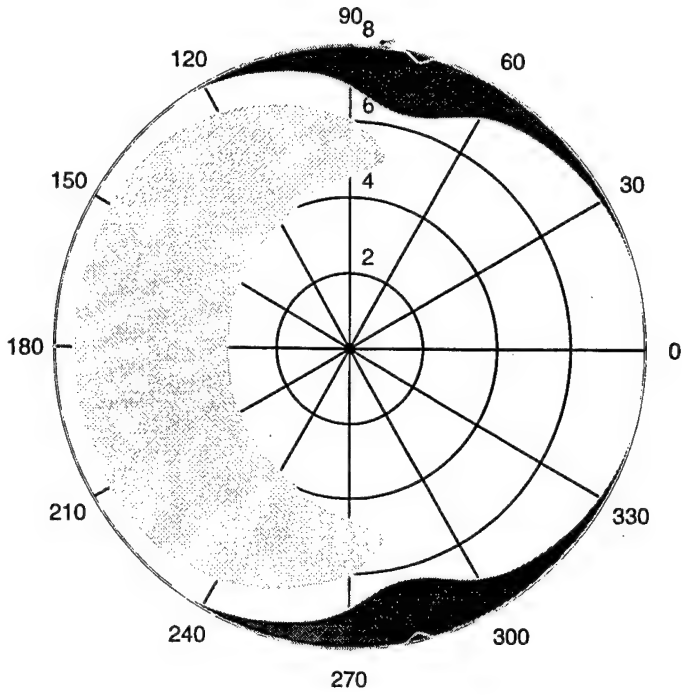

Figure 147. Sea state-polar plot, showing SOE for U=3 Knots and 15D Water Depth

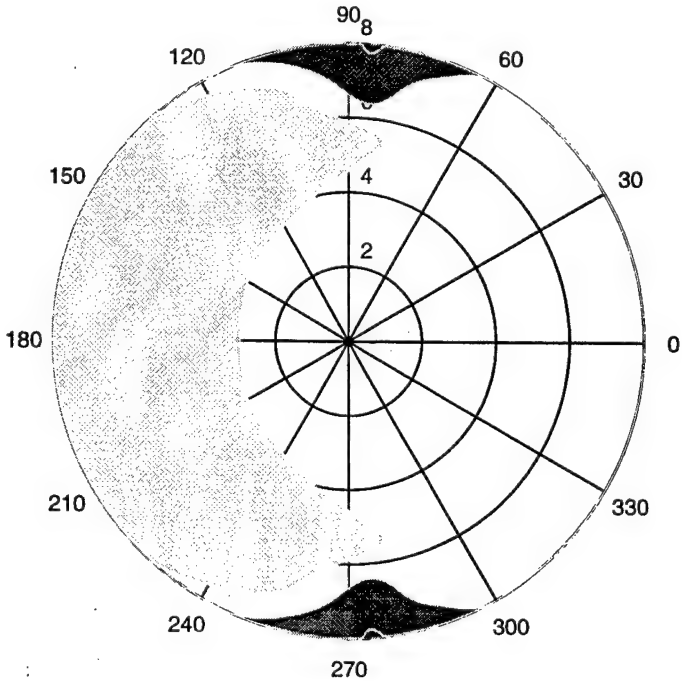

Figure 148. Sea state-polar plot, showing SOE for U=5 Knots and 15D Water Depth

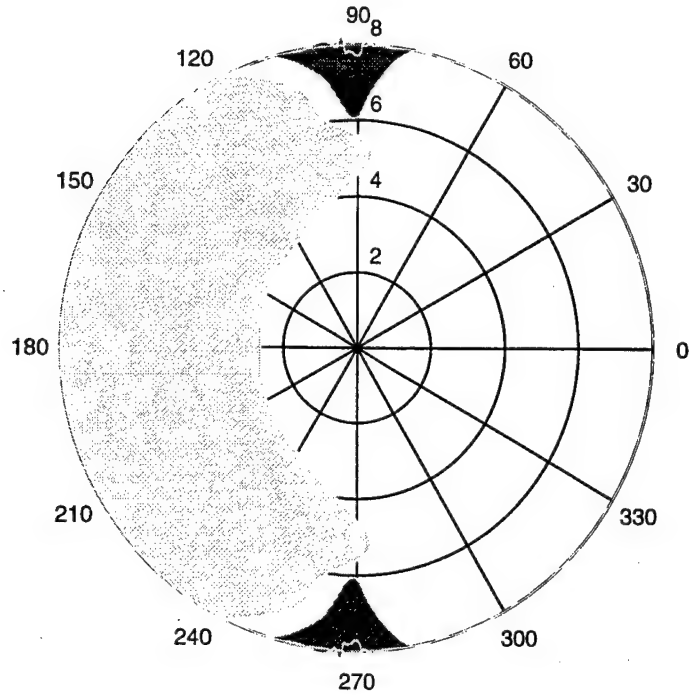

Figure 149. Sea state-polar plot, showing SOE for U=8 Knots and 15D Water Depth

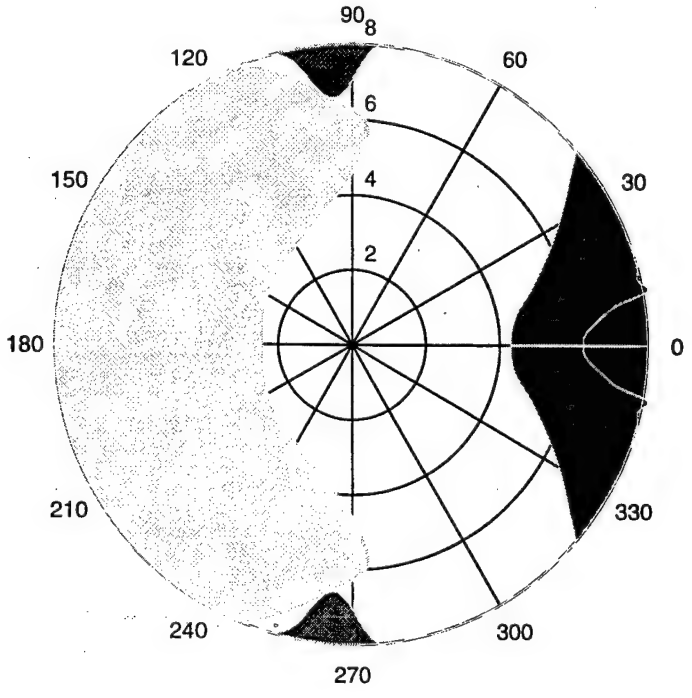

Figure 150. Sea state-polar plot, showing SOE for U=11 Knots and 15D Water Depth

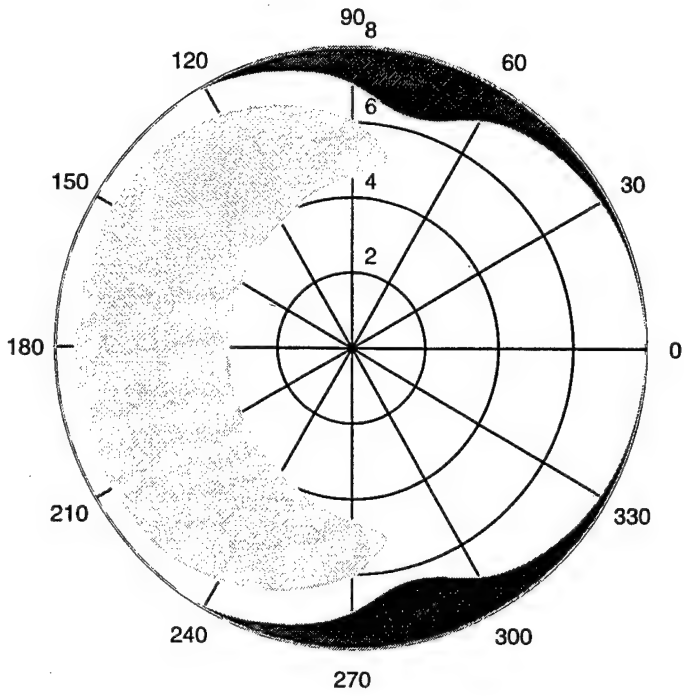

Figure 151. Sea state-polar plot, showing SOE for U=3 Knots and 20D Water Depth

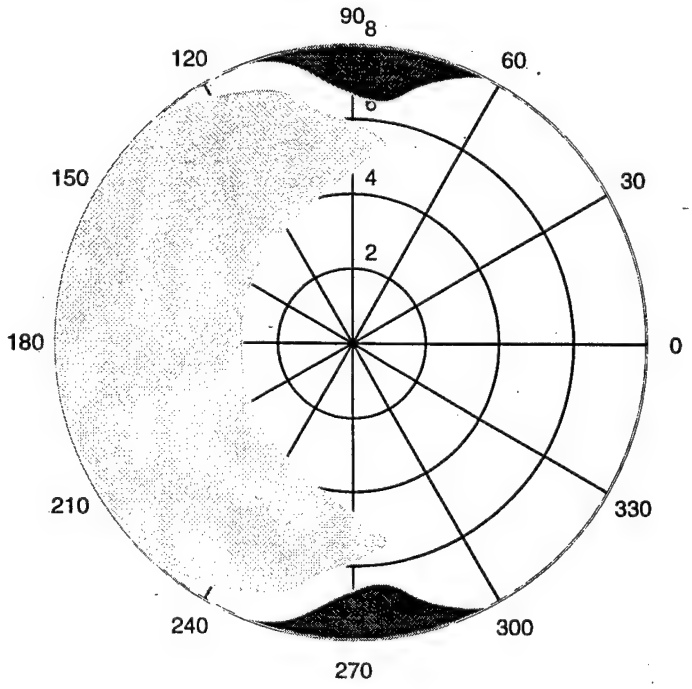

Figure 152. Sea state-polar plot, showing SOE for U=5 Knots and 20D Water Depth

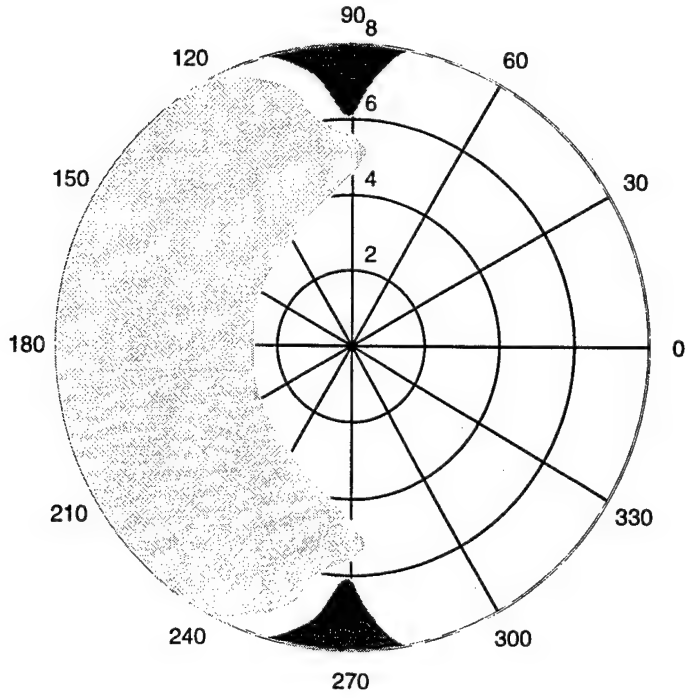

Figure 153. Sea state-polar plot, showing SOE for U=8 Knots and 20D Water Depth

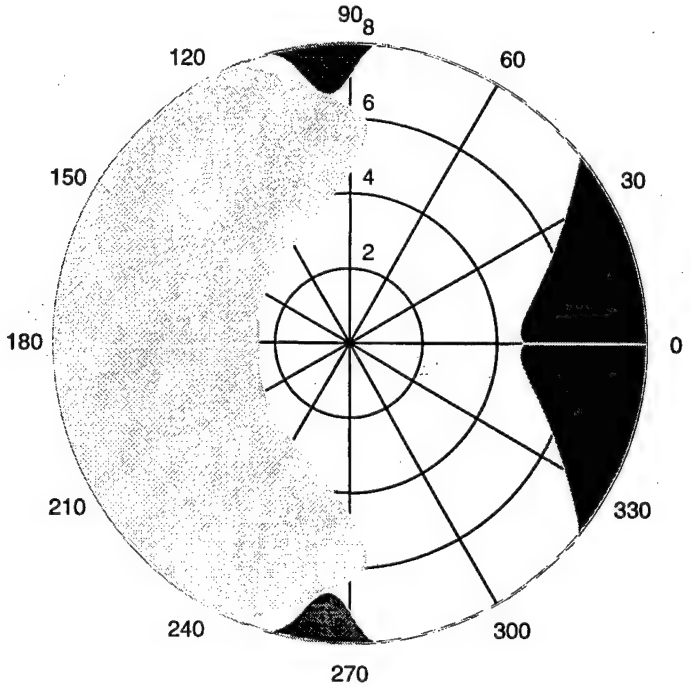

Figure 154. Sea state-polar plot, showing SOE for U=11 Knots and 20D Water Depth

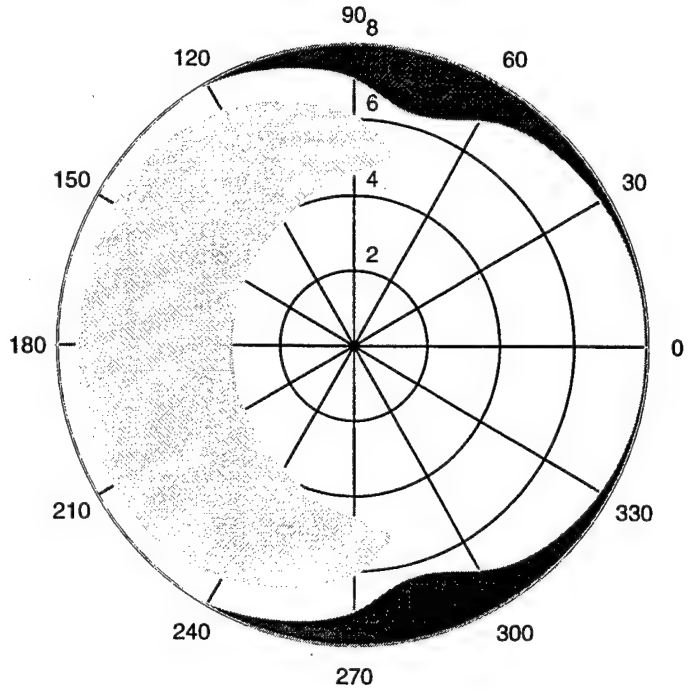

Figure 155. Sea state-polar plot, showing SOE for U=3 Knots and 30D Water Depth

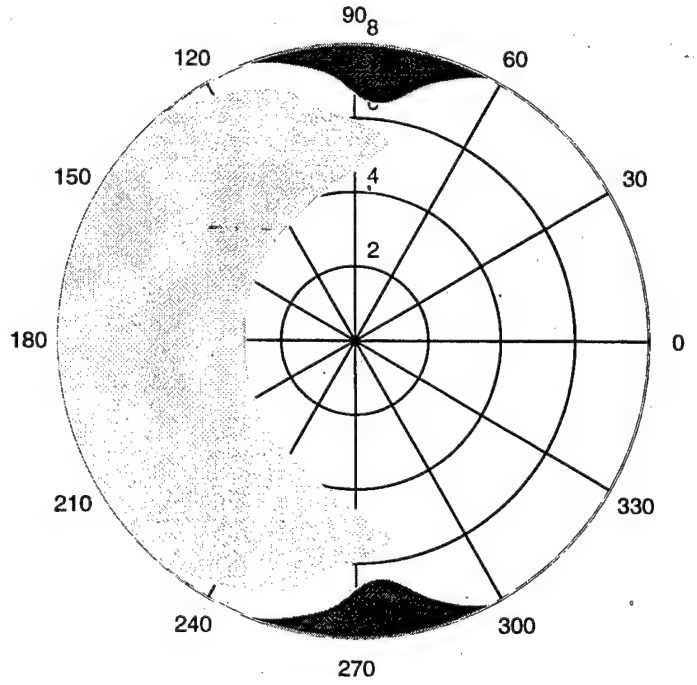

Figure 156. Sea state-polar plot, showing SOE for U=5 Knots and 30D Water Depth

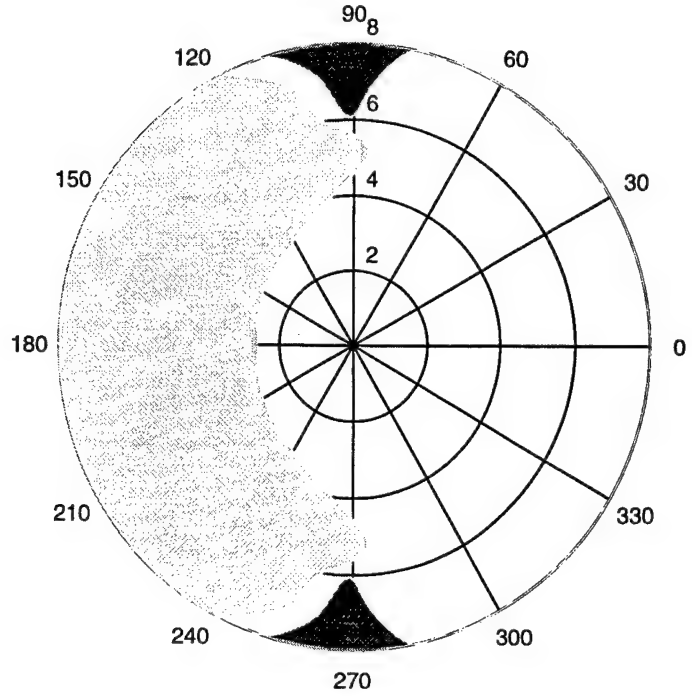

Figure 157. Sea state-polar plot, showing SOE for U=8 Knots and 30D Water Depth

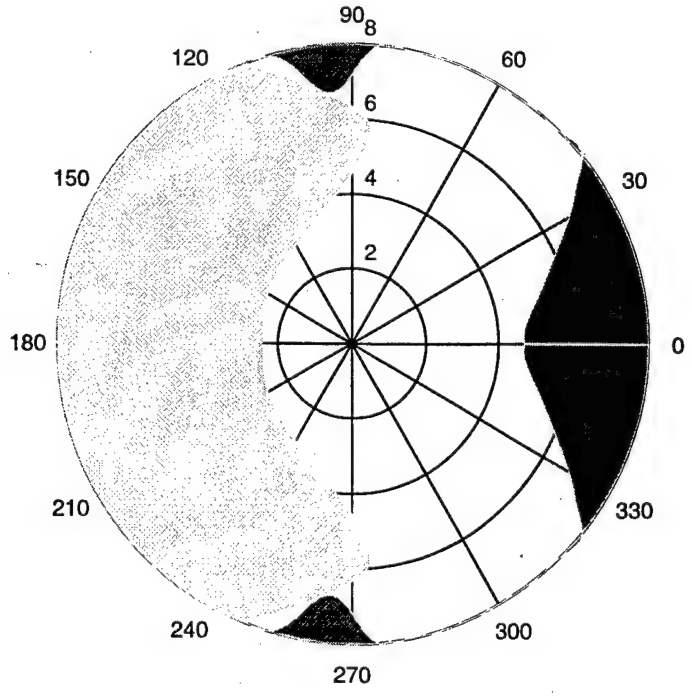

Figure 158. Sea state-polar plot, showing SOE for U=11 Knots and 30D Water Depth

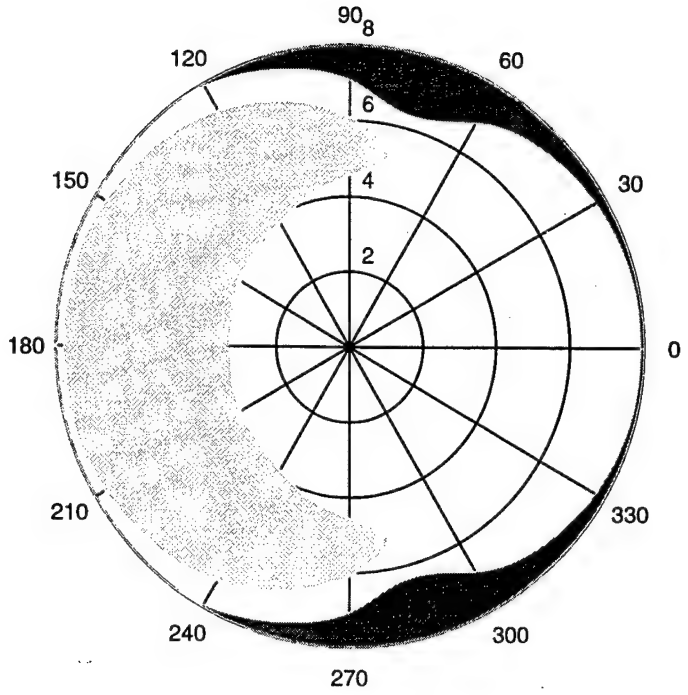

Figure 159. Sea state-polar plot, showing SOE for U=3 Knots and 40D Water Depth

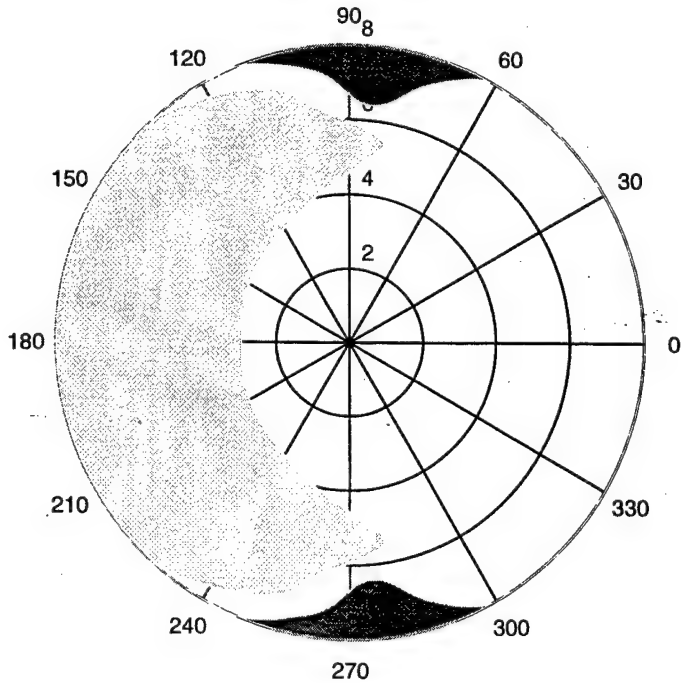

Figure 160. Sea state-polar plot, showing SOE for U=5 Knots and 40D Water Depth

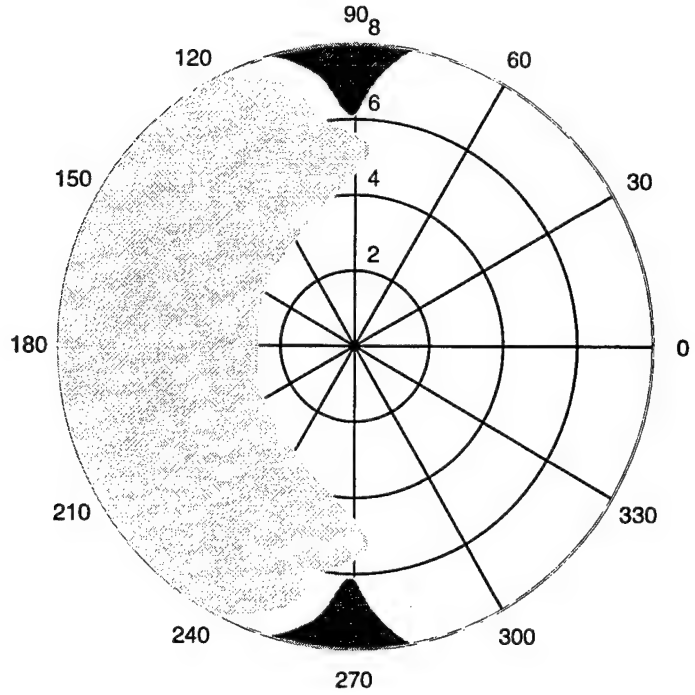

Figure 161. Sea state-polar plot, showing SOE for U=8 Knots and 40D Water Depth

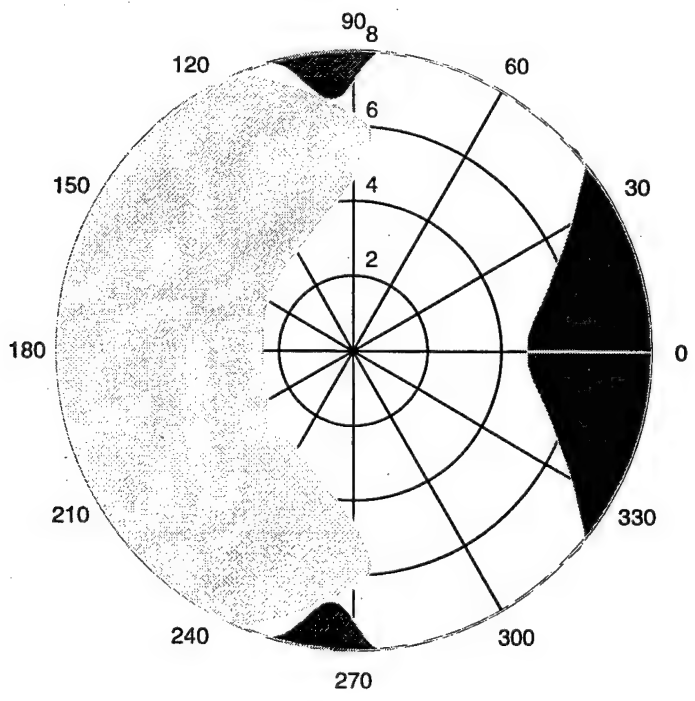

Figure 162. Sea state-polar plot, showing SOE for U=11 Knots and 40D Water Depth

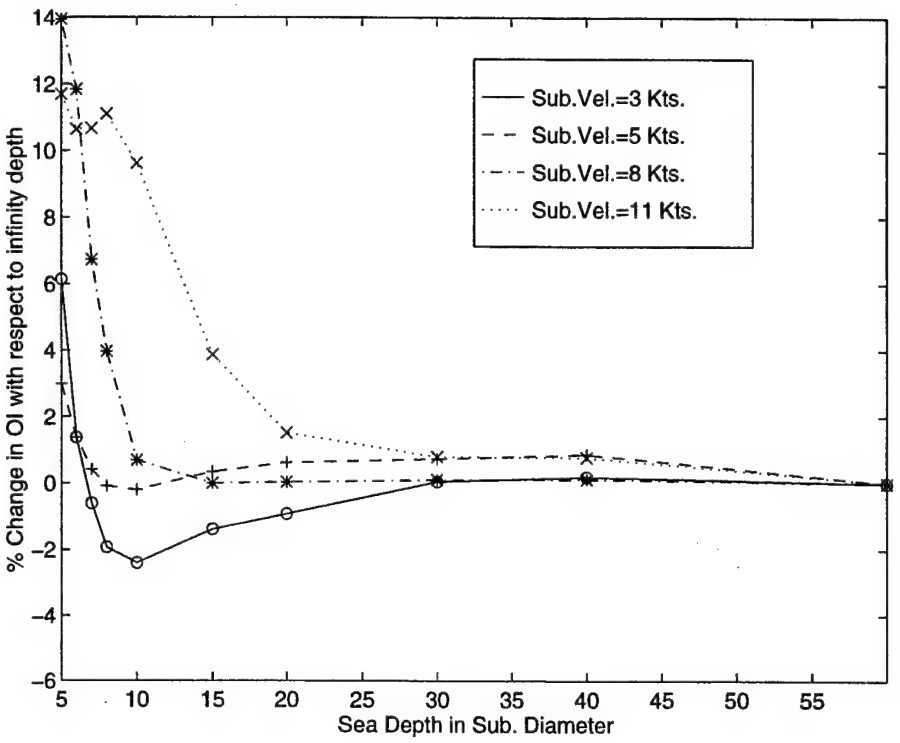

Figure 163. Change in OI with respect to infinite depth vs. Water Depth

V. CONCLUSIONS AND RECOMMENDATIONS

A. CONCLUSIONS

In this study we have evaluated the vertical plane response of submersible vehicles in the proximity of a free surface in deep and shallow waters. A potential flow, strip theory solver is used for the computations. For deep water operations periscope submergence and sail broaching criteria are used to map the operability envelope of the vehicle for different sea directions, sea states, operating depths and vehicle speeds. The operability of the vehicle is quantified by calculating a certain operability index. For shallow water operations in addition to the above two criteria, a third criterion is considered which is the collision of the vehicle with the sea-bed. The primary conclusions from this study are summarized below:

1. For the periscope submergence criterion head seas appear to cause larger number of violations than following seas regardless of the water depth. Also, the operability index does not change much with water depth. The effect of shallow water on this criterion is insignificant. An optimum operating depth can be found which minimizes the expected number of periscope submergence events. This depth is a weak function of vehicle speed.
2. For the sail broaching criterion the operability index does not appear to depend on sea direction in a consistent way. Higher sea states correspond to smaller operability indices for a given sea direction. The operability index does not change significantly with speed or operating depth and it generally increases with increasing operating depth. For the sail broaching criterion, water depth has a more important effect than for periscope submergence on both the value of the operability index and the shape of

the polar plots. In general, the operability index is decreasing with decreasing water depth.

3. For the collision criterion in shallow water, the operability index decreases as the water depth becomes smaller. The shape of the polar plots changes significantly with water depth.
4. For all criteria combined, it appears that certain combinations of vehicle speed and operating depth may result in higher values for the operability index. It should be mentioned that this depends on the relative magnitude of the individual criteria. In general, the sail broaching criterion dominates the collision criterion for the parameters selected in this study. It can be seen that, in general, the operability index is decreasing for decreasing water depth. Shallow water effects seem to be insignificant for depths exceeding 30 submarine diameters.

B. RECOMMENDATIONS

The following is a list of recommendations for further research on near surface response of submersible vehicles:

1. For periscope submergence in a given sea direction the motion point appears to move more in phase with the incoming waves as sea states become more severe. Even though the criterion is not exceeded in such high sea states, the average wave height may exceed the exposed periscope length. Since the periscope moves in phase with the waves, the operator's visual horizon may be very small. This can cause the operations to be difficult to conduct even though the criterion is not violated. Such situations should be analyzed with proper simulation studies.

2. Evaluate the effect of different geometric hull parameters, on the operability index. Such parameters may be, for example, the length, diameter, and prismatic coefficients of the hull.
3. Evaluate the effects of second order wave forces and motions on vehicle response. Even though these motions are slowly varying and can be controlled to a certain extent, they may alter both the values of the operability indices and the shape of the corresponding polar plots.

LIST OF REFERENCES

1. Crook, T. P., (1994), *An Initial Assessment of Free Surface Effects on Submerged Bodies*, M. S. Thesis, Naval Postgraduate School, Monterey, California

2. Friedland, B., (1986), *Control System Design*, McGraw-Hill

3. Beck, R. F., and Troesch, A. W., (1989), *Documentation and User's Manual for the Computer Program SHIPMO.BM*, Report No. 89-2

4. Jackson, H. A., (1992), *Fundamentals of Submarine Concept Design*, Proceedings SNAME Annual Meeting 1992 Paper No. 15

5. Allmendinger, E. E., (1990), *Submersible Vehicle Systems Design*, The Society of Naval Architectures and Marine Engineers

6. Papoulias, F. A.,(1993), *Dynamics of Marine Vehicles*, Informal Lecture Notes for ME4823, Naval Postgraduate School, Monterey, California

INITIAL DISTRIBUTION LIST

		No. Copies
1.	Defense Technical Information Center 8725 John J. Kingman Rd., STE 0944 Ft. Belvoir, VA 22060-6218	2
2.	Dudley Knox Library Naval Postgraduate School 411 Dyer Rd. Monterey, California 93943-5101	2
3.	Chairman, Code ME Department of Mechanical Engineering Naval Postgraduate School Monterey, CA 93943-5000	1
4.	Professor Fotis A. Papoulias, Code ME/PA Department of Mechanical Engineering Naval Postgraduate School Monterey, CA 93943-5000	6
5.	Naval Engineering Curricular Office, Code 34 Naval Postgraduate School Monterey, CA 93943-5000	1
6.	Deniz Kuvvetleri Komutanlığı Personel Daire Başkanlığı Bakanlıklar, Ankara, Turkey	2
7.	Gölcük Tersanesi Komutanlığı Gölcük, Kocaeli, Turkey	1
8.	Taşkızak Tersanesi Komutanlığı Kasımpaşa, İstanbul, Turkey	1
9.	Deniz Harp Okulu Komutanlığı Tuzla, İstanbul, Turkey 81704	1
10.	Denizaltı Filosu Komutanlığı Gölcük, Kocaeli, Turkey	1

11.	İ. T. Ü. Gemi İnşa ve Deniz Bilimleri Fakültesi Kütüphanesi Maslak, İstanbul, Turkey 80626	1
12.	Ufuk Toprak Yahya Kaptan Sitesi Blok F-19 Daire 17 İzmit, Kocaeli, Turkey	2